NASA CONTRACTOR REPORT

NASA CR-2417

NASA CR-2417

ANALYSIS OF SONIC BOOM MEASUREMENTS NEAR SHOCK WAVE EXTREMITIES FOR FLIGHT NEAR MACH 1.0 AND FOR AIRPLANE ACCELERATIONS

by George T. Haglund and Edward J. Kane

Prepared by
BOEING COMMERCIAL AIRPLANE COMPANY
Seattle, Wash. 98124
for Langley Research Center

NATIONAL AERONAUTICS AND SPACE ADMINISTRATION • WASHINGTON, D. C. • JULY 1974

1. Report No.	2. Government Accession No.	3. Recipient's Catalog No.
NASA CR-2417		

4. Title and Subtitle	5. Report Date
ANALYSIS OF SONIC BOOM MEASUREMENTS NEAR SHOCK WAVE EXTREMITIES FOR FLIGHT NEAR MACH 1.0 AND FOR AIRPLANE ACCELERATIONS	JULY 1974
	6. Performing Organization Code
7. Author(s)	8. Performing Organization Report No.
George T. Haglund and Edward J. Kane	D6-22547
	10. Work Unit No.
9. Performing Organization Name and Address	
Boeing Commercial Airplane Company P.O. Box 3707 Seattle, WA 98124	11. Contract or Grant No. NAS1-10992
	13. Type of Report and Period Covered
12. Sponsoring Agency Name and Address	Contractor Report
National Aeronautics and Space Administration Washington, DC 20546	14. Sponsoring Agency Code

15. Supplementary Notes

Appendix by K.-Y. Fung and A. R. Seebass is based on research supported by NASA through NASA Grant NGR 33-010-054.

Final Report

16. Abstract

The sonic boom flight test program conducted by the NASA Langley Research Center over the instrumented Bren tower during the summer and fall of 1970 has provided unique data on sonic boom characteristics near the shock wave extremity. Initial analyses of these data were conducted by NASA Langley personnel and a more detailed analysis by the Boeing Company. This report presents the results of a further in-depth study of selected flights. The goals of this analysis were to define more exactly the sonic boom characteristics for each flight condition and to provide information that may be necessary to avoid objectionable sonic boom noise during future airplane operations.

The analysis of the 14 low-altitude transonic flights showed that the prevailing meteorological conditions influence the vertical extent of attached shock waves during near-sonic flight ($M < 1.0$). Consideration of the acoustic disturbances below the cutoff altitude during threshold Mach number flight has shown that a theoretical safe altitude appears to be valid over a wide range of meteorological conditions and provides a reasonable estimate of the airplane ground speed reduction to avoid sonic boom noise during threshold Mach number flight. Recent theoretical results for the acoustic pressure waves below the threshold Mach number caustic showed excellent agreement with observations near the caustic, but the predicted overpressure levels were significantly lower than those observed far from the caustic. The analysis of caustics produced by inadvertent low-magnitude accelerations during flight at Mach numbers slightly greater than the threshold Mach number showed that folds and associated caustics were produced by slight changes in the airplane ground speed. These caustic intensities ranged from 1 to 3 times the nominal steady, level flight intensity.

A consideration of the effect of acceleration magnitude on caustic intensity for the longitudinal acceleration flights and the inadvertent low-magnitude accelerations during flight near the threshold Mach number indicates that stronger caustics were produced by the higher acceleration magnitudes. This result suggests that a method to alleviate the caustic produced during acceleration from subsonic to supersonic speeds is to accelerate slowly through the threshold Mach number. A maneuver designed to eliminate the acceleration caustic was also investigated.

17. Key Words (Suggested by Author(s))

Airplane
Caustic
Cutoff
Flight Test
Focus
Noise
Pressure
Sonic Boom
Supersonic
Transonic

18. Distribution Statement

Unclassified - Unlimited

STAR Category: 02

19. Security Classif. (of this report)	20. Security Classif. (of this page)	21. No. of Pages	22. Price*
Unclassified	Unclassified	132	$4.75

*For sale by the National Technical Information Service, Springfield, Virginia 22151

CONTENTS

ANALYSIS OF SONIC BOOM MEASUREMENTS NEAR SHOCK WAVE EXTREMITIES FOR FLIGHT NEAR MACH 1.0 AND FOR AIRPLANE ACCELERATIONS

George T. Haglund and Edward J. Kane
Boeing Commercial Airplane Company

SUMMARY

The initial analysis of the sonic boom measurements obtained by NASA Langley Research Center during the 1970 BREN tower flight test program indicated that unique data had been measured near the shock wave extremity. This report presents the results of a more detailed study of selected flights. The analysis of the 14 low-altitude transonic flights showed that the prevailing meteorological conditions influence the vertical extent of attached shock waves during near-sonic flight ($M < 1.0$). At Mach 0.98, the lower extremity of the shock wave on one flight extended to 480 m (1600 ft) beneath the airplane, while under different meteorological conditions it extended to only about 170 m (560 ft). Consideration of the acoustic disturbances below the cutoff altitude during threshold Mach number flight has shown that a theoretical safe altitude appears to be valid over a wide range of meteorological conditions and provides a reasonable estimate of the airplane ground speed reduction to avoid sonic boom noise during threshold Mach number flight. Recent theoretical results for the acoustic pressure waves below the threshold Mach number caustic showed excellent agreement with observations near the caustic, but the predicted overpressure levels were significantly lower than those observed far from the caustic. The analysis of caustics produced by inadvertent low-magnitude accelerations during flight at Mach numbers slightly greater than the threshold Mach number showed that folds and associated caustics were produced by slight changes in the airplane ground speed. These caustic intensities ranged from one to three times the nominal steady, level flight intensity.

A consideration of the effect of acceleration magnitude on caustic intensity for the longitudinal acceleration flights and the inadvertent low-magnitude accelerations during flight near the threshold Mach number indicates that stronger caustics were produced by the higher acceleration magnitudes. The maximum caustic intensity measured was about five times the nominal, steady, level overpressure and was produced by an acceleration magnitude of about 1.5 m/sec^2 (4.9 ft/sec^2). An amplification of about 2 is suggested for acceleration magnitude of about 0.3 m/sec^2 (1.0 ft/sec^2). This result suggests that a method to alleviate the caustic produced during acceleration from subsonic to supersonic speeds is to accelerate slowly through the threshold Mach

number. A maneuver designed to eliminate the transonic acceleration caustic was also investigated. Although the maneuver shows promise, further study is needed.

INTRODUCTION

The sonic boom flight test program conducted by the NASA Langley Research Center over the instrumented BREN tower during the summer and fall of 1970 has provided unique data on sonic boom characteristics near the shock wave extremity. Initial analyses of these data were conducted by NASA personnel (refs. 1 and 2), and a more detailed analysis is given in reference 3. This report presents the results of a further in-depth study of selected flights. The goals of this analysis were to define more exactly the sonic boom characteristics for each flight condition and to provide information that may be necessary to avoid objectionable sonic boom noise during future airplane operations.

During the BREN tower flight test program, measurements near the shock wave extremity were obtained by four types of flights. Seventy-nine of the 121 flights were made near the threshold Mach number to investigate sonic boom phenomena associated with low Mach number supersonic flight where the sonic booms do not reach the ground because they are cut off by atmospheric temperature and wind gradients. The test results for these flights are given in references 1 and 3. Nineteen flights were longitudinal accelerations from subsonic to supersonic speeds which produced caustics at the shock wave extremity. These results are reported in reference 3. Measurements near the lateral cutoff location of the sonic boom carpet were provided by nine flights at Mach 1.3 and are summarized in references 2 and 3. In addition, 14 flights were conducted at speeds close to Mach 1.0 at about 1 km (3000 ft) above the ground to provide measurements of the vertical extent of attached shock waves. The data from these low-altitude transonic flights had not been completely analyzed and reported previously.

The analysis given in this report focused on several aspects of the measurements, including:

- Analysis of the low-altitude transonic flight test data, with emphasis on the effect of meteorological conditions on the propagation of attached shock waves
- Determination of an empirical "safety factor" or safe sonic boom cutoff altitude during steady threshold Mach number flight
- Identification of the effects of low-magnitude accelerations near the threshold Mach number

- More detailed study of the caustics formed during acceleration from subsonic to supersonic speeds.

Since the low-altitude transonic flight test data had not been completely analyzed and reported previously, these data deserved detailed analysis. The objective of these flights was to determine the vertical extent and nature of the attached shock waves and whether these shock waves extend many body lengths to the ground. The flight Mach number ranged from Mach 0.95 to 1.00; with one flight at Mach 1.05. Five of these flights produced sonic booms on the ground.

Two different aspects of the threshold Mach number flight test data appeared to merit additional study. The analysis of reference 3 showed that a theoretical safety factor for specifying an airplane ground speed sufficient to control sonic boom noise on the ground during threshold Mach number operation was valid and warranted further study. The nature of the acoustic noise below the cutoff altitude during threshold Mach number flight was analyzed and is compared with a recent theoretical result. The other aspect studied was the effect of slight accelerations during flight near the threshold Mach number. The preliminary analysis of reference 3 indicated that, in several cases, caustics were produced by low-magnitude accelerations or variations in the airplane ground speed.

Several aspects of the longitudinal acceleration flight test data were also particularly interesting. Since six of the 19 flights produced caustics on the microphone array, very valuable information on shock wave characteristics near caustics was obtained. Identification of pressure signature changes and characteristics just before, at, and beyond the caustic are of particular interest since they may help in defining the physical processes associated with caustic phenomena. The analysis indicated that the effect of acceleration magnitude is an important consideration.

In conjunction with the analysis of the measured data near caustics produced by accelerations, several theoretical analyses were conducted to determine methods for alleviating these caustics. The acceleration phase of supersonic flight from subsonic to supersonic speeds is particularly important in terms of sonic boom, since the caustic results in magnified sonic boom intensity over a small ground area. The fact that the caustics produced by low-magnitude accelerations were weaker than those produced by higher magnitude accelerations suggested that a method for alleviating these caustics was to accelerate relatively slowly through the past the threshold Mach number. A maneuver suggested for completely eliminating the transonic acceleration caustic was also investigated.

The presentation of the test results and analysis in this report begins with the near-sonic test data analysis. This is followed by an analysis of the safety factor during threshold Mach number flight and the analysis of low-magnitude acceleration effects during flight near the threshold Mach number. The longitudinal acceleration caustic data analysis is then given, followed by the

theoretical study of methods for alleviating the transonic acceleration caustic. Appendix A contains a discussion of the possibility of sonic boom generation during cruise slightly below Mach 1.0. Appendix B was written by Mr. K.-Y. Fung and Dr. A. R. Seebass of Cornell University and contains the application of a theoretical method for calculating the acoustic pressure field below the threshold Mach number caustic for the BREN tower flight test conditions.

SYMBOLS

A	airplane acceleration
a	sound speed
a*	sound speed using virtual temperature, T_v
c_o	Snell's law invariant
c_p	pressure coefficient, $\Delta P/q$
D	drag, distance
g	acceleration of gravity
h	airplane altitude above mean sea level
K_R	ground reflection coefficient
L	sonic boom signature wavelength
M	airplane Mach number = V/a
M_o	pilot-read Mach number
M_q	Mach number increment associated with perturbation velocity (eq. 8)
M_S	local shock Mach number (eq. 9)
M_{SB}	lowest Mach number for subsonic sonic boom (eqs. A3 through A5)
M_T	threshold Mach number (eq. 17)
M_{TW}	Mach number associated with gradients of temperature and wind (eqs. 4 and 5)
$\vec{n}$	unit vector normal to wave front

n_L	lift (normal) load factor
n_T	thrust (axial) load factor
n_N	acceleration vector normal to Mach cone (eq. 23)
N	nondimensionalized theoretical sound function below threshold Mach number caustic
P	pressure
q	dynamic pressure; also perturbation velocity associated with the perturbation pressure ΔP in a plane-wave shock system
R	relative curvature of caustic relative to ray (eq. 13); also gas constant
S	separation distance between leading and trailing shocks produced by acceleration
t_a	time along airplane trajectory
T	air temperature; also thrust
t_{ref}	reference time used for shock wave profile calculations
t_o	shock wave arrival time
u	horizontal wind speed
u_n	component of horizontal wind in plane of the normal to the shock wave = $u \cos(\psi - \eta)$
V	airplane velocity relative to atmosphere, Ma_o
V_G	airplane ground speed, $(Ma_o - u_n)$
V_p	shock propagation velocity, $(a - u_n)$
$V_{p_{mic}}$	shock propagation speed determined from shock wave arrival times over ground microphone array (eq. 11)
V_{ps}	shock propagation speed normal to the shock wave surface

V_p^* shock propagation velocity with increase because of water vapor, (a^*-u_n)

W airplane weight

(X,Y,Z) reference coordinate system: east, north, and above ground, respectively

y vertical distance below cutoff altitude

Z_c sonic boom cutoff altitude during threshold Mach number flight

Z_s theoretical minimum altitude above the ground for which cutoff can occur to obtain low-intensity acoustic-like disturbances at ground during threshold Mach number flight

α shock wave angle of incidence

α_G ground slope

β Prandtl-Glauert parameter, $(M^2 - 1)^{1/2}$

γ ratio of specific heats; also airplane climb angle

Δ perturbation from undisturbed value

η direction from which wind blows

θ inclination angle of wave normal $\vec{n}$ below horizontal (eq. 1)

λ sonic boom signature half wavelength

μ Mach angle, $\sin^{-1}(1/M)$

υ heading angle of wave normal $\vec{n}$

ρ atmospheric density

ϕ azimuth angle of wave normal from vertical plane; also velocity potential

ψ airplane heading angle

SUBSCRIPTS

G	ground level
N	incoming N-wave signal
max	maximum
REF	reference value
T	tower
o	initial value at airplane altitude

ANALYSIS OF NEAR-SONIC FLIGHT TEST DATA

This section contains the results of the analysis of sonic boom measurements obtained from the 14 low-altitude flights at near-sonic speeds. During several of these flights, the attached shocks associated with flight at speeds close to the speed of sound were recorded on the BREN tower. These flights were given particular emphasis in the analysis and discussion.

BACKGROUND

During the early 1960s there were a number of "accidental" sonic booms produced by airplanes that appeared to be flying at subsonic speeds. Shortly after that, Barger (ref. 4) proposed a mechanism for "subsonic sonic boom" in an effort to explain these inadvertent boom occurrences. (This is evaluated in appendix A.) Airplanes flying near Mach 1.0 have shock waves attached to them, and the purpose of this test was to determine how far these shock waves extend from the airplane in the real atmosphere and to determine under what conditions they may continue to exist long distances away from it. A recent study has indicated that cruise Mach numbers as high as Mach 0.98 can be flown with fairly reasonable lift-to-drag ratios by use of the supercritical airfoil and refined area ruling techniques (ref. 5).

Since the objective of the near-sonic flights was to determine the vertical extent and nature of the attached shock waves during near-sonic flight, the test airplanes were flown at an altitude of about 850 m (2800 ft) above the ground at Mach numbers ranging from 0.95 to 1.00. An additional flight was made at Mach 1.05. Table 1 summarizes the airplane flight conditions and observed sonic boom characteristics. The airplanes were beacon equipped and tracked by radar. The airplane altitude, Mach number, and weight (obtained from the fuel on board) are given in table 1, along with the boom time at tower microphone T-1 and the maximum observed overpressure recorded by any of the tower and ground microphones. Two different F-104 airplanes were used in the tests, as indicated in table 1. The airplane heading for these flights was 035 true and the "steady point" was about 8 km (5 st mi) from the tower.

The distinguishing feature of the data given in table 1 is the large difference in the observed sonic booms on the BREN tower for similar flight conditions. For example, of the three flights at Mach 0.98 only two produced booms and only one of the two flights at Mach 0.99 produced a sonic boom on the tower. Much of the analysis was concerned with this apparent discrepancy.

During the near-sonic tests several changes were made from the basic microphone setup as given in figure 3 of reference 2. Ground microphones G-5 and G-10 were positioned 242 m (800 ft) from the tower on a line normal to the flight path in line with microphones G-15 and G-16. In

TABLE 1.—SUMMARY OF TRANSONIC FLIGHTS, SEPTEMBER 1, 1970

Bongo-pass	Pass	Airplane altitude MSL, h		Airplane ground speed, V_G		Calculated Mach number, M_{calc}	Pilot-read Mach number M_o	Airplane weight, W		Boom time at microphone T-1 PDT	Maximum observed overpressure			Subjective boom character	Airplane no.
		m	ft	m/sec	ft/sec			kg	lb		N/m^2	lb/ft^2	Microphone		
1-1	067	[a]1980	[a]6500	334.1	1096	[b]0.959	0.95	8575	18 900	[c]0845	—	—	—	Engine noise only	1
1-2	068	1950	6400	338.3	1110	0.971	0.96	8230	18 150	[c]0853	—	—	—	Engine noise only	1
1-3	069	1980	6500	341.7	1121	0.981	0.97	7895	17 400	[c]090	—	—	—	Engine noise only	1
1-4	070	1965	6450	371.9	1220	1.069	1.05	7485	16 500	0906:50.27	596.6	12.46	G-1	Heavy double boom	1
2-1	071	1930	6330	350.5	1150	1.006	0.98	8435	18 600	0920:32.59	293.6	6.133	T-15	Boom	2
2-2	072	1890	6200	345.0	1132	0.990	0.97	7940	17 500	0928:22.51	—	—	—	Rumble plus engine noise	2
2-3	073	1875	6150	349.9	1148	1.003	0.98	7485	16 500	0936:24.33	68.7	1.435	T-13, G-3	Boom	2
3-1	074	1980	6500	347.8	1141	0.997	0.99	8460	18 650	1037:38.39	134.0	2.798	T-15	Boom	1
3-2	075	1995	6550	342.6	1124	0.982	0.98	7895	17 400	1046:53.19	—	—	—	Engine noise	1
3-3	076	1890	6200	351.4	1153	1.007	1.00	7305	16 100	1055:03.64	464.0	9.691	G-1	Sharp boom, rumble	1
4-1	077	2010	6600	331.9	1089	0.953	0.96	8620	19 000	[c]1240	—	—	—	Engine noise and possible very light rumbles	1
4-2	078	2010	6600	336.5	1104	0.965	0.965	8210	18 100	[c]1248	—	—	—		1
4-3	079	2010	6600	340.8	1118	0.980	0.99	7800	17 200	[c]1256	—	—	—		1
4-4	080	1980	6500	345.0	1132	0.993	1.00	7350	16 200	[c]1303	—	—	—		1

[a] The ground level at the BREN tower is 1112.5 m (3650 ft) MSL.

[b] The error in this calculation is about +0.01 Mach number due to inaccuracies in radar ground speed and wind speed.

[c] Approximate time of airplane passage over BREN tower.

addition, only tower microphones T-1, T-3, T-5, T-7, T-9, T-11, T-13, and T-15 were used for these flights, and in many cases the pressure signatures observed by tower microphones T-9 and T-13 were unusable due to excess background noise. Figure 1 gives the microphone locations schematically for reference.

DATA ANALYSIS METHODS

The techniques used in analyzing the near-sonic flight test data are given in this section for reference. These include the conversion of gradients of temperature and wind into a Mach number gradient, the calculation of the Mach number gradient associated with the shock wave strength, and the calculation of shock wave profiles.

Conversion of Temperature and Wind Gradients to a Mach Number Gradient

In determining the effect of temperature and wind gradients it is convenient to convert them into a Mach number gradient. This can be accomplished by beginning with the equation describing the inclination angle of the shock wave with the horizontal. In the notation of references 3 and 6, this is:

$$\cos \theta = \frac{a(z)}{c_o + u_n(z)} \tag{1}$$

For steady, level flight and the $\phi = 0$ ray (directly beneath the airplane) this becomes:

$$\cos \theta = \frac{a(z)}{(M_o a_o - u_{n_o}) + u_n(z)} \tag{2}$$

where M_o is the airplane Mach number. The angle θ can be converted to a Mach number directly related to the gradients of temperature and wind by use of the simple relationship

$$\cos \theta = 1/M_{TW} \tag{3}$$

Equation (2) then gives

$$M_{TW} = \frac{(M_o a_o - u_{n_o}) + u_n(z)}{a(z)} \tag{4}$$

where M_{TW} is the required Mach number that includes the effect of temperature and wind variations beneath the airplane. A slightly different form of equation is also useful:

$$(M_{TW} - M_o) \equiv \Delta M_{TW} = M_o\left[\frac{a_o - a(z)}{a(z)}\right] + \left[\frac{u_n(z) - u_{n_o}}{a(z)}\right] \quad (5)$$

For the case when $(M_{TW} - M_o)$ is positive in an altitude layer proceeding from the airplane to the ground, the shock wave will be refracted toward the ground. In this case cutoff due to atmospheric refraction cannot occur. This condition occurs when $a_o > a(z)$ and/or $u_n(z) > u_{n_o}$ (in more common terms, when a temperature inversion exists, when a tailwind decreases toward the ground, or when a headwind increases toward the ground).

Perturbation Mach Number

At high subsonic Mach numbers, shock waves are produced locally as the airflow becomes supersonic over certain portions of the airplane. These shock waves extend beneath the airplane but normally die out rather quickly with altitude. Thus, a Mach number gradient is produced locally around the airplane and can be estimated from the maximum strength of the local shock wave overpressure, ΔP_{max}. For a plane-wave system the overpressure is given (ref. 6) as:

$$\Delta P_{max} = \rho a q_{max} \quad (6)$$

where ρ = density, a = sound speed, and $(q_{max})\vec{n}$ is the maximum perturbation velocity normal to the wave front. The Mach number change, ΔM_q, associated with this perturbation velocity is

$$\Delta M_q = q_{max}/a = \frac{\Delta P_{max}}{\rho a^2} \quad (7)$$

Using the equation of state and $a = (\gamma RT)^{1/2}$ this becomes

$$\Delta M_q = \frac{1}{\gamma}\,\frac{\Delta P_{max}}{P} \quad (8)$$

which is the desired relationship. Values of ΔM_q are given in a later figure, calculated for a Mach 1.05 flight. The variation of ΔM_q with airplane Mach number was not accounted for.

Local Shock Mach Number and Subsonic Sonic Boom

In determining the effect of temperature and wind gradients and the airplane-induced Mach number gradient it is convenient to think in terms of a local shock Mach number, M_S. This is defined as

$$M_S = M_o + \Delta M_{TW} + \Delta M_q \quad (9)$$

In the case when M_S increases from the airplane toward the ground it is expected that the shocks produced during high subsonic flight may penetrate further below the airplane or even extend to the ground, since cutoff due to atmospheric refraction cannot occur. Figure 2 shows the effect of the wind gradients (a tailwind decreasing toward the ground or a headwind increasing toward the ground) that may cause attached shock waves from subsonic aircraft to extend to the ground. The local shock Mach number, M_S, is also indicated schematically for these wind gradients. Some time ago, in an effort to explain "accidental" booms produced by apparently subsonic airplanes, Barger (ref. 4) proposed that this meteorological condition may actually *produce* sonic booms during flight near the speed of sound. A much more likely mechanism is the propagation of *existing* shock waves (due to local supersonic flow over portions of near-sonic airplanes) to lower altitudes by these meteorological conditions. Appendix A contains a more detailed discussion of the generation of sonic boom by subsonic airplanes.

Shock Wave Profiles

The sonic boom measurements on the tower provided the capability to calculate the shock wave shapes and locations at a reference time in the vertical plane. This required a conversion from time to distance, since the shock wave front swept past the fixed tower at a given velocity, $V_{p_{mic}}$. The shift in distance from the tower, ΔX, corresponding to differences in shock arrival time, t_o, from a reference time, t_{ref}, is:

$$\Delta X = (t_{ref} - t_o)\ V_{p_{mic}} \tag{10}$$

The reference time, t_{ref}, was taken as the arrival time at tower microphone T-1.

The shock wave propagation velocity, $V_{p_{mic}}$, can be calculated from the shock wave arrival times on the ground microphone array from the following equation:

$$V_{p_{mic}} = \frac{\Delta X}{t_o\,(G\text{-}14) - t_o\,(G\text{-}1)} \tag{11}$$

where:

ΔX = 975.4 m (3200 ft)

$t_o(\ )$ = shock wave arrival time at microphone ( ).

An associated calculation is the conversion of the observed pressure signatures (overpressure versus time) from the time scale to a distance scale (overpressure versus distance). By making this conversion, shock wave profiles and observed pressure signatures could be placed on the same graph using a common distance scale.

METEOROLOGICAL CONDITIONS

During the transonic flights the meteorological conditions were very important for understanding the boom exposures on the BREN tower. During the early morning hours the winds observed on the BREN tower were light and variable, with speeds generally less than 2 m/sec (6.6 ft/sec). At the airplane altitude a 4 m/sec (13 ft/sec) tailwind prevailed. Since the temperature gradient between the airplane and the tower top was small, the wind gradient was the predominant meteorological factor. The tailwind decreasing toward the ground is favorable for sonic boom propagation to the ground and existed during passes 067 through 073.

At about 1000 PDT a transition took place in the meteorological conditions that made sonic boom propagation to the ground unfavorable. Changes occurred in both the temperature and wind conditions. Since clear skies prevailed the temperature near the ground increased with time, which made the temperature lapse rate of greater magnitude (and less favorable for sonic boom propagation). Associated with the steepening temperature lapse rate in the kilometer nearest the ground was the breakdown of the nocturnal wind flow and the establishment of a southerly to southwesterly wind regime that prevailed through the remainder of the day. During passes 074, 075, and 076 the wind speeds on the tower were about 4 m/sec (13 ft/sec), and during passes 077 through 080 the wind speeds had increased further to over 6 m/sec (20 ft/sec). Thus, very little, if any, wind gradient existed between the airplane and the tower top. This condition, combined with the relatively steep temperature lapse rate, will produce early cutoff of attached shock waves on near-sonic aircraft.

ANALYSIS OF THE MACH 1.05 FLIGHT

The one low-altitude flight made at Mach 1.05 produced an interesting set of data, which is summarized in this section and compared with theoretical calculations. Since the airplane altitude was 853 m (2800 ft) above the ground or 396 m (1300 ft) above the top of the BREN tower, the observed pressure signatures are near-field signatures that have not yet reached their asymptotic far-field shape. For this reason they are of value and interest.

Figure 3 shows the shock wave profile and tower pressure signatures to the same distance scale for this flight. The observed shock wave front was determined by analysis of the shock wave arrival times at the tower. A theoretical shock front shape is also given for the airplane ground speed as calculated from the shock arrival times along the ground microphone array.

Figure 4 gives a detailed comparison of the observed and calculated pressure signatures. In general, there is good agreement between theory and experiment for both overpressure and signature length. The reflected theoretical signatures were calculated using a "mirror-image" atmosphere below ground level.

The signatures in figures 3 and 4 illustrate the "aging" process rather well. The merging of the two intermediate shocks, the signature lengthening, and the rapid overpressure decay with distance from the airplane are all aging processes. Such good agreement between theory and experiment would not normally be expected so close to the airplane. The good agreement over this altitude range in the near field is probably due to the slenderness of the F-104 airplane. Figure 5 gives a more detailed comparison of the observed and theoretical maximum bow overpressure. In several cases "spikes" were observed due to small-scale atmospheric turbulence; for these cases a more representative maximum overpressure is also given. For convenience, the ground-reflected values are given below ground level. The parameter ΔM_q as calculated from the theoretical ΔP_{max} values is also shown in figure 5. This was used in the analysis of the remaining transonic data.

The pressure signatures measured on the ground are presented in figure 6. These are similar in shape to those measured near the tower base, except that the overpressures are stronger by a factor of about 1.85 due to ground reflection.

ANALYSIS OF THE TWO MACH 1.00 FLIGHTS

As shown in table 1, passes 076 and 080 were at Mach 1.00. In spite of the fact that the flight conditions were almost identical for these two flights, pass 080 produced no sonic boom on the BREN tower, while the other flight produced well-defined incident and reflected shock waves. This apparent discrepancy can be explained by the difference in the meteorological conditions for these two flights. Figure 7 shows the local shock Mach number profiles for these two cases and the observed maximum overpressure of the incident bow shock. During pass 076 the meteorological conditions were such that the local shock Mach number, M_S, was above 1.0 except near the tower base. Lower M_S values prevailed during pass 080 due to the slightly different meteorological conditions, which apparently caused cutoff of the shock wave above the tower. It may also be significant that pass 076 was at a 90 m (300 ft) lower altitude than pass 080. This is reflected in higher ΔM_q values for pass 076.

The measured pressure signatures and shock wave profile for pass 076 are given in figure 8. The pressure signatures and shock front are to the same distance scale; a corresponding time scale is also given with the intensity scale for the pressure signatures. The pressure signatures show considerable variability due to the effects of small-scale atmospheric turbulence. Airplane accelerations are also evident since the incident shock front has an opposite curvature from what the prevailing wind and temperature effects alone would produce. Over the depth of the tower, M_S decreases, which corresponds to a condition where the shock wave should be more vertical at the tower base than at the tower top—the opposite is true, however.

The measured pressure signatures on the ground for pass 076 are displayed in figure 9. The significant feature of these signatures is the relatively long duration (in excess of 0.1 sec) compared to those measured during pass 070 (0.07 to 0.08 sec). Another significant feature is the relatively ill-defined tail shock.

ANALYSIS OF THE SUBSONIC FLIGHTS

In addition to the two flights at Mach 1.00 discussed in the previous section, there were five flights at subsonic Mach numbers that are of particular interest. For similar flight conditions quite different sonic boom characteristics were observed on the BREN tower, depending on the prevailing meteorological conditions. The two flights at Mach 0.99 will be discussed first, followed by the three Mach 0.98 flights.

The shock Mach number profile is shown in figure 10 for passes 074 and 079. Both of these passes were made by test airplane number 1 at a pilot-read Mach number of 0.99 and at essentially the same altitude. Pass 074 produced an interesting, fairly intense pressure signature at the tower top, shown in figure 11 with the shock front profile. On the other hand, no significant disturbances were produced during pass 079. The shock Mach number profiles in figure 10 indicate that meteorological conditions were more favorable for shock wave propagation during pass 074, which produced shocks at the tower top but low-intensity acoustic-like disturbances at the ground. Observers at the ground rated the disturbance as a "boom," however.

Three flights were made at Mach 0.98. Passes 071 and 073 were made by test airplane number 1 at airplane altitudes above the ground of 817 m (2680 ft) and 762 m (2500 ft), respectively. Pass 075 was made by airplane number 2 at an altitude of 884 m (2900 ft). Despite these similar flight conditions, quite different boom characteristics were produced on the BREN tower. The shock Mach number profiles and observed maximum overpressures are given in figure 12. The most favorable conditions for shock wave propagation existed during pass 071 ($M_S > M_O$) and a strong shock wave occurred at the tower top, while least favorable conditions existed during

pass 075 ($M_S < M_o$), and a very low-intensity pressure wave occurred. The observed sonic boom on the tower again appears to be determined by the meteorological conditions.

The observed pressure signatures and shock wave profiles are given in figures 13 and 14 for passes 071 and 073, respectively. The pressure signature at microphone T-15 in figure 13 is very similar to signatures produced during supersonic flight. This suggests that shock waves are produced near the airplane nose (canopy) and tail during slightly subsonic flight (or the airplane could have been slightly supersonic during part of its flight). Shock waves are still present at microphone T-11, but below that altitude the signature deteriorates rapidly to a rounded, low-intensity, acoustic-like disturbance. The pressure signatures in figure 14 for pass 073 are fairly low in intensity (about 50 N/m^2 (1.0 lb/ft^2)) and exhibit the characteristics of acoustic noise. The lower extremity of the shock wave in this case appears to have been above the tower top, but conditions may have been more favorable for the propagation of the acoustic disturbances.

The shock wave profiles in figures 11, 13, and 14 are somewhat surprising in that the lower extremities of the shock waves do not seem to be associated with the cutoff phenomena. During cutoff the shock wave becomes vertical ($\theta = 0$) at some altitude. Several hundred feet below cutoff the signals become acoustic in nature and can propagate for some distance (ref. 2). For these cases, however, the shock wave at its lower extremity has an appreciable angle to the vertical ($\theta > 0$) and cutoff has not been reached. Thus, it would appear that the shock wave deterioration is associated with the local Mach number gradient produced by the local supersonic flow over the near-sonic airplane. Meteorological conditions can extend the lower extremity of the shock waves, but for these cases the lower extremity occurs before cutoff.

Six additional subsonic passes were made at Mach numbers ranging from 0.95 to 0.97. These passes produced engine noise only, or very slight rumbles associated with low-intensity, acoustic-like disturbances. The supersonic flow and attached shock waves were probably not strong enough to persist for any appreciable distance below the airplane at these lower Mach numbers.

The major conclusion of this section is that the meteorological conditions determine the vertical extent of attached shock waves during near-sonic flight. This conclusion is supported by the data given in figures 15 and 16. Figure 15 shows the observed boom characteristics at the tower top as a function of the airplane Mach number M_o and the local shock Mach number, M_S, at the tower top. In all cases when $M_S < M_o$ (an unfavorable meteorological condition for shock wave propagation) no disturbances were observed. On the other hand, for $M_S > M_o$, strong shock waves were observed when $M_o > 0.985$, acoustic-like disturbances occurred for $0.975 < M_o < 0.985$, and no disturbances were observed for $M_o < 0.975$.

Figure 16 indicates the effect of meteorological conditions (ΔM_{TW}) on the vertical extent of the shock waves for several airplane Mach numbers. The altitude of the shock wave lower extremity was estimated from the M_S profile for four of the six cases since it occurred above the BREN tower. For this reason these data should be considered to be schematic, but they illustrate the effect rather well. An "equivalent wind speed change" is given for ΔM_{TW} to indicate the actual wind increment required between the airplane and the tower top. This was calculated by assuming that all of the ΔM_{TW} was due to a wind gradient alone. For no gradient ($\Delta M_{TW} = 0$) the shock wave extremities are 185 m (600 ft) and 400 m (1300 ft) for Mach 0.98 and 0.99, respectively. At Mach 0.98 the shock wave extremity varied from about 170 m (560 ft) to 480 m (1600 ft) due to the different meteorological conditions, and thus both airplane Mach number and meteorological conditions are important influences on the altitude extension of the attached shock waves. It is not clear, however, how much farther the shock waves would have propagated under more favorable meteorological conditions.

ANALYSIS OF SAFETY FACTOR DURING THRESHOLD MACH NUMBER FLIGHT

This section contains the results of a detailed study of 29 threshold Mach number flights for which rumbles or low booms were observed. For these flights, cutoff occurred above the BREN tower. The results presented in this section include the determination of the validity of a theoretical safe altitude for sonic boom cutoff to avoid objectionable noise at the ground, and a discussion of the nature of the acoustic disturbances measured below the cutoff altitude.

BACKGROUND

The attractiveness of commercial operation at speeds slightly below the threshold Mach number is primarily due to the avoidance of sonic boom noise at the ground. Such flights produce a caustic at some altitude above the ground, however, and significant acoustic noise perceived as heavy rumbles or low booms can propagate to the ground. Thus, if objectionable noise is to be avoided with a high degree of assurance, some method is needed to determine the allowable "safe" airplane ground speed in terms of the known prevailing meteorological conditions. A theoretical "safe altitude" for sonic boom cutoff has been derived for this purpose. The 1970 BREN tower tests provide an excellent set of data for verifying this theoretical safe cutoff altitude under a variety of meteorological conditions.

Preliminary results of the analysis of the safety factor during threshold Mach number flight for these data was given in reference 3. That analysis showed that low rumbles were produced on the ground when the airplane ground speed was at least 6 m/sec (19.7 ft/sec) lower than the maximum shock propagation speed. In addition, it was shown that the theoretical safe altitude for sonic boom cutoff agreed fairly well with the observations, although the safe altitude was underestimated somewhat.

In the present analysis several changes were made in the method used in reference 3 for determining the safe cutoff altitude. These are detailed in the following paragraphs, along with the definition of the theoretical safe altitude.

ANALYSIS OF SAFE CUTOFF ALTITUDE AND SPEED SAFETY FACTOR

Theory

Since amplified shock waves occur at the cutoff altitude, cutoff must occur at some distance above the ground to avoid objectionable disturbances at the ground. The safe cutoff altitude has been defined to be the lowest altitude reached by the shock wave; a buffer zone between there and the ground is required to attenuate the acoustic signal propagating from the shock to a relatively small intensity. The depth of this buffer zone below the cutoff altitude is given as

$$\Delta Z_s = (R)^{1/3} (L)^{2/3} \tag{12}$$

where L is the signal length and R depends on the meteorological conditions.

$$R = \frac{-a}{\partial(a - u_n)/\partial z} = \frac{-a}{\partial V_p/\partial z} \tag{13}$$

where

a = sound speed

u_n = wind speed along flight path for ray directly beneath airplane (tailwind negative) = $u \cos(\psi - \eta)$

u = horizontal wind speed

$(a - u_n) = V_p$ = shock propagation speed

The parameter R is the relative curvature of the caustic relative to the ray and is inversely proportional to the lapse rate of the shock propagation speed.

Since cutoff at the safe altitude is produced by a reduction in the airplane ground speed, it is convenient to convert the buffer zone depth into an increment of propagation speed (airplane ground speed) to obtain

$$\Delta V_s = (a)^{1/3} \left\{ L (\partial V_p/\partial z) \right\}^{2/3} \tag{14}$$

Thus, the theoretical requirement for acceptable sonic boom noise at the ground can be expressed as

$$V_{G_{safe}} = \left(V_{p_{max}} - \Delta V_s\right) \tag{15}$$

where $V_{p_{max}}$ is the maximum shock propagation speed $(a - u_n)$ between the airplane and the ground. Normally, this maximum occurs at or near the ground, but occasionally it occurs well above the ground (an inversion). In the latter case the "buffer zone" and safe altitude must be calculated with respect to the altitude where the maximum V_p occurs. This is illustrated in figure 17. In the case when an inversion exists, use of the propagation speed at the ground, V_{p_G}, is conservative (that is, a higher ground speed could be flown) but has several operational advantages. These include:

- It is easy to monitor and to measure.
- The resulting block time reduction is insignificant.
- It can be obtained with currently available meteorological data-gathering methods.

Figure 17 also illustrates the relationship between ΔZ_s and ΔV_s. The safe cutoff altitude is expressed as

$$Z_s = Z(V_{p_{max}}) + \Delta Z_s \tag{16}$$

Theoretical buffer zone depths and corresponding ground speed decrements are given in figure 18 for various values of lapse rate, $-\partial V_p/\partial Z$. These data are given for several signal lengths, including 91.4 m (300 ft), 61 m (200 ft), 30.5 m (100 ft), and 47.85 m (157 ft). The signal length of 47.85 m (157 ft) is typical of pressure signatures measured on the BREN tower near caustics produced by threshold Mach number flight. As noted in reference 3 a characteristic feature of pressure signatures near caustics is a significant lengthening (as well as amplification). Since the caustic pressure signature is the one that determines the acoustic field below cutoff, its characteristic length should be used. In previous work (ref. 3) a length of 39.6 m (130 ft) was used and is more representative of measured signatures at the ground away from caustics for an airplane Mach number of about 1.2.

It should be noted that the buffer zone depth, ΔZ_s, is inversely related to the lapse rate while the speed safety factor is directly related to the lapse rate. As the lapse rate approaches zero, the safety factor approaches zero, and the safe altitude approaches infinity.

The theory is valid over a wide range of meteorological conditions, but fails for several special conditions. For the theory to be valid the ratio L/R must be small. For small R (of the order of several thousand meters) the theory fails since L/R is "large" and ΔZ_s will be underestimated. Small R corresponds meteorologically to a very large value of $-\partial V_p/\partial z$ (of the order 0.05) and is not possible in the real atmosphere. This corresponds to a very large ΔV_s and a small ΔZ_s (see fig. 18). Another requirement is that R must be positive ($\partial V_p/\partial z$ negative). Under normal conditions this requirement is met. In the case when a temperature inversion exists, however, or a tailwind increases in strength above the ground, R may be negative. Under these conditions cutoff must occur above the inversion. For this reason the safe altitude must be calculated with respect to the altitude where the maximum V_p occurs. A third requirement is that $\partial V_p/\partial z$ and R should be approximately constant with altitude. In some cases this requirement is not strictly met. In calculating the theoretical safe altitude, however, an average or "effective" R was calculated by an iteration technique. The observed meteorological conditions were used in calculating R, ΔZ_s, and ΔV_s. The results of the ΔZ_s and ΔV_s theoretical calculations are given in table 2. A wide range of meteorological conditions occurred during these flights, with average $\partial V_p/\partial z$ values in the lower atmosphere ranging from -0.001 to -0.017. The eight flights on October 23 and 30 were not considered in this analysis since a significant inversion existed, and the upper-level meteorological conditions were not known accurately enough.

Comparison of Theory With Experiment

Table 2 contains a summary of the important calculated and observed parameters. The theoretical safe altitude increment for "no boom," ΔZ_s, is given, along with ΔV_s, the corresponding airplane ground speed decrement with respect to the maximum propagation speed, $V_{p_{max}}^*$. The safe altitude is calculated with respect to the altitude where the maximum shock propagation speed occurs. The approximate actual sonic boom cutoff altitude, Z_c, and the airplane ground speed decrement, $\Delta V_o = (V_{p_{max}}^* - V_G)$, were calculated from the observed airplane ground speed. Two nondimensionalized parameters are also given in table 2. They are the observed fractions of the safe altitude and ground speed decrement, $(Z_c - Z_s)/\Delta Z_s$ and $(\Delta V_o - \Delta V_s)/\Delta V_s$. The quantity $(\Delta V_o - \Delta V_s)$ is simply V_G("safe") - V_G. Other information in table 2 includes the average $V_p/\partial z$ within Z_s below the cutoff altitude, the observed sonic boom characteristics, and average maximum sonic boom intensities on the tower and on the ground.

Figure 19 shows the variation of the average tower maximum overpressure with the parameter $(Z_c - Z_s)/\Delta Z_s$. The safe altitude as defined earlier does appear to be a useful criterion since a transition occurs from low rumbles to moderate rumbles and low booms for cutoff near the safe altitude ($Z_c = Z_s$). In addition, the overpressures increase rather sharply closer to the caustic. These data also indicate that low-intensity disturbances (less than 5 N/m^2 (0.10 lb/ft^2)) can propagate to the ground even though cutoff occurs well above the "safe" cutoff altitude. For cutoff near the safe

TABLE 2.–SUMMARY OF RUMBLE AND LOW BOOM CASES, THRESHOLD MACH NUMBER FLIGHT, NONINVERSION CASES

A. METRIC UNITS

Date	Bongo-Pass	Pass	$Vp^{\cdot}_{max}$	Altitude of Vp_{max}	Average R	Safe altitude increment, ΔZ_s	Speed safety factor, ΔV_s	Airplane ground speed, V_G	ΔV_o	Z_c[a]	(Z_c-Z_s)	$\frac{(Z_c-Z_s)}{\Delta}$	$\frac{(\Delta V_o-\Delta V_s)}{\Delta}$	Average $\partial v_p/\partial z$ cutoff	$\overline{\Delta P_G}_{max}$	$\overline{\Delta P_T}_{max}$	Category[b]
			m/sec	m MSL	m	m	m/sec	m/sec	m/sec	m MSL	m			sec^{-1}	N/m^2	N/m^2	
8-24	1-1	001	348.3	1138	54 990	501	3.18	341.4	6.94	3931	2292	4.56	1.18	-0.0031	0.0	0.0	R1
	1-3	003	350.9	1138	67 820	538	2.77	345.0	5.91	3109	1433	2.66	1.13	-0.0029	2.82	3.21	R2
	2-2	005	350.7	1113	32 890	423	4.49	342.9	7.83	3689	2153	5.10	0.74	-0.0044	3.26	2.50	R2
	3-1	007	352.6	1245	54 620	500	3.20	348.4	4.18	2164	419	0.82	0.31	-0.0022	3.40	2.40	R2
	3-2	008	353.0	1245	40 810	454	3.89	347.5	5.52	2469	770	1.70	0.42	-0.0021	2.98	2.98	R2
	3-3	009	352.3	1288	41 270	455	3.86	348.7	3.66	1645	-98	-0.21	-0.05	-0.0103	6.03	6.96	R3
8-25	1-1	014	355.7	1331	18 610	349	6.52	349.3	6.43	1646	-34	-0.10	-0.01	-0.0180	9.67	8.93	R3
	2-3	019	353.4	1128	65 860	532	2.82	346.3	7.13	2408	748	1.41	1.53	-0.0051	7.13	2.75	R2
	3-2	022	354.7	1113	48 050	479	3.49	348.4	6.28	2012	420	0.88	0.80	-0.0064	5.22	3.19	R2
	3-3	023	356.2	1128	26 780	395	5.12	351.1	5.09	1525	2	0.00	-0.01	-0.0130	10.61	11.85	R4
	4-1	025	356.8	1138	75 120	556	2.58	349.6	7.19	2118	424	0.76	1.79	-0.0107	9.58	7.76	R2
	4-3	027	355.8	1113	32 980	423	4.49	355.1	0.67	1128	-408	-0.97	-0.85	---	16.61	13.83	R3
8-31	1-3	053	352.2	1113	103 160	618	2.09	349.0	3.17	2058	327	0.53	-0.08	-0.0031	6.94	4.67	R2
	2-1	055	352.6	1113	75 320	557	2.58	349.9	2.71	1693	23	0.04	0.05	-0.0046	10.66	5.10	R4
	2-2	056	352.7	1160	64 070	527	2.87	349.9	2.74	1646	-41	-0.08	-0.05	-0.0057	18.75	8.91	R4
	3-1	059	353.5	1160	80 320	569	2.47	352.4	1.13	1204	-525	-0.92	-0.54	---	7.42	10.84	R4
	4-2	064	357.0	1160	48 070	479	3.48	353.9	2.99	1524	-115	-0.24	-0.14	-0.0080	14.48	16.61	R4
10-27	2-1	089	329.7	1128	24 420	383	5.27	352.2	4.45	1416	-95	-0.25	-0.16	-0.0105	8.38	15.38	R3
	2-2	090	329.8	1113	31 840	418	4.43	321.6	8.23	1830	299	0.71	0.85	-0.0128	13.55	9.60	R2
	2-3	091	330.2	1202	30 940	414	4.49	328.0	2.16	1341	-275	-0.67	-0.52	-0.0114	18.98	15.57	R4
10-28	1-2	096	332.5	1113	75 870	568	2.48	327.4	5.12	3323	1652	2.96	1.06	-0.0043	7.80	3.0	R2
	1-3	097	333.1	1113	105 720	623	1.99	331.0	2.07	1768	32	0.05	0.04	-0.0037	10.68	14.34	R3
	2-1	098	334.2	1113	32 290	420	4.39	327.7	6.58	3231	1699	4.05	0.50	-0.0043	8.57	4.0	R2
	2-2	099	334.2	1128	36 520	437	4.04	327.7	6.74	3231	1666	3.81	0.67	-0.0043	0.0	0.0	R1
	2-3	100	336.3	1113	52 770	494	3.17	327.7	8.60	3231	1624	3.28	1.71	-0.0043	0.0	0.0	R1
10-29	1-4	107	337.6	1113	306 070	889	0.99	336.8	0.79	1708	-294	-0.33	-0.20	-0.0013	13.33	8.77	R4
	2-4	111	346.9	1113	19 550	355	6.23	339.9	7.04	1555	87	0.24	0.13	-0.0158	10.49	9.18	R2
	2-5	112	344.3	1245	35 360	433	4.18	340.8	3.51	1524	-154	-0.36	-0.16	-0.0120	7.52	14.08	R4
	3-3	115	347.2	1288	18 410	347	6.49	339.2	7.92	1678	43	0.12	0.22	-0.0200	6.66	7.74	R2

[a] Altitude of ground is 1112.5 m (3650 ft) MSL

[b] Categories: R1 = no rumble; R2 = low rumble; R3 = moderate to heavy rumble; R4 = light boom

TABLE 2.–SUMMARY OF RUMBLE AND LOW BOOM CASES, THRESHOLD MACH NUMBER FLIGHT, NONINVERSION CASES

B. ENGLISH UNITS

Date	Bongo-pass	Pass	$V_{p_{max}}$	Altitude of $V_{p_{max}}$	Average R	Safe altitude increment, ΔZ_s	Speed safety factor, ΔV_s	Airplane ground speed, V_G	ΔV_o	Z_c[a]	$(Z_c - Z_s)$	$\frac{(Z_c - Z_s)}{\Delta Z_s}$	$\frac{\Delta V_o - \Delta V_s}{\Delta V_s}$	Average $\partial V_p / \partial Z$ cutoff	$\overline{\Delta P_G}_{max}$	$\overline{\Delta P_T}_{max}$	Category[b]
			ft/sec	ft MSL	ft	ft	sec	ft/sec	ft/sec	ft MSL	ft			sec^{-1}	lb/ft^2	lb/ft^2	
8-24	1-1	001	1142.7	3735	180 400	1644	10.44	1120	22.7	12 900	7520	4.56	1.18	-0.0031	~0.0	~0.0	R1
	1-3	003	1151.4	3735	222 500	1764	9.08	1132	19.4	10 200	4700	2.66	1.13	-0.0029	0.059	0.067	R2
	2-2	005	1150.7	3650	107 900	1386	14.72	1125	25.7	12 100	7065	5.10	0.74	-0.0044	0.068	0.052	R2
	3-1	007	1156.7	4085	179 200	1641	10.50	1143	13.7	7 100	1375	0.82	0.31	-0.0022	0.071	0.050	R2
	3-2	008	1158.2	4085	133 900	1489	12.75	1140	18.2	8 100	2525	1.70	0.42	-0.0021	0.062	0.062	R2
	3-3	009	1156.0	4225	136 400	1494	12.65	1144	12.0	5 400	-320	-0.21	-0.05	-0.0103	0.126	0.145	R3
8-25	1-1	014	1167.1	4365	61 060	1146	21.38	1146	21.1	5 400	-110	-0.10	-0.01	-0.0180	0.202	0.186	R3
	2-3	019	1159.5	3700	216 100	1746	9.24	1136	23.4	7 900	2455	1.41	1.53	-0.0051	0.149	0.057	R2
	3-2	022	1163.6	3650	157 600	1572	11.44	1143	20.6	6 600	1380	0.88	0.80	-0.0064	0.109	0.066	R2
	3-3	023	1168.7	3700	87 850	1295	16.80	1152	16.7	5 000	5	0.0	-0.01	-0.0130	0.225	0.247	R4
	4-1	025	1170.6	3735	246 450	1825	8.48	1147	23.6	6 950	1390	0.76	1.79	-0.0107	0.200	0.162	R2
	4-3	027	1167.2	3650	108 200	1387	14.72	1165	2.2	3 700	-1340	-0.97	-0.85	--	0.347	0.289	R3
8-31	1-3	053	1155.4	3650	338 450	2028	6.86	1145	10.4	6 750	1072	0.53	0.52	-0.0031	0.147	0.097	R2
	2-1	055	1156.9	3650	247 100	1826	8.46	1148	8.9	5 550	75	0.04	0.05	-0.0045	0.226	0.107	R4
	2-2	056	1157.0	3805	210 200	1730	9.40	1148	9.0	5 400	-135	-0.08	-0.05	-0.0057	0.398	0.186	R4
	3-1	059	1159.7	3805	263 500	1866	8.10	1156	3.7	3 950	-1721	-0.92	-0.54	--	0.158	0.226	R4
	4-2	064	1171.2	3805	157 700	1572	11.41	1161	10.2	5 000	-377	-0.24	-0.14	-0.0080	0.308	0.347	R4
10-27	2-1	089	1081.6	3700	80 000	1255	17.28	1067	14.6	4 650	-305	-0.25	-0.16	-0.0105	0.175	0.321	R3
	2-2	090	1082.0	3650	104 450	1371	14.52	1055	27.0	6 000	980	0.71	0.85	-0.0128	0.283	0.200	R2
	2-3	091	1083.2	3945	101 500	1357	14.75	1076	7.2	4 400	-900	-0.67	-0.52	-0.0144	0.403	0.325	R4
10-28	1-2	096	1090.8	3650	248 900	1831	8.13	1074	16.8	10 900	5420	2.96	1.06	-0.0043	0.163	0.08	R2
	1-3	097	1092.8	3650	346 850	2045	6.52	1086	6.8	5 800	105	0.05	0.04	-0.0037	0.223	0.299	R3
	2-1	098	1096.6	3650	105 950	1377	14.40	1075	21.6	10 600	5575	4.05	0.50	-0.0043	0.179	0.13	R2
	2-2	099	1097.1	3700	119 800	1435	13.26	1075	22.1	10 600	5465	3.81	0.67	-0.0043	0.0	0.0	R1
	2-3	100	1093.9	3650	173 150	1622	10.40	1075	18.9	10 600	5330	3.28	0.82	-0.0043	0.0	0.0	R1
10-29	1-4	107	1107.6	3650	1 004 150	2917	3.24	1105	2.6	5 600	-970	-0.33	-0.20	-0.0013	0.283	0.183	R4
	2-4	111	1138.1	3650	64 150	1165	20.43	1115	23.1	5 100	285	0.24	0.13	-0.0158	0.219	0.192	R2
	2-5	112	1129.5	4085	116 000	1420	13.70	1118	11.5	5 000	-505	-0.36	-0.16	-0.0120	0.160	0.294	R4
	3-3	115	1139.0	4225	60 400	1140	21.30	1113	26.0	5 500	135	0.12	0.22	-0.0200	0.139	0.162	R2

[a]Altitude of ground is 1112.5m (3650 ft) MSL

[b]Categories: R1 = no rumble; R2 = low rumble;
R3 = moderate to heavy rumble; R4 = light boom

altitude (airplane ground speed near "safe" ground speed) overpressure intensities less than 10 N/m^2 (0.21 lb/ft^2) were observed. Table 3 summarizes these conclusions, and compares the average maximum overpressures with steady, level flight and those observed at the caustic.

TABLE 3.–SUMMARY OF OBSERVED FREE-AIR SONIC BOOM INTENSITIES FOR CUTOFF ABOVE THE GROUND

Cutoff location	$\frac{(Z_c - Z_s)}{\Delta Z_s}$	Range of average ΔP_{max} on tower		Boom character
		N/m^2	lb/ft^2	
Cutoff well above safe altitude	>1.0	0 to 4	0.0 to 0.08	No rumble to low rumble
Cutoff between one and two ΔZ_s above ground	0.0 to 1.0	2 to 10	0.04 to 0.21	Low rumble
Cutoff below safe altitude but above ground	-0.8 to 0.0	5 to 17	0.10 to 0.35	Moderate rumble to low boom
Caustic on tower	---	25 to 51	0.52 to 1.06	Boom
Steady, level flight at about Mach 1.2; no cutoff	---	~28.7	~0.60	Boom

In earlier work (ref. 3) it was determined that the maximum overpressure observed at cutoff during threshold Mach number flight was 50.8 N/m^2 (1.06 lb/ft^2) during the BREN tower tests. Higher intensities were observed but were associated with slight accelerations (and in one case atmospheric turbulence). During steady, level flight well above the threshold Mach number, the nominal maximum intensity is about 28.7 N/m^2 (0.60 lb/ft^2).

The effect of propagation lapse rate is given in figure 20. These data do not indicate a clear-cut effect except at the small values of $-\partial V_p/\partial z$. Thus, the theory appears to be valid for a relatively large range of propagation speed lapse rate. A more accurate analysis of this effect is not possible due to the inaccuracies in the observed airplane ground speed and the meteorological data. The data in figures 19 and 20, however, indicate that the concept of a safe cutoff altitude based on the prevailing meteorological conditions and signature length does have merit.

PRESSURE SIGNATURE CHARACTERISTICS BELOW CUTOFF

The psychoacoustic response to sonic boom disturbances in the free field is determined primarily by the detailed pressure wave observed. Below cutoff the pressure waves are considerably different from those observed at or above the cutoff altitude; pressure waves below cutoff are

generally rounded and frequently without true shocks, are of relatively low magnitude, and are perceived as rumbles similar to distant thunder. In this section maximum overpressures and detailed pressure signatures for several flights are presented and discussed, and recent theoretical results are compared with these observations.

Maximum Overpressure

One of the most convenient and significant pressure signature characteristics is the maximum overpressure. For several flights, caustics were observed near the top of the BREN tower and measurements were obtained just below the caustic. These observations of maximum overpressure are given in figure 21. Similar data are given in figure 22 for flights on August 24, when measurements were obtained over a large range of $y/\Delta Z_S$. The maximum overpressure predicted by linear acoustic theory (see appendix B) is also given for comparison. The theoretical values agree well just below the caustic but predict significantly lower values than those observed far from the caustic. Figure 23 gives the range of overpressures observed for all cases. It appears that low-intensity acoustic waves can propagate considerable distances in certain cases even when cutoff has occurred several kilometers above the ground.

Detailed Pressure Signatures

For six flights, caustics due to shock wave cutoff were produced on the tower. The pressure signatures observed near the caustic altitude are given in figure 24. A theoretical N-wave pressure signature (see appendix B) was also calculated at a distance of about 15 m (50 ft) below the caustic. This theoretical signature is an excellent representation of signatures observed near the caustic. A theoretical sonic boom pressure signature that applies above the caustic is also given in figure 24. The caustic observed during pass 063 appears to have been affected by atmospheric turbulence.

Theoretical and observed pressure signatures are compared below the caustic for two cases in figure 25. The theoretical signatures have been matched with the appropriate observed signature at the approximate distance from the caustic. As noted in the previous section, the predicted maximum overpressure damps very quickly with increasing distance from the caustic compared to the observed data.

Measured pressure signatures below cutoff observed on the BREN tower are given in figures 26 through 30. Figure 26 gives signatures measured during pass 111. The signatures have a shape similar to that of a caustic but with low intensity; the pressure peaks are rounded and no shocks are evident. The onset of the pressure rise occurs almost simultaneously over the depth of the tower and there is very little ground reflection. Figure 27 shows signatures for a similar case, except that an inversion existed in the shock propagation speed profile so that the acoustic wave was oriented like a shock wave, occurring at the tower top first.

The pressure signatures observed during pass 090 are given in figure 28. Several incident pressure waves, and also reflected waves, can be seen. The incident wave occurred first at the tower base. Pressure signatures in figures 29 and 30 for passes 097 and 122, respectively, are similar except that an inversion existed. Since the angle of incidence of the acoustic wave was relatively large for these two cases, the reflected waves are more evident. During pass 097, figure 29, it appears that the airplane ground speed was higher uptrack of the tower, which produced the caustic closer to the ground there. After ground reflection these more caustic-like signatures then intercepted the tower. In figure 30 three incident and reflected pressure waves are evident, produced by variations in the airplane ground speed. These last two cases indicate the complexity of the shock pattern produced during flight near the threshold Mach number when the airplane ground speed varies slightly. Similar maneuver effects are presented in more detail in a later section for cases when shock waves occurred on the ground.

OPERATIONAL ASPECTS OF THRESHOLD MACH NUMBER FLIGHT

The 1970 BREN tower tests have demonstrated the ability to predict with reasonable accuracy the airplane speed required for shock wave cutoff near the ground during threshold Mach number flight, have helped to define more exactly the behavior of shock waves near cutoff, and have helped identify the nature of the associated sonic boom noise. Sustained flight near the threshold Mach number is a much more complex problem, however, since the airplane speed must be specified accurately in terms of the refractive properties of the atmosphere at each point along the flight path to avoid objectionable noise at the ground. Methods for assuring "boom-safe" operation are discussed in this section. These include (1) using airplane ground speed and the shock propagation speed instead of airplane Mach number and threshold Mach number to specify the allowable airplane speed, (2) using ground meteorological data only, (3) accounting for the shock propagation distance, and (4) the effects of meteorological variations. In addition, a few comments are given with respect to airplane systems and a "total" speed safety factor. Finally, methods are summarized for calculating the speed safety factor for adequate sonic boom attenuation based on the results of the data analysis of earlier sections.

Speed Specification

In specifying the airplane speed for shock wave cutoff, two approaches can be taken. One is to use the airplane Mach number, and the other is to use the airplane ground speed. The threshold Mach number, M_T, has been defined to be the maximum airplane Mach number for which complete shock wave refraction can occur at or above the ground. For cutoff directly beneath the airplane the equation defining the threshold Mach number is, in the notation of refs. 3 and 6:

$$M_T = \frac{1}{a_o}\left[\left\{ a(z) - u_n(z) \right\}_{max} + u_{n_o}\right] \tag{17}$$

Alternately, equation (17) can be rewritten as:

$$V_G = \left\{ a(z) - u_n(z) \right\}_{max} = V_{p_{max}} \tag{18}$$

where

V_G = airplane ground speed for flight at the threshold Mach number

= $(M_T)(a_o) - u_{n_o}$

Equation (18) simply states that for flight at the threshold Mach number, defined by equation (17), the airplane ground speed, V_G, is equal to the maximum shock propagation in the direction of flight speed, $V_{p_{max}}$, beneath the airplane. Comparison of these two equations indicates the reason that specification of the allowable airplane ground speed is a more practical speed control method. The allowable airplane Mach number is dependent on the temperature and wind at both the airplane altitude and the cutoff altitude, while the allowable airplane ground speed is dependent only on the conditions at the cutoff altitude. Since the threshold Mach number is dependent on the sound and wind speeds at both the airplane and cutoff altitudes, these data would be required to calculate it. Wind and ambient temperature at the airplane altitude would be difficult to measury continuously. In addition, significant variations of wind at the airplane altitude can occur over relatively short flight path distances, with corresponding variations in the threshold Mach number. Since it is desired to achieve cutoff near the ground, only the ground conditions would have to be monitored to specify the allowable airplane ground speed, and this value would be flown. The airplane Mach number would be allowed to vary as a function of the local conditions at altitude.

Another associated consideration is the comparative accuracy of a Machmeter versus inertial navigation systems. An inertial navigation system provides an accurate measure of airplane ground speed. It is highly unlikely that a Machmeter could ever approach the accuracy of an inertial navigation system due to inherent measurement and calibration errors at speeds near Mach 1.0. Since the ground speed safety factor required for noise attenuation below cutoff is 6.7 kt (11.3 ft/sec) under standard day conditions (signal length of 91.4 m (300 ft)), the speed accuracy must be at least within that accuracy. In terms of airplane Mach number the 6.7 kt (11.3 ft/sec) is only a Mach number increment of about 0.012.

Use Of Ground Meteorological Data

Of primary importance is the determination of the meteorological conditions along the flight path and the resulting allowable airplane ground speed. Use of ground meteorological data alone is the most practical method since hourly observations of ground meteorological data (temperature and wind) are available at over 500 locations in the continental United States on a routine basis. These data are available in real time over the National Weather Service teletype communications facilities and could be used for preflight planning as well as during flight. Upper air rawinsonde data could also be used, but these are only available at 12-hour intervals at about 68 locations. Variations in the upper level winds in space and time, however, can be considerable and are difficult to predict.

Use of ground meteorological data means that in some cases a slight ground speed penalty will occur (i.e., the airplane could be flown faster than the ground meteorological conditions alone would indicate with no boom on the ground). This situation occurs when there is an inversion in the V_p profile because of a temperature inversion and/or strong tailwinds aloft. Normally only a relatively small airplane ground speed penalty will result from using ground meteorological data alone.

In terms of the meteorological condition at the ground, the allowable airplane ground speed is

$$V_G = (V_{p_G} - \Delta V) = (a_G - u_{n_G}) - \Delta V \tag{19}$$

where

a_G = ambient sound speed near ground

u_{n_G} = wind speed component along flight path (tailwind negative) near ground

ΔV = ground speed safety factor

For calculation purposes this can be expressed as

$$V_G = 29.04 \left\{T\,(°R)\right\}^{1/2} - u \cos(\psi - \eta) - \Delta V \tag{20}$$

where T(°R) = ambient air temperature in degrees Rankine near the ground, and u, ΔV, and V_G are in knots.

Necessity for Anticipating Meteorological Variations

During threshold Mach number flight the shock waves produced at flight altitude travel a considerable distance through the atmosphere before being cutoff in the lower atmosphere. This means that variations in the shock propagation speed at the ground must be "anticipated" by appropriate changes in the airplane ground speed by at least this propagation distance. Changes in topography would also have to be anticipated in the same manner. For example, during a westbound flight it may be necessary to decrease the airplane ground speed as the east slope of the Rocky Mountains is approached to avoid placing sonic booms on the ground. Figure 31 shows the variation of the shock wave propagation distance and threshold Mach number for various wind conditions at the airplane altitude. For these flight and atmospheric conditions the propagation distance varies from about 20 miles to over 50 miles. Adjustments to the airplane ground speed would be made at distances of this order prior to passing over the point of interest.

Other Meteorological Effects

Important micrometeorological variations are due to wind gusts caused by topographical features and meso-scale meteorological disturbances. Figure 32 shows the effect of wind gusts on the allowable ground speed, where gusts are considered to be variations from the mean wind speed. From this analysis it can be seen that this effect can be important, particularly when ground meteorological data are used. These variations can affect both $V_{p_{max}}$ and ΔV_s.

Airplane Systems

An additional ground speed decrement, ΔV_A, to allow for airplane ground speed variations induced by the pilot and/or throttle setting may be necessary. The accuracy of the inertial navigation system (V_G sensors) may also be significant.

Total Speed Safety Factor

During threshold Mach number operation it will be necessary to determine a total ground speed safety factor (ΔV in equation 20) to assure boom-safe operation. This total safety factor would consist of several factors and could be expressed as

$$V_G\,(\text{safe}) = V_{p_G} - \Delta V \qquad (21)$$

V_{p_G} = shock propagation speed near ground

$\Delta V = \Delta V_s + \Delta V_G + \Delta V_A$

where

ΔV = total speed safety factor decrement

ΔV_S = speed safety factor decrement required for cutoff at safe altitude above ground for adequate noise attenuation

ΔV_G = speed safety factor decrement required to account for wind gusts and meso-scale meteorological variations

ΔV_A = speed safety factor decrement required to account for variations in the speed specification system and ground speed accuracy

Methods for Calculating the Speed Safety Factor for Adequate Noise Attenuation Below Cutoff

The analysis in previous sections has shown that the theoretical "safe" altitude is a useful method for determining the airplane ground reduction for safe sonic boom cutoff. The method used to determine it, however, is dependent to a large degree on the available meteorological data. Ideally, tower measurements of temperature and wind would be available in real time. An average gradient of shock propagation speed should be calculated above the altitude of the maximum shock propatation speed. The allowable airplane ground speed is then calculated as

$$V_G\,(\text{safe}) = V_{p_{max}} - \Delta V_S - \Delta V_G - \Delta V_A \qquad (22)$$

where

$\Delta V_S = (R)^{1/3}\,(L)^{2/3}$

$R = \dfrac{-a}{\partial V_p / \partial z}$

L = signal length

In the absence of tower meteorological data, upper air meteorological data must be used to obtain the propagation speed lapse rate. As a last resort a conservative value of about 6 m/sec (12 kt) can be used.

ANALYSIS OF LOW-MAGNITUDE ACCELERATION EFFECTS DURING THRESHOLD MACH NUMBER FLIGHT

BACKGROUND

During the 1970 BREN tower program there were 31 threshold Mach number flights which were at sufficiently high Mach numbers to produce well-defined sonic booms on the ground. These are listed in table 9 of reference 3. The initial analysis of these data in reference 3 indicated that about half of these flights resulted in caustics that were produced by variations in the airplane ground speed rather than by cutoff. In most of these cases, the shock waves were within several degrees of cutoff so that it was clear that the caustics were not associated with the cutoff condition. Some of these caustics produced by low-magnitude accelerations are analyzed in this section. This analysis indicates the sensitivity of shock wave propagation and intensities to slight variations in ground speed near the cutoff condition, and it provides insight into the caustic mechanism for these flights.

METHOD OF CALCULATION

To provide a sound basis for a study of the maneuver effects and to aid in the interpretation of the test data, calculations were made of shock wave vertical profiles. Shock wave locations in the vertical plane can be determined after a relatively large number of ray trajectories have been calculated. The method of geometrical acoustics (as in ref. 6) was used to calculate the ray trajectories from the known airplane trajectory and meteorological conditions. In the method of geometrical acoustics the sonic boom signal is propagated along rays, each ray being the trajectory of a point on the wave front. Since steady ray geometry is assumed, only the wavefront emanating from the nose of the airplane is considered (the wavefront associated with the tail shock, for example, will have nearly the same shape and location as the wavefront from the airplane nose).

The shock front location and vertical profile can be calculated from the ray trajectory data by interpolating in time for the shock location at a reference time. For convenience the reference time was taken as the observed sonic boom arrival time at tower microphone T-1. This provided a comparison between theory and experiment for both the shock location (and arrival time) and the shock front shape at the reference time. Observed shock wave profiles are provided by the observed tower pressure signatures. In comparing theory and experiment, only the onset of bow shocks is considered.

In several cases caustics were produced on the part of the shock wave that had been reflected from the ground uptrack of the tower and then intercepted the tower. To calculate theoretical shock wave profiles for these cases required the use of a "mirror-image" atmosphere below ground level. The calculated shock front below ground level was then rotated 180° with respect to the ground plane to place it above the ground. In addition, it was necessary to rotate the shock wave backward about 2° in the plane of the tower due to the effect of the 1° terrain slope uptrack of the tower (see ref. 3).

The analysis of these data was restricted to flights for which detailed radar data were available. Since airplane ground speed has a significant effect on sonic boom propagation at low supersonic Mach numbers, the unsmoothed radar data were used. Constant airplane altitude and zero climb angle were assumed, however, since they vary only slightly and have a negligible effect compared to ground speed changes. The cases analyzed included 10 of the 14 flights classified as "B3" (indicating that acceleration effects were evident) in table 9 of reference 3. In addition, three "B2" category flights (indicating no-acceleration flights) were analyzed (passes 018, 028, and 116). Thus, 13 flights are included in this section and are summarized in table 4. The results of the data analysis are given in the next two subsections; detailed tower pressure signatures are included for seven cases.

ACCELERATION MAGNITUDE AND CAUSTIC INTENSITY

In this section observed and calculated caustic locations and shock wave profiles are compared. The calculated shock wave profiles permit the correlation of the observed shock wave characteristics and caustics with the portion of the airplane trajectory which produced them. For six flights it was possible to relate an acceleration magnitude with an observed caustic on the BREN tower. These six flights are summarized in table 4. Calculated shock wave profiles and observed tower pressure signatures are given for four of these cases in figures 33 through 36 (passes 017, 018, 106 and 116, respectively).

Table 4 also gives the error in the calculated shock location at the reference time (arrival time at tower microphone T-1). This was converted to an error in time by using the airplane ground speed. These times differ slightly from those given in table 9 of reference 3, because unsmoothed radar data were used in the present study, whereas smoothed radar data were used in reference 3. In addition, the integration step size for the numerical calculations was larger for the present analysis. In most of the shock profile plots the calculated shock profile was positioned to agree with the observed shock profile (generally at microphone T-1) so that shock profile shapes could be compared easily.

TABLE 4.–SUMMARY OF LOW-MAGNITUDE ACCELERATION THRESHOLD MACH NUMBER FLIGHTS

Date	Bongo-pass	Pass	Shock arrival time at mic. T-1, PDT	Average ΔP_{max} on tower		Maximum ΔP_{max} observed on tower			Acceleration, A		Observed shock wave characteristics	Characteristics of calculated shock profile	Error in calculated shock location at reference time at T 1	
				N/m^2	lb/ft^2	N/m^2	lb/ft^2	Mic. no.	m/sec^2	ft/sec^2			Distance, m(ft)	Time, sec
A. CASES FOR WHICH ACCELERATION RATE COULD BE CALCULATED														
8-25	2-1	017	0937:38.928	29.1	0.680	82.4	1.72	T-14	0.65	2.12	Caustic at tower top preceded by another shock wave	Excellent agreement with observation; caustic at tower top with another incident wave	136(446)	-0.38
	2-2	018	0948:50.403	29.7	0.620	62.0	1.295	T-8	0.55	1.80	Three incident shocks, caustics at T-8 and on reflected shock	Caustic on both incident and reflected waves	94(308)	-0.26
	3-4	024	1112:02.955	33.2	0.684	63.2	1.32	T-6	0.44	1.43	Caustic between T-5, -6	Caustic at 100 m (330 ft)	35 (115)	-0.10
8-31	4-4	066	1143:57.200	30.1	0.628	70.4	1.47	T-12	0.69	2.255	Caustic at T-12	Two incident waves that cross near midtower; caustic above tower	84(276)	-0.23
10-29	1-3	106	0856:36.848	31.0	0.647	40.6	0.847	T-7	0.25	0.81	At least three incident shocks; caustic near midtower	Two incident waves that cross at 180 m (600 ft); caustics above and below tower	756(-2480)	2.19
10-30	1-1	116	0908:23.564	25.6	0.535	47.0	0.981	T-1	0.30	0.99	Caustic at tower base	Caustic near tower base and 175 m (575 ft)	837(-2746)	2.41
B. OTHER CASES														
8-24	2-1	004	0937:17.832	23.8	0.765	36.6	0.765	T-5	–		At least three incident shocks but no caustic	Five incident shocks and two caustics	65(213)	0.18
8-25	2-4	020	1009:30.824	29.4	0.614	44.9	0.937	T-4	–		Several incident shocks; weak caustic at T-4; weak reflection	Four incident shocks and several caustics	60(197)	-0.17
	4-4	028	1148:56.207	48.2	1.007	79.0	1.65	T-4	–		Several incident shocks; caustic at T-4; weak reflection	One incident wave with noncaustic focusing at 220 m (700 ft)	245(804)	-0.88
8-31	3-3	061	1058:28.566	40.3	0.842	56.6	1.183	T-10	–		Several incident shocks; caustic at T-7 and also on reflected wave	Two incident shocks; caustic	329 (1079)	-0.88
10-30	4-3	065	1133:42.590	40.8	0.852	57.6	1.203	T-12	–		Several incident waves; caustic on reflected wave at T-12	Two incident shocks; two caustics above and below tower	140(459)	-0.39
	1-2	117	0919:09.237	31.7	0.662	37.4	0.782	T-5	–		Caustic at T-5	Complex shock profile	-392(-2926)	2.57
	1-4	119	0939:30.391	19.5	0.408	35.6	0.743	T-14	–		Weak incident shock; caustic-like signal on reflection at T-15	One incident shock wave	898(-2946)	2.58

Shock wave profiles are given in figure 33 for pass 017. The onset of each calculated incident shock wave is given by a dashed line. The shock wave onset is defined as the location of the bow shock at the reference time. No ground-reflected shock waves were calculated for this case. Excellent agreement is indicated at the tower top since a caustic is preceded by another shock wave for both the calculated and the observed profiles. On the lower part of the tower, agreement is not as good since the first incident wave at the tower top is calculated to have a much higher angle of incidence that that observed, and thus trails behind the other incident waves on the bottom part of the tower. The airplane ground speed variation for this case is given in the insert. Note the ground speed increase over the flight time for which the caustic was produced (67 to 70 sec). The caustic in this case was produced by the decreasing, then increasing ground speed which results in a foldover of the shock front. The insert diagram of the airplane ground speed variation in figure 33 also gives the airplane ground speed corresponding to the threshold Mach number, which is noted as the "threshold V_G."

The shock wave profiles shown in figure 34 for pass 018 are particularly interesting since a double caustic (or double foldover) is predicted on the incident shock wave. Evidence of multiple shocks can be seen on the observed pressure signatures and the signature at microphone T-8 is caustic-like. The first foldover was caused by an airplane ground speed decrease and the subsequent increase between 70 and 75 seconds, and the second foldover was caused by the increasing ground speed followed by the decreasing ground speed between 75 and 80 seconds. For this case, ground-reflected shock waves were also calculated by using a mirror-image atmosphere below ground level. Several caustics are predicted due to airplane ground speed increases beginning at flight times of 50 and 62 seconds. Interestingly, caustic-like pressure signatures did occur on the reflected wave near the calculated locations.

The caustic produced during pass 106, shown in figure 35, is less complex. Two pressure signatures are evident near the tower top. This is particularly evident at T-14 (note tail shocks also). These two signatures progressively merge toward midtower with a caustic-like signature at microphones T-7 and T-8. Two incident shock waves were calculated with caustics both above and below the tower (i.e., on reflected wave). Since the shock wave arrival time predicted by theory was over 2 seconds too late (see table 4) compared to the observed arrival time, it appears that the caustic predicted to be below the tower corresponds to the one that actually occurred at midtower. This was produced by the ground speed variation near 40 seconds. Slight inaccuracies in the meteorological conditions can have a large effect on the calculated wavefront shapes and locations. The 2-second error in the predicted arrival times for the cases on October 29 and 30 (see table 4) indicates that for these cases the observed meteorological conditions may not have been representative of the actual propagation conditions along the boom path. The calculated shock profiles are still valid, however, and indicate the portion of flight track which produced the caustic.

Shock profiles for another caustic case, pass 116, are given in figure 36. The decreasing airplane speed followed by the increasing speed after the flight time of 26 seconds produced a predicted caustic at tower microphone T-6, and a second caustic is predicted (but not shown) on the ground-reflected wave near the tower base due to the ground speed change near 50 seconds. The signatures near the tower top are also interesting since two incident signatures are evident (note particularly the tail shocks). As for the previous case, pass 106, these two signatures merge to form the caustic, and the caustic predicted to occur below the tower (produced near a flight time of 40 seconds) correlates with it.

Two other caustic cases, passes 024 and 026, are summarized in table 4. In each of these cases the predicted caustic location agreed reasonably well with the caustic location observed on the tower, and it was possible to calculate an acceleration magnitude associated with the caustic. These results are given in table 4 and figure 37 for the available six cases. A rather significant increase in caustic intensity with increasing acceleration magnitude is indicated by these data. In each case the acceleration magnitude was calculated over a 3-second interval over which the airplane ground speed was increasing. With current methods it is not possible to predict the intensity at a caustic, but these experimental results may prove helpful in evaluating future methods. The effect of acceleration magnitude is discussed in a later section in the context of using a slow acceleration to alleviate the caustic produced during transonic acceleration.

OTHER MANEUVER EFFECTS

Additional results of the comparison of observed and calculated caustic locations and shock wave profiles are presented in this section. For these cases it was not possible to determine an acceleration magnitude associated with the observed caustics due to uncertainties in correlating the observed caustics with the airplane maneuvers, but the maneuver effects are of interest. These seven cases are summarized in table 4; calculated shock wave profiles and observed pressure signatures are given in figures 38 through 41 for passes 004, 028, 117, and 119.

Maneuver effects were particularly evident during pass 004 since a "triple boom" was observed. The calculated and observed shock wave profiles are given in figure 38 for this case; an observed pressure signature at ground microphone G-7 near the tower base is also given. Although two caustics were predicted on the tower, none were evident. (Tower pressure signatures for this case were not of sufficient quality for presentation). The ground speed variation shown in figure 38 shows that the caustics were produced by ground speed variations near 42 and 53 seconds. Since the ground speed at 42 seconds is below the "threshold" value, this caustic would be cut off before reaching the ground. In spite of the two predicted caustics, the observed and calculated shock fronts agree reasonably well. The acoustic wave ahead of the shock waves was probably a precursor or an acoustic signal propagating from a cutoff shock wave produced at an earlier flight time.

The calculated shock wavefront for pass 028, shown in figure 38 along with the observed pressure signatures, is somewhat unusual. Noncaustic focusing is predicted between tower microphones T-6 and T-8 because of the slowly increasing ground speed between 66 and 70 seconds. Focused waves did occur between microphones T-3 and T-9. The observed pressure waves are very complex, however, and correlation with the calculated shock wave is difficult.

The calculations and observations for pass 117 in figure 40 are similar to those for passes 106 and 116. At the tower top three incident shock waves can be seen (again note the tail shocks, as well). Two of these shock waves are fairly weak initially, but they merge to form the caustic near microphones T-6 and T-5. The calculated shock fronts agree reasonably well, and a caustic is predicted below the tower due to the ground speed variation at 23 seconds. A second caustic is predicted above the tower (produced near a flight time of 28 seconds), and a third one is predicted below ground level by the maneuver near 36 seconds. It is not clear in this case which of the three predicted caustics correlates with the observed caustic. As for passes 106 and 116 it is probably one of the caustics predicted to occur below the tower.

The case shown in figure 41 is interesting because it shows the effect of a deceleration near the threshold Mach number. The reflected shock wave is fairly strong near the tower top and decreases in strength progressively to the ground and then upward on the incident wave. The calculated shock front agrees reasonably well with the observed shock front, and the airplane speeds associated with the calculated shock wave show that the airplane was decelerating near the threshold Mach number. It appears likely, however, that actual cutoff occurred above the tower and that the actual threshold V_G was about 347.5 m/sec (1140 ft/sec). An inversion existed in this case so that cutoff would occur above the tower. Since the shock propagation speed decreases toward the ground, the acoustic wave is oriented like a shock wave. As the airplane speed decreased, cutoff occurred at higher altitudes above the ground resulting in the lower intensities for the later flight times.

Calculations were also made for passes 020, 161, and 065. These results are summarized in table 4 and are similar to results for other cases.

The cases considered in this section, except for pass 119 (fig. 41), were those for which the airplane ground speeds were greater than the threshold value. The ground speed variations that produced the caustics ranged from about 3 to 10 m/sec (10 to 30 ft/sec). Such variations in ground speed are not unusual for lightweight, high thrust-to-weight ratio airplanes since slight changes in throttle setting (in an effort to fly constant Mach number) produce relatively large speed changes. Wind and temperature variations at the airplane altitude may also cause speed variations. Commercial airplanes with much greater inertia and a lower thrust-to-weight ratio would probably exhibit less speed variation than the F-104 airplanes used in these tests.

The analysis of those selected cases for which the airplane Mach number was greater than the threshold value has shown that very slight changes in the airplane ground speed can produce folds and associated caustics. In general, a fold on the wavefront during flight near the threshold Mach number may be produced whenever the airplane acceleration changes sign, i.e., from increasing speed to decreasing speed or from decreasing to increasing speed. In several cases it was possible to correlate the acceleration magnitude with the measured caustic on the BREN tower. These data indicate an increase in caustic intensity with increasing acceleration magnitude. The wave folding produced by slight airplane ground speed changes in most cases explained the multiple shock waves observed on the BREN tower.

These experimental observations of the wave-folding mechanism for caustic formation tend to verify qualitatively a recent theoretical study of the flow field associated with a sonic boom focus (ref 7). In that study it was found that wave folding occurs for weak shocks according to geometrical accoustics but does not occur for strong shocks with relative overpressures, $\Delta P/P$ of the order of unity or higher. Whitham (ref. 8) hypothesized that a shock will straighten out without foldover, which appears to be true for strong shocks only.

ANALYSIS OF LONGITUDINAL ACCELERATION FLIGHT TEST DATA

In this section the results are given of a detailed study of the seven flights for which measurements were obtained near caustics produced by longitudinal accelerations.

BACKGROUND

Experimental flight test programs have been very helpful in defining the nature of sonic boom near caustics produced by longitudinal accelerations. The initial analysis of the 19 BREN tower acceleration flights in reference 3 indicated that measurements had been obtained very close to the caustic. These measurements showed that nonlinear effects become important within about 400 m (1300 ft) downtrack of the caustic-ground intersection and within 150 m (500 ft) vertically above the caustic. Within 30 m (100 ft) of the caustic itself, nonlinear effects predominate and transform the incoming N-wave into a U-wave. Measurements were also obtained well uptrack and downtrack of the caustic-ground intersection, but the measurements close to the caustic are particularly interesting since current theoretical methods are invalid there. In the last several years significant advances have been made in theoretically describing the pressure field in the vicinity of a caustic (refs. 7 and 9 through 12). These methods, however, need further refinement before specific results can be obtained.

In the analysis of these data, essentially the same methods were used as in the analysis of the low-magnitude acceleration threshold Mach number flights. Shock wave profiles were calculated using the unsmoothed radar airplane trajectory data and the observed meteorological conditions. These calculated shock wave profiles aid in the interpretation of the test results and make it possible to calculate airplane acceleration magnitudes associated with the measured caustics. A discussion of the shock wave characteristics near caustics and detailed documentation of the observed pressure signatures are given to aid theoreticians in their attempts to provide realistic theoretical results near caustics.

SHOCK WAVE PROFILES–THEORY AND EXPERIMENT

Observed and calculated shock wave profiles are given in figures 42 through 47 for passes 045, 046, 088, 092, 093, and 094, respectively. A comparison of these results is given in table 5; observed and calculated shock wave characteristics are summarized and the errors in the arrival time at microphone T-1 are also given. It was not possible to calculate a shock wave profile for pass 047 due to unacceptable radar data.

The results for passes 045 and 046 are very similar. In each case the calculated caustic is predicted to occur uptrack of the tower on the ground and to pass over the tower, while the actual caustic occurred on the lower part of the tower. This discrepancy is due to the fact that the

TABLE 5.—COMPARISON OF THEORETICAL AND EXPERIMENTAL SHOCK WAVE PROFILES FOR LONGITUDINAL ACCELERATIONS

Date	Bongo-pass	Pass	Reference time (boom time at mic. T-1), PDT	Observed shock wave characteristics	Agreement between theory and experiment	Calculated shock front characteristics	Error in calculated shock location at reference time at T-1	
							Distance error, m(ft)	Time error, sec
8-28	3-2	045	1043:48.723	Caustic incident on tower at microphone T-3	Poor	Caustic predicted to occur uptrack of tower on ground and pass over tower after reflection	+147 (482)	-0.4
8-28	3-3	046	1055:28.108	Caustic incident on tower at microphone T-1; relatively large acceleration magnitude apparently produced a stronger caustic	Poor	Caustic predicted to occur uptrack of tower on ground and intercept tower after ground reflection	+184 (604)	-0.5
10-27	1-3	088	0904:13.733	Anomalous extra shock front precedes caustic; caustic incident on tower at microphone T-2	Poor	Caustic predicted at about 100 m (300 ft) lower altitude than observed	-1156 (-3793)	+3.2
10-27	3-1	092	1146:53.628	Weak caustic reflected from ground uptrack of tower and observed on tower at microphone T-9	Excellent	Caustic predicted to occur on tower after ground reflection about 30 m (100 ft) higher than observed	-88 (-289)	+0.25
10-27	3-2	093	1158:34.954	Caustic incident on tower at microphone T-5, -6	Excellent	Caustic predicted to occur at about 100 m (300 ft) lower altitude than observed	-55 (-180)	+0.15
10-27	3-3	094	1210:49.308	Caustic incident on tower at microphone T-6	Excellent	Caustic predicted to occur at 150 m (500 ft) lower altitude than observed	-101 (-331)	+0.3

observed upper level winds were not representative of the conditions along the boom propagation path. Only a slight decrease in the tailwind component at the airplane altitude would cause the calculated caustic location to agree better with the observed location. A reduction in the tailwind component would also give better agreement for the arrival times at microphone T-1 (see table 5).

A major and significant difference between the observed shock waves for passes 045 and 046 in figures 42 and 43 is the angle between the leading and trailing shock waves just above the caustic where they merge to form the caustic. The angle for pass 046 is significantly greater than for pass 045, suggesting a higher airplane acceleration magnitude and caustic intensity. The effect of acceleration magnitude on caustic intensity is considered in more detail in a later section.

The results for pass 088 are given in figure 44. During this pass an extra shock wave precedes the caustic. This extra shock wave, however, was not predicted from the available flight track and meteorological data. Another caustic must have occurred uptrack of the tower (negative distance, D, from tower). Passes 092 and 094 in figures 45 and 47, respectively, also exhibited extra shock waves. In each case these extra shock waves and caustics were not predicted by the theoretical calculations. In the experimental flight test program "Jericho-Carton" (ref. 13) similar results were noted. For one case of a relatively slow acceleration, four caustics were observed and it was concluded that they are due to slight variations in the acceleration magnitude and undulations in the airplane flight path.

For comparison of the calculated and observed shock wave profiles for pass 092, it was necessary to consider the effect of ground reflection. Since the caustic occurred on the tower after ground reflection, the observed shock wave profile was "unreflected" (placing the caustic below ground level). To obtain the corresponding theoretical calculations a mirror-image atmosphere below ground level was used. The results are shown in figure 45. The agreement between theory and experiment is excellent; the error in arrival time is only 0.25 seconds, or an 88 m (289 ft) distance error at the reference time at microphone T-1. The caustic locations also agree very closely, with the predicted caustic 30 m (100 ft) above the observed caustic. Similar results were obtained for passes 093 and 094 in figures 46 and 47, respectively. The caustics were predicted to occur slightly behind and below the observed caustics. In some cases the trailing shock was predicted to occur ahead of the leading shock wave. This did not occur in actuality for these flights and is due to the calculation method. The focusing effect produced by the accelerations is clearly evident in the theoretical calculations near the caustic, however, with many rays converging there. The caustic-forming mechanism is illustrated very well by these calculations. A fold is produced as a direct result of the acceleration, with the caustic occurring at the lowest extension of the shock wave at the tip of the fold.

SHOCK WAVE CHARACTERISTICS NEAR CAUSTICS

Observed pressure signatures are given in figures 48 through 54 for the seven longitudinal accelerations that produced caustics on the microphone network. Pressure signatures observed on both the tower and the ground are plotted on the figures; the ground pressure signatures have been positioned at the approximate altitude at which that part of the shock wave intercepted the tower. In addition, for clarity the effect of ground reflection was eliminated in some cases by positioning the signatures below ground level. The horizontal and vertical scales are the same in these figures so that angles of incidence can be read directly; the pressure signatures are to this same distance scale. A time scale and the maximum overpressure for each signature are also given. The onset of each bow shock wave has been drawn in on these figures to aid in interpreting them.

The pressure signatures observed during pass 045 in figure 48 are typical of those observed near caustics. The leading N-wave and trailing U-wave (that has passed through the caustic) are fairly close together at the tower top and merge to form the caustic near the tower base. The ground-observed pressure signatures, G-8 through G-14, give much the same picture as the tower signatures. Below the caustic in the "shadow" region the sonic boom disturbances degenerate into low-magnitude acoustic disturbances. It appears that the leading and trailing signatures each produce a corresponding acoustic counterpart below the caustic; the shock waves have been drawn below the caustic to illustrate this effect.

The data for pass 046 are given in figure 49, where again the caustic was produced near the tower base. In contrast to pass 045, however, the leading and trailing shocks are separated by a much larger distance near the tower top. This caustic was the most intense that was observed. A secondary caustic apparently also occurred on the leading shock wave. The focusing of both the N-wave and the U-wave is evident as the caustic is approached.

The pressure signatures given in figure 50 for pass 047 are similar to those for pass 045, except that near the caustic the signatures exhibit more of the N-wave shape than the U-wave shape. Below the caustic the disturbances attenuate rapidly with distance.

Pass 088 produced an interesting shock wave profile, as shown in figure 51. Caustics were produced on the incident shock wave near the tower top and on the trailing shock waves near the tower base. The caustic on the trailing shock waves appears to result from the merging of three low-intensity pressure signatures. This complex shock wave pattern was apparently produced by an undulation in the flight path (see the previous subsection). The reflected waves observed on the tower (not shown in figure 51) were acoustic in nature.

The caustic observed during pass 092 occurred on the ground just before microphone G-1 and on the tower after ground reflection. In figure 52 the shock waves have been positioned below ground level for clarity and for ease of comparison with previous cases. This was the weakest caustic observed; ground reflection may have affected the magnitude. A second leading shock, although weak, appears on the lower part of the tower. The data for pass 093 in figure 53 also show three incident shock waves which interact in a complex manner near midtower. The pressure signatures for pass 094 in figure 54 show a less complex caustic formed by the merging of two shock waves.

The pressure signatures given in detail in figures 48 through 54 suggest several significant features typical of caustic phenomena. These can be conveniently separated into characteristics above the caustic, at the caustic, and below the caustic. Above the caustic at least two shock waves exist; one is the leading N-wave and the other is the trailing U-wave which passed through the caustic earlier and was transformed from N-wave to U-wave by the nonlinear effects which predominate at the caustic. As the caustic is approached these two shock waves begin to merge and eventually are superimposed. Simultaneously, however, both the N-wave and U-wave are focused as the caustic is approached. The calculated shock wave profiles in the previous subsection illustrated that both shock waves are focused. These focused shock waves are superimposed in a linear manner up to at least within 30 m (100 ft) of the caustic (ref. 3). Thus, the basic nonlinearity appears to be associated with the effect of focusing on the initial N-wave, which results in the transformation to the U-wave. To obtain realistic pressure signatures above the caustic it will be necessary to consider both the incoming N-wave and the outgoing U-wave. It appears that these could be calculated separately, however, and superimposed linearly.

Below the caustic the disturbance attenuates rapidly to an acoustic disturbance. This occurs because the caustic is the lowest extremity of the shock wave. Acoustic disturbances propagate from the caustic, however, into the "shadow" region. In many cases acoustic pressure waves can be seen which correspond to both the incoming N-wave and the outgoing U-wave.

EFFECT OF ACCELERATION MAGNITUDE

The acceleration magnitude for each flight was calculated over a 6-second flight time interval during which the measured caustic was produced. These data are given in table 6, along with the maximum observed overpressure on the tower near the caustic. Another measure of the acceleration magnitude is the difference in the angles of incidence of the leading and trailing shocks. In reference 3 the distance S was calculated between the leading and trailing shocks at a distance of 300 m (1000 ft) above the caustic, and these correlated well with the calculated acceleration magnitude. A more general measure of the shock separation is the difference in the angles of incidence of the leading and trailing shocks (bow shocks). These are also given in table 6 and are

TABLE 6.–EFFECT OF ACCELERATION MAGNITUDE ON CAUSTIC STRENGTH

Date	Bongo-pass	Pass	Maximum overpressure on tower near caustic			Difference in angles of incidence of leading and trailing shocks, $\Delta\theta$		Calculated airplane acceleration, A	
			N/m^2	lb/ft^2	Mic no.	Rad	Deg	m/sec^2	ft/sec^2
8-28	3-2	045	109.6	2.29	T-2	0.03491	2.0	1.27	4.2
	3-3	046	134.5	2.81	T-2	0.12741	7.3	1.48	4.9
	3-4	047	93.4	1.95	T-4	0.03840	2.2	1.25	4.1
10-27	1-3	088	112.0	2.34	T-2	0.09306	5.3	1.34	4.4
	3-1	092	56.9	1.12	[a]T-9	0.04538	2.6	1.23	4.05
	3-2	093	107.3	2.24	T-7	0.09948	5.7	1.36	4.5
	3-3	094	80.0	1.67	T-5	0.07156	4.1	1.26	4.1

[a]The caustic occurred on the tower after ground reflection

plotted in figure 55. A general trend toward increasing caustic intensity with increasing acceleration magnitude is indicated by these results. Some scatter due to atmospheric effects is to be expected.

These results for the effect of acceleration magnitude are compared in figure 56 with the results obtained from the analysis of low-magnitude accelerations near the threshold Mach number (see the previous section and figure 37 for those results). These data together also suggest a general increase of caustic intensity with increasing acceleration. A band of intensities is indicated in figure 56. This suggests an upper bound for the magnification at the caustic produced by longitudinal acceleration as three to five times the nominal steady, level overpressure. In view of the small number of data points, however, further flight tests would be needed to establish the maximum intensity with certainty.

The results of the extensive French experimental program "Jericho-Carton" are reported in reference 13. One of the major goals of that program was to determine the effect of acceleration magnitude and lateral spread on the caustic intensity produced by rectilinear acceleration. Although experimental results were obtained for 26 flights, there was no conclusive evidence that acceleration magnitude influenced the caustic intensity (see fig. 26 of ref. 13). This is in contrast to the results given here, where it appears that there is an effect. There may be several reasons for the different conclusions from these two studies. No description is given in reference 13 of the method used to calculate the acceleration magnitudes. In this study, theoretical ray calculations were used to

determine the portion of the flight path which produced the observed caustic, and the acceleration magnitude was calculated over a 6-second interval from detailed radar ground speed observations. These acceleration magnitudes correlate well with the observed separations of the leading and trailing shock waves (see fig. 49).

Another difference is the measurement of the caustic intensity. During exercise Jericho-Carton, 48 microphones were positioned along a single line 4890 m (16 000 ft) long. This long line of microphones was required to ensure that the portion of the shock wave of interest was observed, but meant that the distance between microphones had to be compromised to from 100 m (330 ft) to 120 m (394 ft). In most cases, then, the caustic occurred between two microphones. During the BREN tower test program, on the other hand, a much shorter line of microphones was used (975 m (3200 ft)), with a distance between microphones of 61 m (200 ft). This relatively short line on the ground was possible because of the use of the BREN tower with microphones spaced 30.5 m (100 ft) apart on the tower. In all cases the caustic intensity was taken from the tower measurements, which provide a more accurate measure of caustic intensity for two reasons. First of all, the 31.5 m (100 ft) microphone spacing on the tower ensures that an observation is obtained near the caustic. Secondly, the effects of ground reflection are eliminated by using tower observations. These differences in the determination of acceleration magnitude and measurement of the caustic intensity may account for the different conclusions for the effect of acceleration magnitude on caustic intensity. Further flight tests are needed, however, to provide more definitive information.

STUDY OF METHODS FOR ALLEVIATING THE TRANSONIC ACCELERATION CAUSTIC

BACKGROUND

The normal transonic acceleration of supersonic airplanes produces a relatively small region on the ground where a caustic occurs. The pressure signature data given in the previous section were measured in this caustic region. The large-scale shock wave patterns in the vertical plane of the airplane and the horizontal ground plane are given in figures 57 and 58, respectively, for constant accelerations of 0.04 and 0.10 g at 10 670 m (35 000 ft) in the standard atmosphere. The caustic occurs at the extremity of the fold or cusp and is a direct result of the acceleration. Several ray trajectories have been given in figure 57 to aid in understanding the formation of the caustic. Within several pressure signature wavelengths of the caustic, magnified sonic boom intensities occur, and within one wavelength the magnification is several-fold.

The effects of maneuvers on sonic boom have been studied by several investigators during the last several years. A comprehensive study of maneuvers typical of large SST-type airplanes (ref. 14) showed that it is possible to perform normal SST flight operations without producing caustics, except during the transonic acceleration phase of flight. Ribner (ref. 15) discussed the procedure of decelerating during supersonic turns to eliminate the caustic. Others (refs. 16 and 17) have considered the pullup-pushover maneuver to produce local reduction of sonic boom intensity.

The data analyses of the effects of accelerations during threshold Mach number flight and longitudinal accelerations given in previous sections suggest that a method to alleviate the transonic acceleration caustic is to accelerate rather slowly. This possibility is discussed in this section. In addition, a transition maneuver suggested by Hayes (ref. 18) was studied to determine if it is possible to eliminate the caustic completely.

LOW-MAGNITUDE ACCELERATION

The variation of caustic intensity with acceleration magnitude for the longitudinal acceleration flights (see fig. 55) and the threshold Mach number flights (see fig. 37) have been combined in figure56. These two sets of data indicate that a slower acceleration produces a less intense caustic. This suggests that a method to alleviate the transonic acceleration caustic is to accelerate slowly through and past the threshold Mach number.

In comparing the shock wave patterns in figures 57 and 58 for the two acceleration rates, several features are evident that indicate a lower caustic intensity for the lower acceleration magnitude. For the slower acceleration the "double boom" and area of magnified sonic boom is spread over a larger ground area; in the vertical plane the leading and trailing shocks are closer together near the caustic, suggesting that the magnification is spread over a larger depth of the atmosphere. In addition, the distance of propagation is significantly longer for the portions of the shock wave which form the caustic at the ground for the slower acceleration case. Thus a weaker signature produced at a Mach number near the threshold value is amplified at the caustic. This suggests that the lower limit for the magnification of the acceleration caustic (finite acceleration magnitude) is the same as the magnification at the threshold Mach number caustic (about 2). The data in figure 56 also suggest this conclusion. An acceleration magnitude of about 0.3 m/sec^2 (1.0 ft/sec^2) or less would appear to give an amplification of about 2.

With current prediction methods it is not possible to deal with sonic boom intensities close to caustics, so that no method is available for calculating the variation of caustic intensity with acceleration magnitude. More experimental data would be helpful in establishing this variation. The limited experimental data and an investigation of the shock wave patterns produced by different acceleration magnitudes, however, do suggest a pronounced effect of acceleration magnitude on caustic intensity.

CAUSTIC-ELIMINATION MANEUVER

The caustic-elimination maneuver during transonic acceleration that is the topic of this section was first suggested by Hayes (ref. 18). The basic concept is to use a vertical acceleration (pullup maneuver) to cancel out the focusing caused by the forward acceleration. The maneuver as envisioned by Hayes, however, appears to be reversed. A pushover followed by a pullup was specified in reference 18 as sufficient to eliminate the caustic. A caustic is produced, however, by focusing when the pullup is terminated. A pullup followed by a pushover is required to eliminate the caustic. The preliminary results of a study of this maneuver are given in this section. The mechanism of caustic elimination is described and some indication of its feasibility is given for commercial SST operation.

A convenient starting point for considering the elimination of the caustic produced during transonic acceleration is to consider the acceleration vector normal to the Mach cone directly beneath the airplane ($\phi = 0$). In terms of the axial and lift load factors, n_T and n_L, respectively, this is

$$n_N = \frac{1}{M}\left[n_T - \beta(n_L - 1)\right] \tag{23}$$

In terms of rates of change of Mach number and climb angle, it is

$$n_N = \frac{a_o}{g} \frac{\dot{M}}{M} - \beta \dot{\gamma}. \tag{24}$$

To eliminate the caustic (no focusing) the vertical acceleration component must balance the forward acceleration component ($n_N = 0$). Solving equation 24 with $n_N = 0$ gives

$$\partial \gamma / \partial M = 1/(\beta M). \tag{25}$$

This convenient result specifies how climb angle must vary with Mach number so that no focusing is produced.

To understand the meaning of equation 25 more fully it is necessary to consider the criterion for cutoff of shock waves above the ground. For the case of no wind, directly beneath the airplane, and climb angle not zero, it is

$$\sin(\mu + \gamma) = a_o/a(z). \tag{26}$$

For $\gamma = 0$ and steady flight this gives the well-known result for the threshold Mach number, M_T, as

$$\sin \mu = a_o/a(z) = 1/M_T. \tag{27}$$

In our case, however, γ is not zero and we want to solve for the relationship between γ and M implied by equation 26. Solving for γ gives

$$\gamma = \sin^{-1}(a_o/a(z)) - \sin^{-1}(1/M). \tag{28}$$

Taking the derivative with respect to M and assuming that a_o is constant and cutoff occurs at a constant altitude (constant a(z)), gives

$$\partial \gamma / \partial M = 1/(\beta M).$$

This last result is significant since it is the same result derived for $n_N = 0$ (see eq. 25). This means that cutoff of the shock wave at some constant altitude above the ground is produced when γ is varied according to equation 25 such that no focusing is produced. The pullup cancels the focusing caused by the forward acceleration, producing cutoff at a constant altitude as if the airplane were flying at a lower constant Mach number. The caustic is kept up off the ground by an increase in

climb angle with increasing Mach number. Figure 59 gives the required variation of climb angle with Mach number ($n_N = 0$) for cutoff at several constant altitudes above the ground for an airplane above 11 km (36 000 ft) in the *1962 U.S. Standard Atmosphere.* Mach numbers and climb angles for cutoff at various altitudes above ground can also be determined from these data.

The first part of the maneuver should now be clear. At some Mach number below the threshold value a pullup is initiated to keep the caustic up off the ground and to allow acceleration past the threshold Mach number. At some point, however, the pullup must be terminated. The manner in which it is terminated is crucial; a simple termination of the pullup is not sufficient since a caustic will be produced by the subsequent focusing. The pullup must be followed by a sudden pushover, which produces a sudden decrease in climb angle. The shock wave will thus occur suddenly at the ground and no caustic will form if the pushover and reduction in climb angle are sudden enough (according to Hayes (ref. 18) no caustic will form if the velocity of the caustic over the ground is made to be faster than the speed of sound at ground level).

A specific maneuver was considered to gain insight into the nature of the shock wave when it first appears at the ground due to the sudden pushover. For simplicity, an airplane accelerating from Mach 1.0 in level flight at 11 278 m (37 000 ft) in the standard atmosphere was considered. Before the threshold Mach number of 1.153 is reached, a pullup is initiated to promote cutoff and to allow acceleration to about Mach 1.18. The sudden pushover then produces a lower climb angle and the first boom on the ground. The forward acceleration is also reduced so that it is low enough for no caustic to form at the higher Mach numbers. The Mach number, climb angle profile for this maneuver is given in figure 59. The resulting shock wave patterns in the vertical plane and horizontal (ground) plane are given in figure 60 for the region where the shock wave first reaches the ground. This should be compared with the case of a normal acceleration in figures 57 and 58. A detailed comparison of the shock fronts for a normal 0.04 g acceleration and the caustic-elimination maneuver is given in figure 61. Note that the 0.04 g acceleration caustic is formed by the focusing produced over a significant portion of the flight path. On the other hand, the shock waves for the caustic-elimination maneuver must be very weak since they are produced over a short flight path interval and stretched over a large depth of the atmosphere.

In considering this maneuver for commercial SST operation, several problems are evident. First is the consideration of the thrust required to perform the transition maneuver. For the maneuver as given in figure 52, the maximum (T-D)/W is about 0.07 at about Mach 1.175. This thrust margin is probably excessive for a production model of a commercial SST. On the other hand, the caustic-elimination maneuver of figure 52 has not been optimized for minimum thrust margin. A related consideration is the procedure and methods for performing the maneuver and correlating the changes in forward acceleration and climb angle. As suggested by Hayes in ref. 18 this will probably have to be done by use of a simple computer using information on airplane altitude, Mach number,

climb angle, and acceleration vector. Probably the most crucial problem is the fact that the pullup must be initiated just before the threshold Mach number is reached. Since the threshold Mach number can vary from 1.0 to over 1.3, depending on the particular meteorological conditions between the airplane and the ground, the beginning of the transition maneuver must vary accordingly. The "suddenness" of the change in climb angle during the pushover that is required to produce no caustic also needs to be defined. Thus, more study is required to assess the feasibility of the transition maneuver for commercial SST operation.

CONCLUSIONS

Sonic boom characteristics near the shock wave extremity for several types of flight conditions have been more clearly defined by the detailed analysis of the 1970 BREN tower test program. The major results of the analysis are summarized in this section for the low-altitude near-sonic flights, the threshold Mach number flights, and the longitudinal acceleration flights. The lateral cutoff flight test data were not considered in the present study; those results can be found in references 2 and 3.

The detailed analysis of the low-altitude transonic flight test data has indicated that the prevailing meteorological conditions influence the vertical extent of attached shock waves produced during near-sonic flight. At Mach 0.98, the lower extremity of the shock wave on one flight extended to 480 m (1600 ft) beneath the airplane, while under different meteorological conditions it extended to only about 170 m (560 ft). The airplane Mach number has a direct influence on the vertical extent of attached shock waves; for airplane Mach numbers less than 0.98, the shock waves probably did not extend much more than about 100 m (300 ft) beneath the airplane. The extension of attached shock waves to lower altitudes may explain several "accidental" sonic booms produced by low-altitude, marginally subsonic airplanes (although Machmeter and altimeter errors may also be responsible).

A theoretical safe altitude for sonic boom cutoff during threshold Mach number flight has been shown to be valid within experimental accuracy over a wide range of meteorological conditions. Thus, it should be possible to estimate reasonably well the buffer zone depth (or ground speed reduction) for any airplane and meteorological condition. For cutoff at or above the safe altitude, average maximum free air overpressures of the pressure waves were less than 10 N/m^2 (0.2 lb/ft^2). In some cases, very low intensity acoustic waves (< 4.0 N/m^2 (0.1 lb/ft^2)) propagated to the ground, even though cutoff apparently occurred several kilometers above the ground. Pressure signatures in the vicinity of the caustic exhibit the U-wave rather the N-wave shape. Below cutoff, rounded, low-magnitude acoustic waves occurred. Comparison of a recent theoretical method for calculating the acoustic pressure waves below the threshold Mach number caustic showed excellent agreement with observation near the caustic. Various operational aspects of threshold Mach number operation were considered and problem areas were discussed. These included the use of airplane ground speed for speed specification (instead of Mach number), various meteorological effects, airplane systems, and methods for calculating the speed safety factor.

The analysis of caustics produced by low-magnitude accelerations during flight at Mach numbers slightly greater than the threshold Mach number showed that folds and associated caustics were produced by slight changes in the airplane ground speed. Changes in airplane ground speed were of the order of 3 to 10 m/sec (10 to 30 ft/sec), most likely due to changes in throttle setting as

the pilot attempted to maintain constant Mach number. For these cases, the Mach numbers flown were generally greater than the threshold Mach number. In several cases, it was possible to correlate the airplane acceleration magnitude with the measured caustic on the tower. These results indicate an increase in caustic intensity with increasing acceleration. Caustic intensities ranged from one to three times the nominal, steady, level flight intensity. The wave folding produced by airplane ground speed changes explains the observed multiple shock waves on the BREN tower for the cases considered and tends to verify recent theoretical work which has shown that wave folding occurs for weak shocks.

The analysis of caustics produced by longitudinal accelerations from subsonic to supersonic speeds has shown that, for these cases, acceleration magnitude appears to have an effect on caustic intensity. The maximum caustic intensity observed was about five times the nominal, steady, level overpressure and was produced by an acceleration of 1.5 m/sec^2 (4.9 ft/sec^2). Calculated theoretical shock wave profiles agree reasonably well with the observed shock wave locations and help to illustrate the focusing effect near caustics. The observed pressure signatures are documented in detail.

In conjunction with the analysis of the experimental data, methods to alleviate the caustic produced during the acceleration from subsonic to supersonic speeds were considered. Caustic strength seems to be a function of acceleration magnitude, therefore, low-magnitude acceleration may provide some alleviation of caustic intensity. The limited experimental data suggest an amplification of about 2 for an acceleration magnitude of about 0.3 m/sec^2 (1.0 ft/sec^2), about 1/5 the normal values. In addition, a maneuver was investigated that was designed to eliminate the caustic produced during the acceleration from subsonic to supersonic speeds. Although the maneuver shows promise, further study is needed to determine its feasibility for commercial SST operation.

APPENDIX A

SONIC BOOM GENERATION DURING CRUISE SLIGHTLY BELOW MACH 1.0

This appendix contains a discussion of the possibility of sonic boom generation during cruise slightly below Mach 1.0. Barger (ref. 4) has theorized that it may be possible for a slightly subsonic airplane to generate a sonic boom if certain meteorological conditions exist below the airplane. It would appear to be highly unlikely, however, that meteorological conditions alone could produce shock waves. A necessary condition is that there must be local shock waves present due to local supersonic flow over portions of the subsonic airplane. The criterion for subsonic sonic boom is developed in this appendix from the definition of the threshold Mach number. This criterion is more general and simpler than the one developed in reference 4. The possibility of subsonic sonic boom is then evaluated in relation to the 1970 low-altitude near-sonic flight tests over the BREN tower.

The threshold Mach number has been defined to be the maximum airplane Mach number for which complete shock wave refraction can occur at or above the ground. For cutoff directly beneath the airplane, the equation defining the threshold Mach number is:

$$M_T = (1/a_o) \left\{ [a(z) - u_n(z)]_{max} + u_{n_o} \right\} \tag{A1}$$

where

M_T = threshold Mach number

z = altitude

$a(z)$ = speed of sound at altitude z

$u_n(z)$ = wind component of altitude z parallel to flight path (tailwind is negative)

$[a(z) - u_n(z)]_{max}$ = $V_{p_{max}}$ = maximum shock propagation speed between the airplane and the ground in the direction of flight, with a(z) and u(z) taken at the same altitude

a_o = sound speed at airplane

u_{n_o} = wind speed at airplane (tailwind is negative)

Equation (A1) can be rewritten as

$$V_G = (M_T(a_o) - u_{n_o} = [a(z) - u_n(z)]_{max} \tag{A2}$$

A sonic boom is observed at the ground when the airplane ground speed is greater than the maximum shock wave propagation speed. A solution exists to equation (A2), however, when the Mach number, M_T, is less than 1.0. This occurs when u_{n_o} and a_o are large enough so that the airplane ground speed is equal to $[a(z) + u_n(z)]_{max}$, although M_T is less than 1.0. This can occur with a strong tailwind at the airplane (negative u_{n_o}). The criterion for subsonic sonic boom is simply

$$(1/a_o)\,[a(z) - u_n(z) + u_{n_o}] \leq M_{SB} < 1.0 \tag{A3}$$

where M_{SB} is the lowest Mach number for which subsonic sonic boom can occur.

Since sound speed gradients associated with temperature inversions are normally small, wind gradients are most important. Under constant (or nearly constant) temperature conditions equation (A3) reduces to

$$M_{SB} > 1 + [u_{n_o} - u_n(z)]/a_o \tag{A4}$$

or

$$(1 - M_{SB}) < [u_n(z) - u_{n_o}]/a_o \tag{A5}$$

Equation (A5) is slightly different from equation (4) of reference 4. In the notation used here, equation (4) of reference 4 is $(1 - M_{SB}) < [u_n(z) - u_{n_o}]/(2\,a_o)$. This result is in error since $\cos\gamma$ was assumed constant and should have been treated as a variable with altitude. When this correction is made in the analysis of reference 4 the results then agree.

For M less than 1.0, equation (A5) gives $u_n(z) > u_{n_o}$. Since a positive u_n is a headwind this criterion physically means that the headwind must increase with decreasing altitude from the airplane to the ground, or alternatively, a tailwind must decrease from the airplane toward the ground. For a no-wind condition equation (A3) becomes simply $a(z)/a_o \leq M_{SB} < 1.0$ or $a(z) < a_o$. This condition is called a temperature inversion.

TABLE 7.–COMPARISON OF THEORETICAL MACH NUMBER AND WIND GRADIENT REQUIRED FOR SUBSONIC BOOM WITH OBSERVATION

Pass	Theoretical wind change required for subsonic boom in presence of temperature gradient, $u_n(z) - u_{n_o}$		Observed wind change from airplane to tower top, $u_n(z)_{top} - u_{n_o}$		Theoretical lowest Mach number for subsonic boom, M_{SB}	Pilot-read mach number, M_o	Character of observed boom
	m/sec	ft/sec	m/sec	ft/sec			
071	[a] 7.4	[a] 24.1	2.9	9.5	[b] 0.993	0.98	Boom
072	11.1	36.4	2.1	6.9	0.996	0.97	Rumble
073	7.4	24.1	-0.1	-0.3	1.0018	0.98	Boom
074	4.4	14.5	0.9	3.0	1.0003	0.99	Boom
075	7.8	25.5	0.3	1.0	1.0035	0.98	Engine Noise
076	1.0	3.3	-0.1	-0.3	1.0026	1.00	Boom

[a] Theoretical wind change calculated from $u_n(z) - u_{n_o} = a(z) - a_o M_o$

[b] Theoretical M_{SB} calculated from $M_{SB} \geq (1/a_o)\left[a(z) - u_n(z) + u_{n_o}\right]$

The above criterion does not necessarily mean that shock waves can be produced for all subsonic Mach numbers even if correct temperature and wind conditions occur. To determine the validity of this mechanism for producing sonic boom, the data from the 1970 BREN tower transonic tests were evaluated. The calculated required Mach number and wind increments are given in table 7. For passes 071 and 072, comparison with the observed Mach number and wind increments show that by this criterion sonic booms should not have been observed since the airplane Mach numbers were too low. For passes 073 through 076, the atmospheric gradients were not favorable so again booms should not have occurred, yet booms were observed in three of the four cases. It must be concluded that this mechanism was not important during these tests but that the local shock waves produced by local regions of supersonic flow over the airplane are much more important. It appears to be highly unlikely that atmospheric gradients *alone* can produce shock waves. If shock waves are present, however (due to local supersonic flow over portions of a subsonic airplane), the shock waves may be refracted and propagated toward the ground by these special meteorological conditions. The meteorological conditions specified by the above criterion are precisely those that will refract shock waves toward the ground once they have been produced during near-sonic flight. This refraction of local shock waves (rather than production of shock waves by the atmospheric gradients) may account for inadvertent sonic booms that have occurred in the past where the pilots have believed that they were flying at a low enough Mach number to avoid sonic booms on the ground (Machmeter and/or altimeter inaccuracy could also explain some of the "accidental" boom occurrences).

APPENDIX B

ACOUSTIC BEHAVIOR OF A DISCONTINUOUS SIGNAL NEAR A CAUSTIC

K.-Y. Fung and A. R. Seebass

A recently developed theoretical method for calculating the acoustic pressure field below the threshold Mach number caustic is presented in this appendix. Results are given for an incoming N-wave for the BREN tower flight test conditions.

The equation that describes the behavior of a weak, discontinuous pressure signal near a caustic has been formulated by Guiraud (ref. 9) and Hayes (ref. 10). This equation is nonlinear and consequently difficult to solve. While the linear version of this equation can be solved by Fourier transforms as well as by other means, the resulting solution, while physically simple, is represented by a complicated combination of hypergeometric functions. This linear solution becomes algebraically singular as the signal approaches the caustic and gives rise to a reflected signal that is logarithmically singular.

Because the signal amplifies without limit as it approaches the caustic in the linear theory, it is clear that a nonlinear description is essential. Efforts to determine this nonlinear behavior have met with only partial success (refs. 11, 12, and 19). From these results we can deduce that a shock wave terminates in a weak compression that is formed by coalescing compression waves emanating from a distorted "sonic" line. The sonic line itself runs into this compression; above the junction with the sonic line, the shock becomes stronger and nearly normal; behind this normal portion of the shock the flow is subsonic and a coordinate system fixed to the shock. This normal shock presumably joins the incoming and reflected wave at a single point. The variation of the jump in pressure coefficient through the reflected shock, estimated by Gill (ref. 19), is depicted in figure 62.

It has not been possible to determine the precise details of this nonlinear behavior from field measurements, such as those given in this report or those by Wanner, et al. (refs. 13 and 20), because of practical limits on the spatial resolution obtainable in such tests. Indeed, even laboratory tests (refs. 21 and 22) have not yet achieved the resolution necessary to delineate this structure clearly. Nonlinear effects are, of course, noticeable in the measurements. For example, in the French flight tests, the asymmetry in the reflected wave due to nonlinear steepening can easily be discerned. The linear solution appropriate to the incoming signal usually gives a good representation of the signal on the scales used in experimental measurements, even for the reflected wave, which the linear theory says is logarithmically singular. (Because a logarithmic singularity is a weak one, it appears

---

The research upon which this appendix is based was supported by the NASA through Grant NGR-33-010-054.

finite when plotted at the spatial or temporal resolution typical of experiments.) In addition, below the caustic the signal strength decays rapidly and the signal's evolution may be described by linear equations. Consequently, in this appendix we record the linear solution when the incoming wave is an N-wave.

In dimensional variables the linear solution for threshold operation, in coordinates such that the aircraft's motion is steady, is governed by

$$M^{2'} y \phi_{xx} - \phi_{yy} = 0$$

$$c_p \cong c_{p_N} (y/y_N)^{-1/4} N(x + 2/3 \sqrt{M^{2'}} y^{3/2}) \text{ on } x - 2/3 \sqrt{M^{2'}} y^{3/2} \to \infty \tag{B1}$$

where ϕ is the velocity potential, x the horizontal coordinate decreasing in the direction of flight, y the vertical coordinate, c_p the pressure coefficient, and $M^{2'}$ the vertical gradient of the square of the Mach number, assumed constant. The quantity M is the airplane Mach number based on its ground speed and the ambient sound speed, $M = V/a(z)$. N(t) is the unit N-wave function:

$$N(t) = \begin{cases} 0, & t < -\lambda \\ -t/\lambda, & -\lambda < t < \lambda \\ 0, & t > \lambda \end{cases} \tag{B2}$$

where λ is the half wavelength of the N-wave. The incoming N-wave signal has pressure jumps of magnitude c_{p_N} at

$$x + 2/3 (M^{2'})^{1/2} y^{3/2} = \pm\lambda \text{ for } y = y_N.$$

The solution can be given in terms of hypergeometric functions. This solution, in the nondimensional coordinates x/λ and y/λ, depends upon the single parameter $M^{2'}\lambda$; this is, of course, clear from the above formulation. Typical signatures for three cases are shown (in physical coordinates) in figures 63 through 65. They correspond to $M^{2'}\lambda = 6 \times 10^{-4}$, 11.6×10^{-4}, and 7.8×10^{-4}. For standard day conditions and $\lambda = 23.8$ m (78 ft), $M^{2'}\lambda$ is about 6×10^{-4}

Below the caustic the acoustic signal attenuates both in amplitude and frequency. An observer fixed relative to the ground and situated below the caustic will experience a pressure field given by

$$c_p = c_{p_N} \left[\frac{y}{y_N}\right]^{-1/4} N(Vt/\lambda, 2/3 (M^{2'} |y|^3)^{1/2}/\lambda) \tag{B3}$$

where the nondimensionalized "sound" function N is depicted in figure 66. The maximum pressure that occurs in these signatures is delineated in figure 67 for three values of $M^{2'}\lambda$. Far below the caustic an asymptotic expansion obtains and the pressure decays as $(y/\lambda)^{-13/4}$.

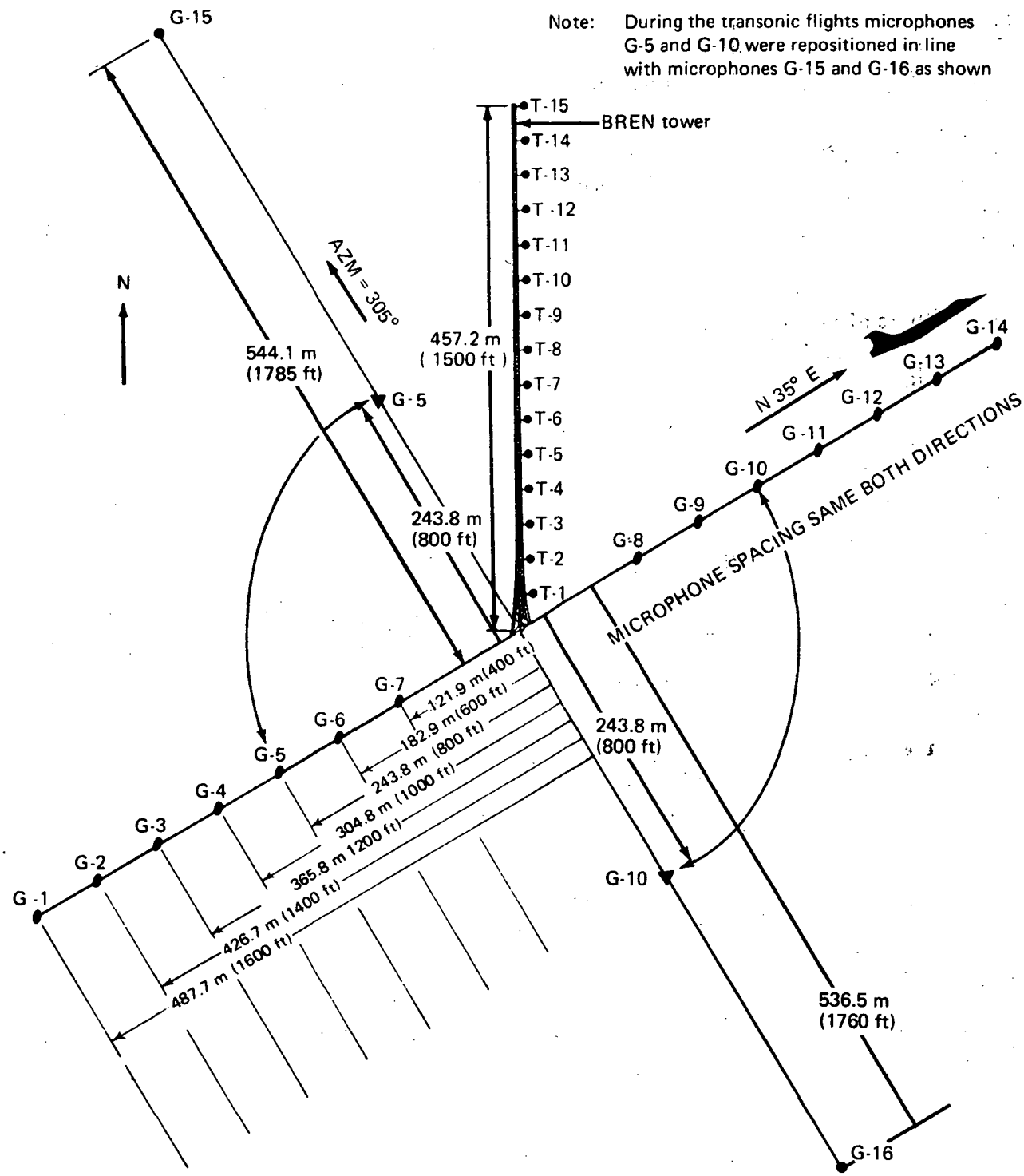

FIGURE 1.—BREN TOWER MICROPHONE ARRAY

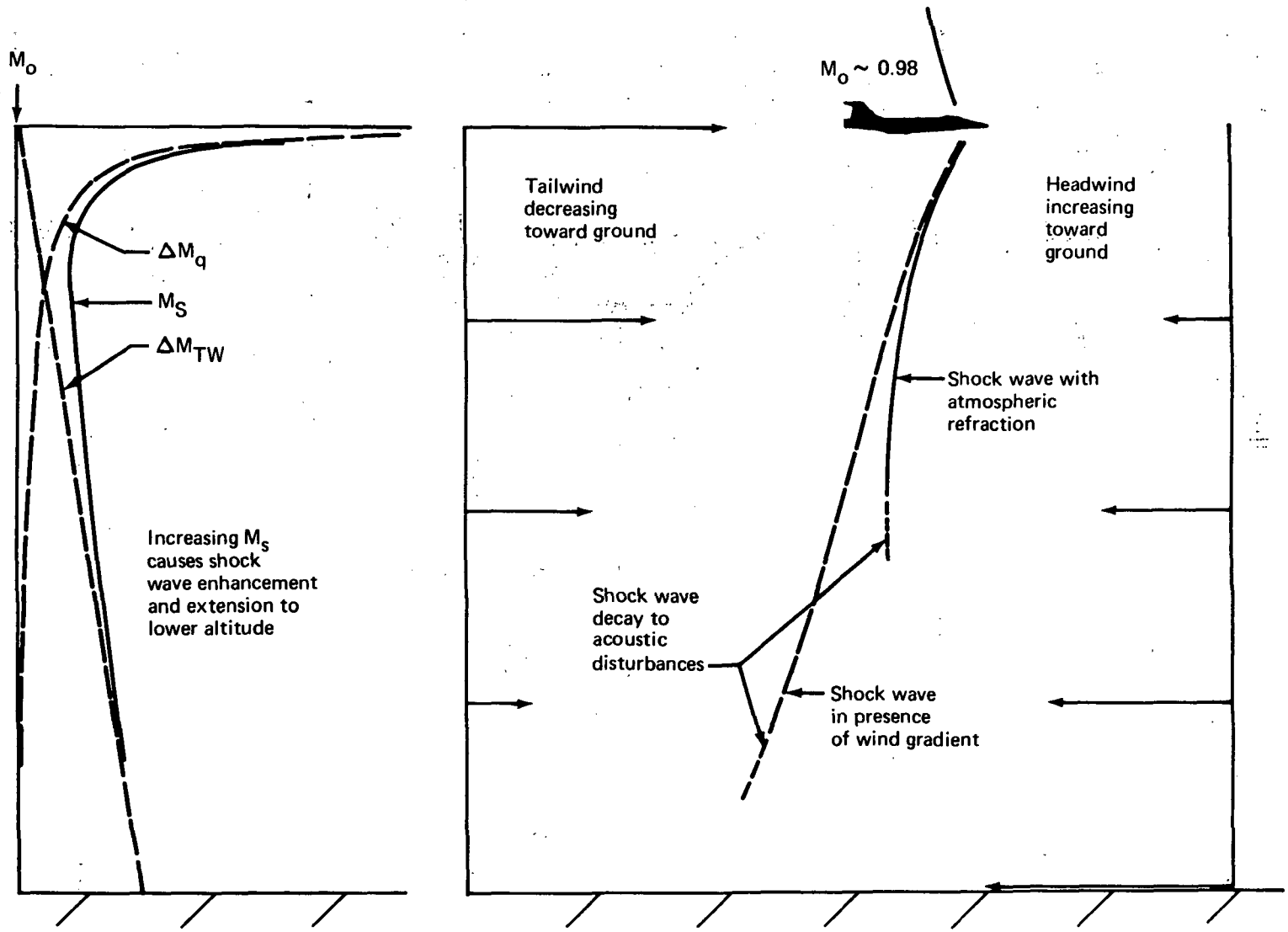

FIGURE 2.–EXTENSION OF ATTACHED SHOCK WAVES TOWARD GROUND BY WIND GRADIENTS DURING NEAR-SONIC FLIGHT

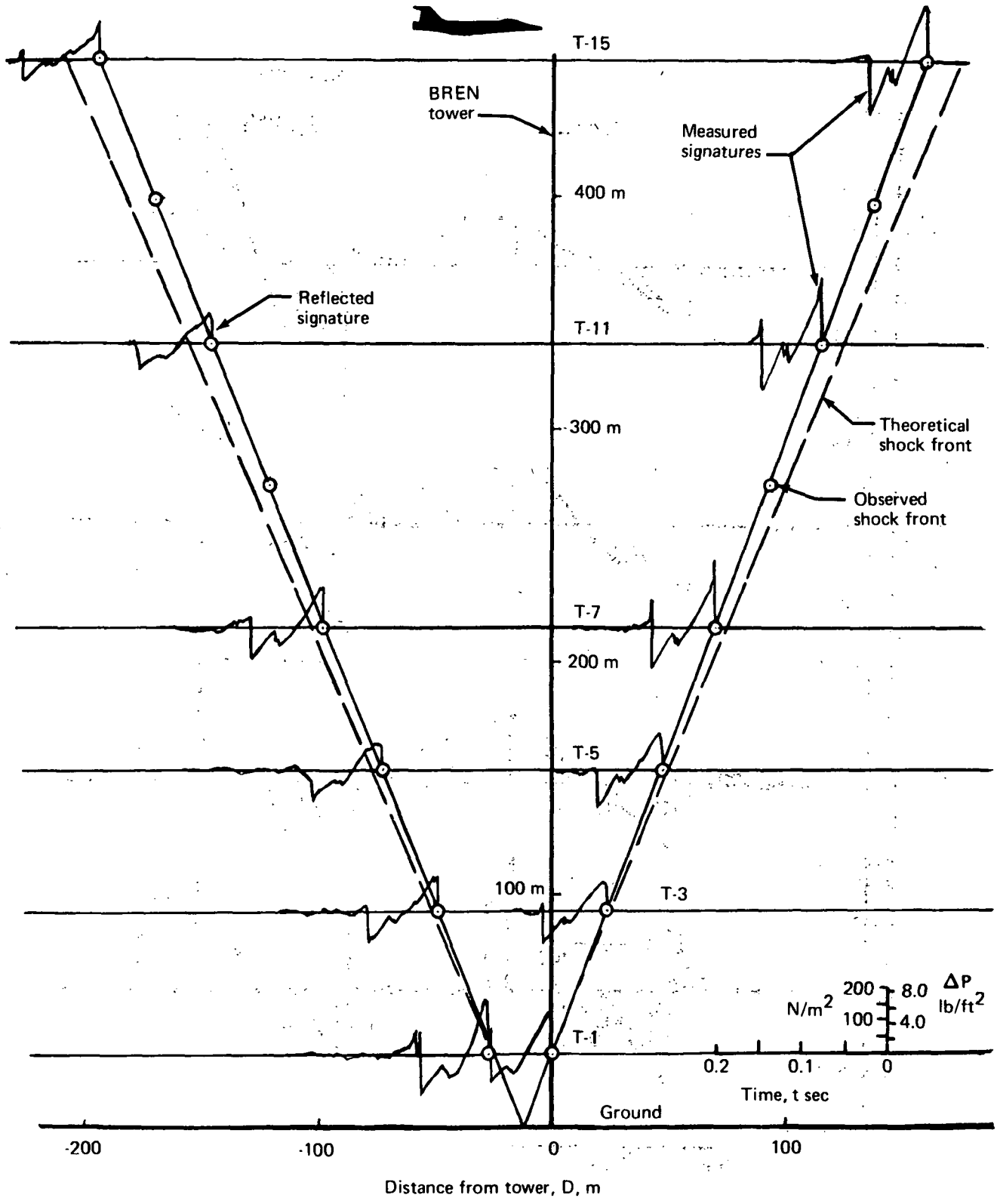

FIGURE 3.–SHOCK WAVE PROFILE AND TOWER PRESSURE SIGNATURES, PASS 070, 1-4, M_o = 1.05, LOW-ALTITUDE NEAR-SONIC FLIGHT

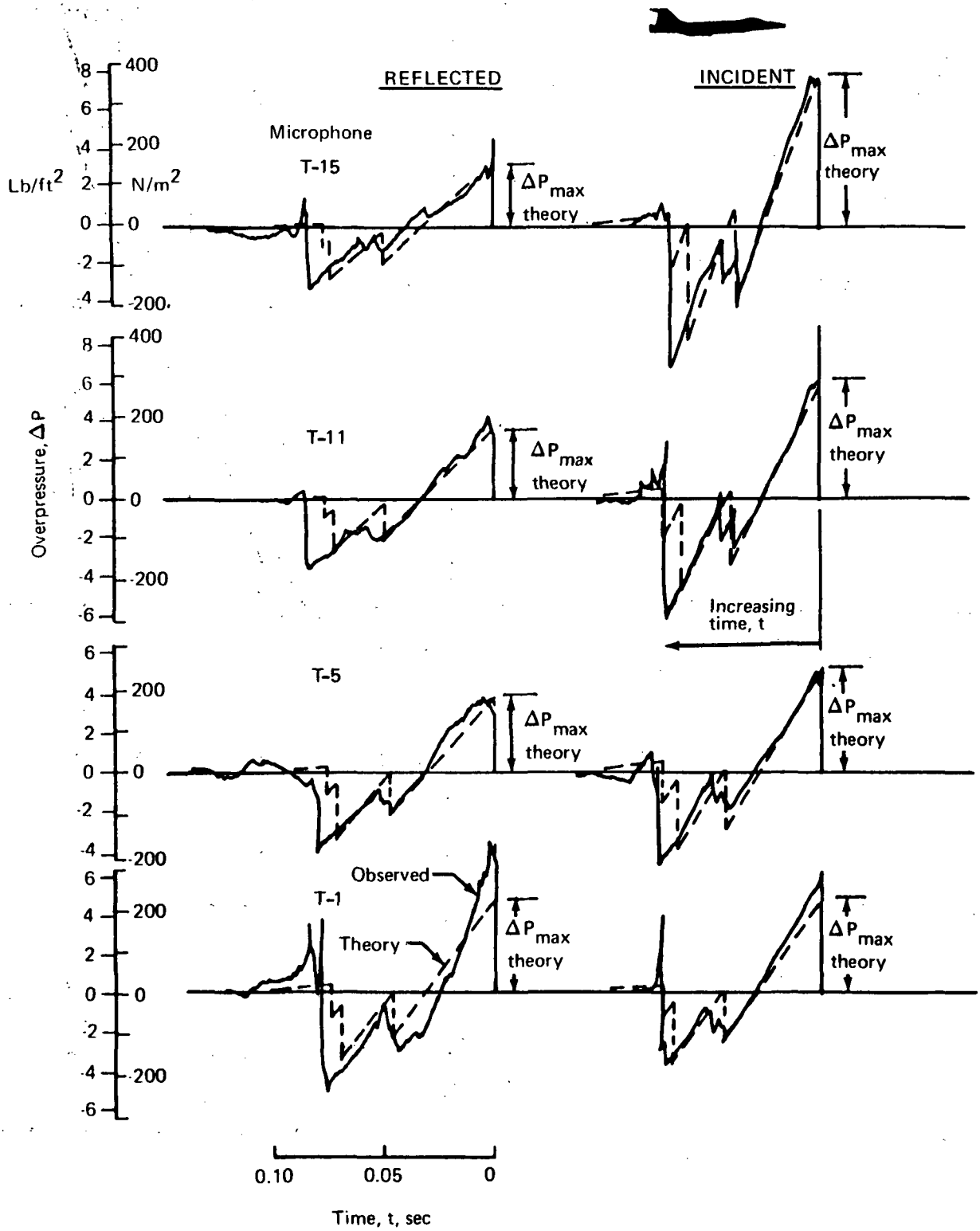

FIGURE 4.–COMPARISON OF CALCULATED AND OBSERVED PRESSURE SIGNATURES FOR PASS 070, M_o = 1.05, LOW-ALTITUDE NEAR-SONIC FLIGHT

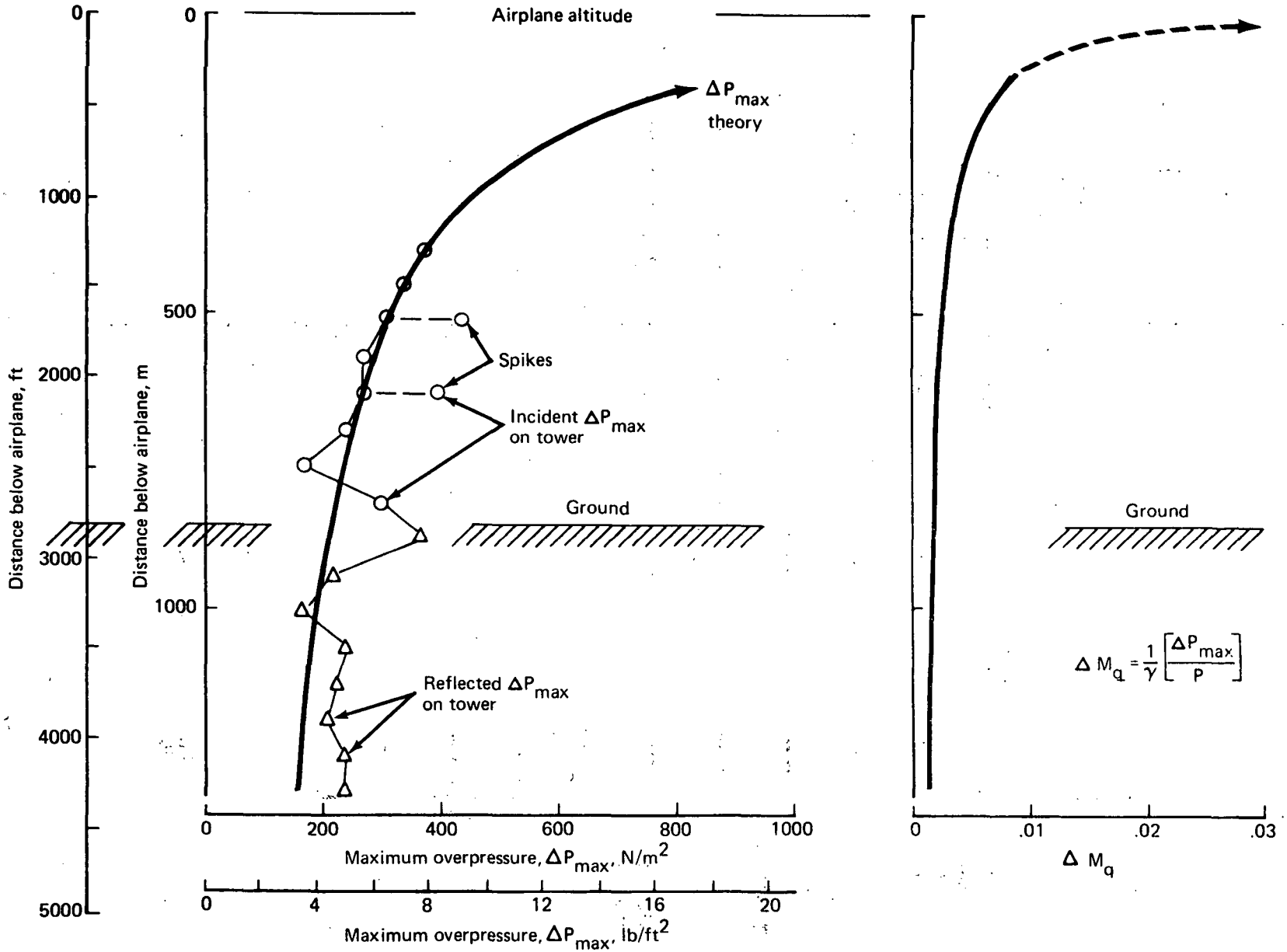

FIGURE 5.—THEORETICAL AND OBSERVED MAXIMUM TOWER OVERPRESSURES AND THEORETICAL ΔM_q FOR PASS 070, LOW-ALTITUDE NEAR-SONIC FLIGHT

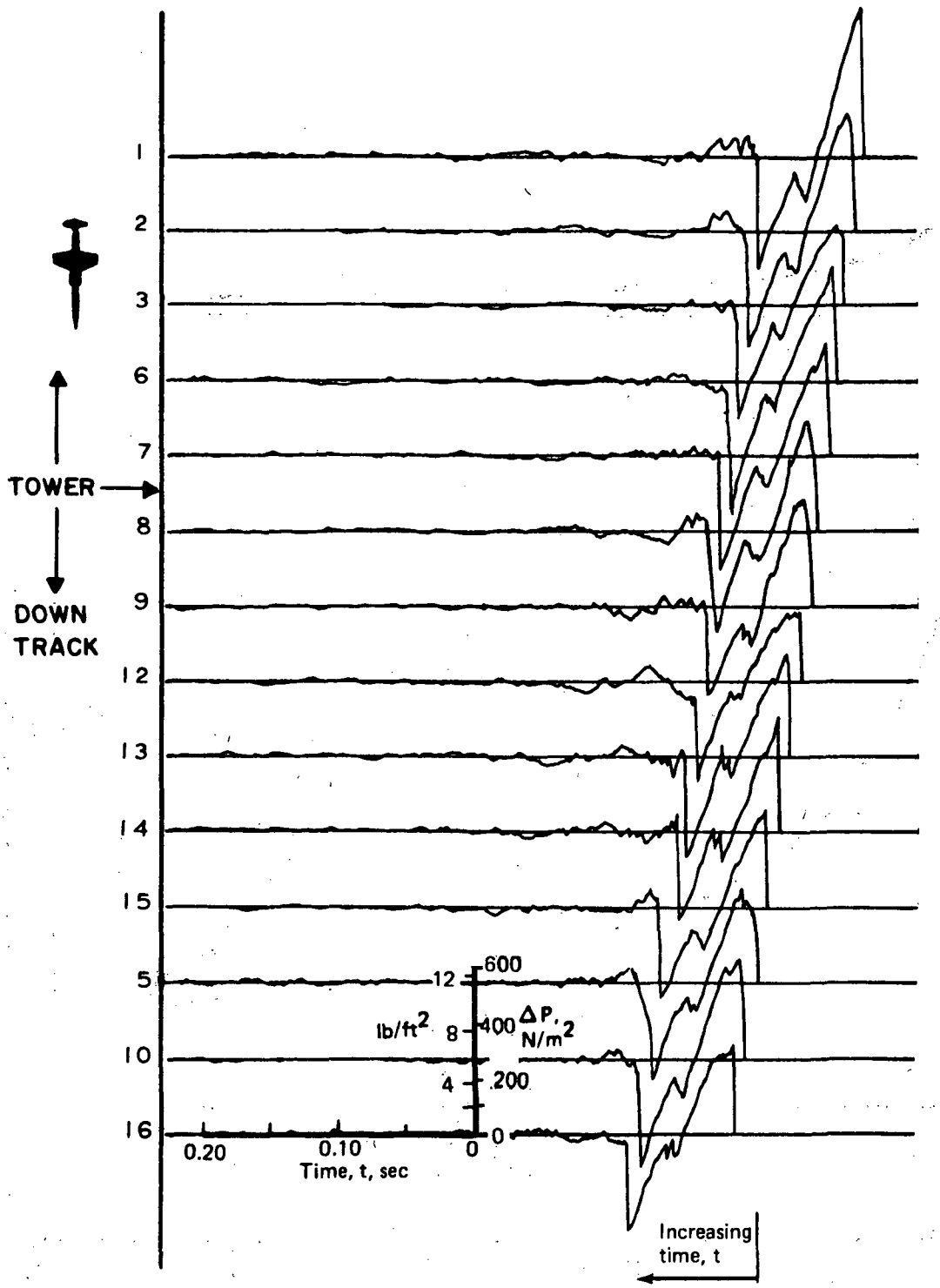

FIGURE 6.—GROUND PRESSURE SIGNATURES FOR PASS 070, M_o = 1.05, LOW-ALTITUDE NEAR-SONIC FLIGHT

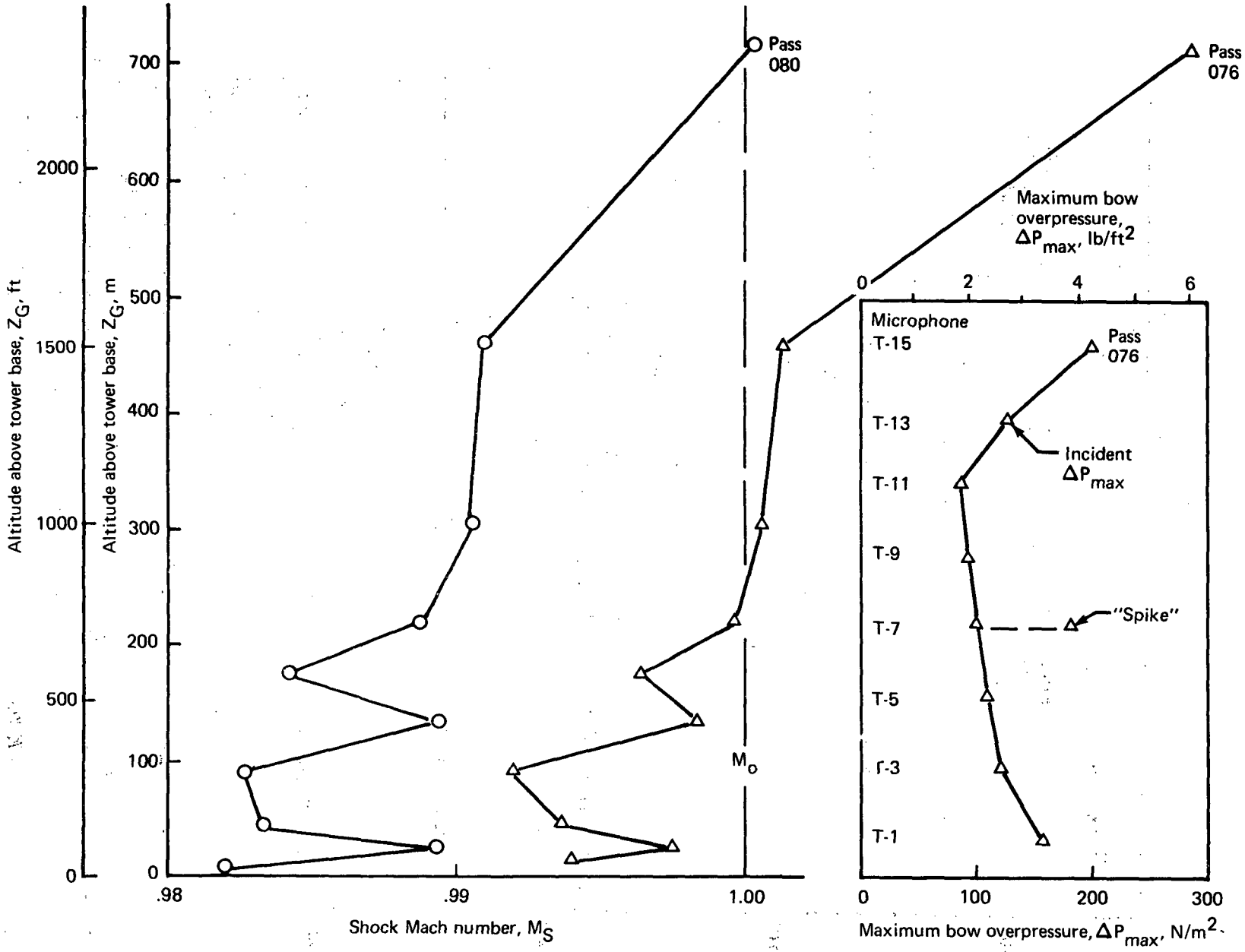

FIGURE 7.–SHOCK MACH NUMBER PROFILES FOR PASSES 076 AND 080, M_o = 1.00, LOW-ALTITUDE NEAR-SONIC FLIGHT

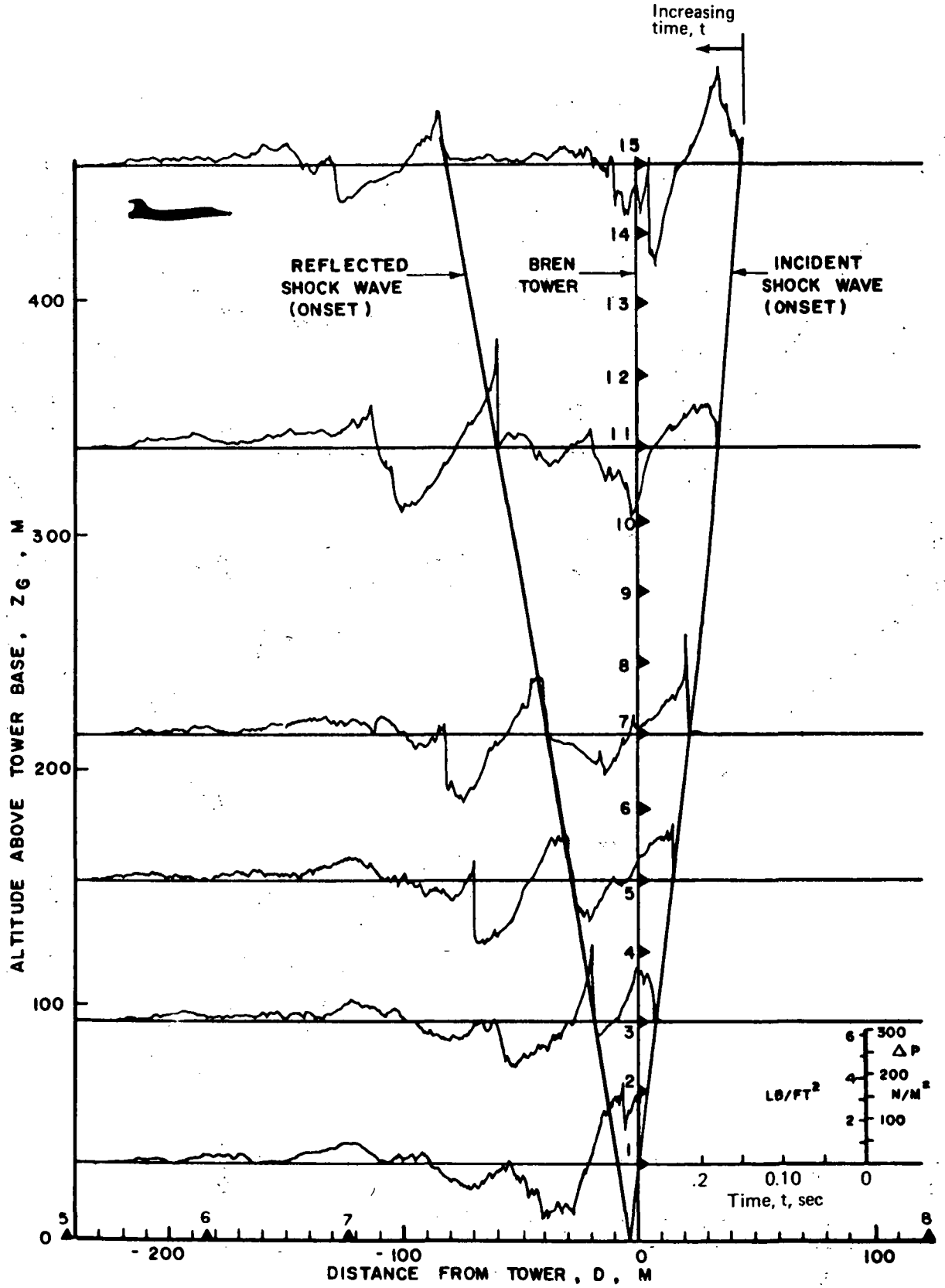

FIGURE 8.—SHOCK WAVE PROFILE AND TOWER PRESSURE SIGNATURES FOR PASS 076, M_O = 1.00, LOW-ALTITUDE NEAR-SONIC FLIGHT

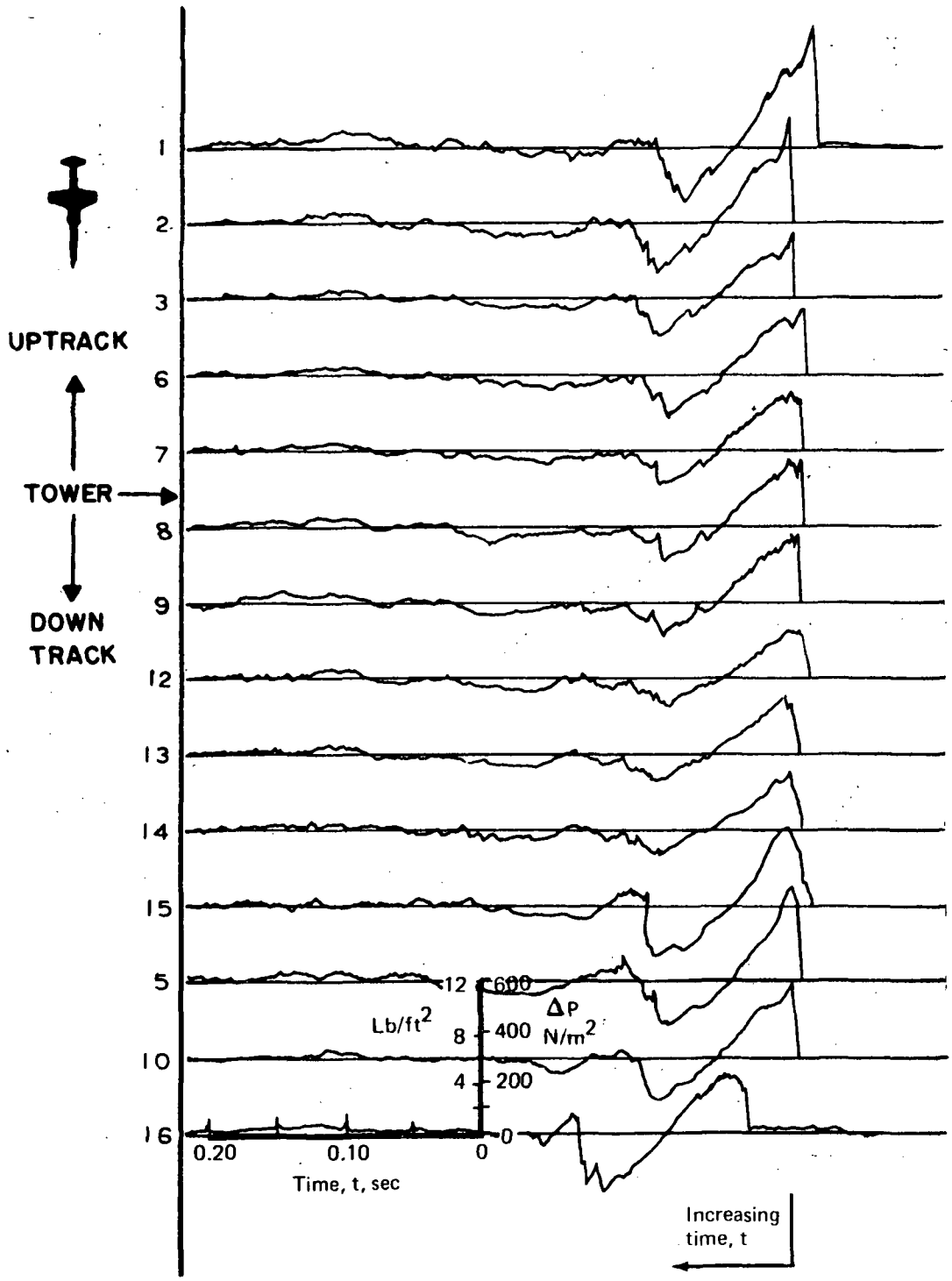

FIGURE 9.—GROUND PRESSURE SIGNATURES FOR PASS 076, M_o = 1.00, LOW-ALTITUDE NEAR-SONIC FLIGHT

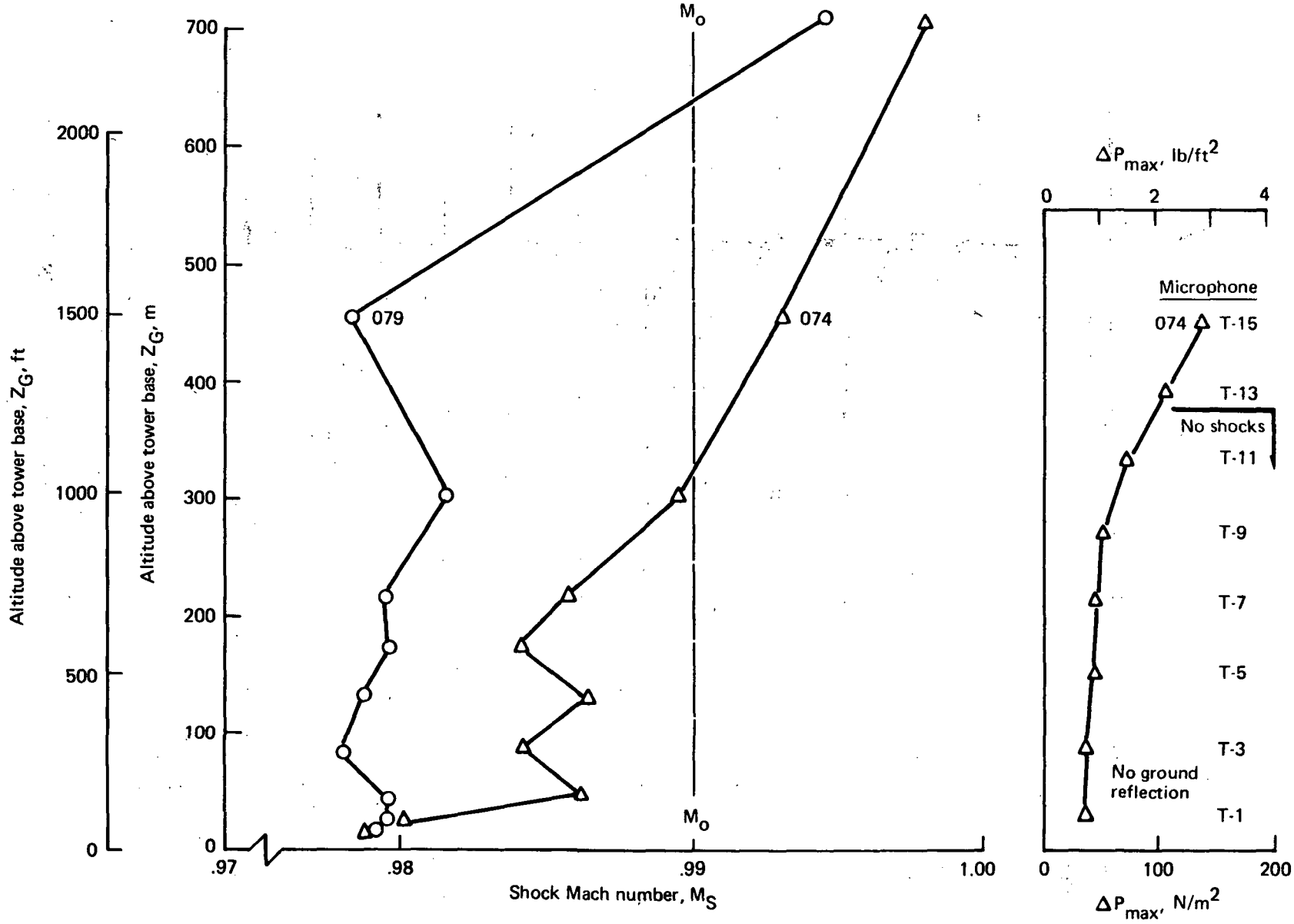

FIGURE 10.–SHOCK MACH NUMBER PROFILES FOR PASSES 074 AND 079, M_o = 0.99, LOW-ALTITUDE NEAR-SONIC FLIGHT

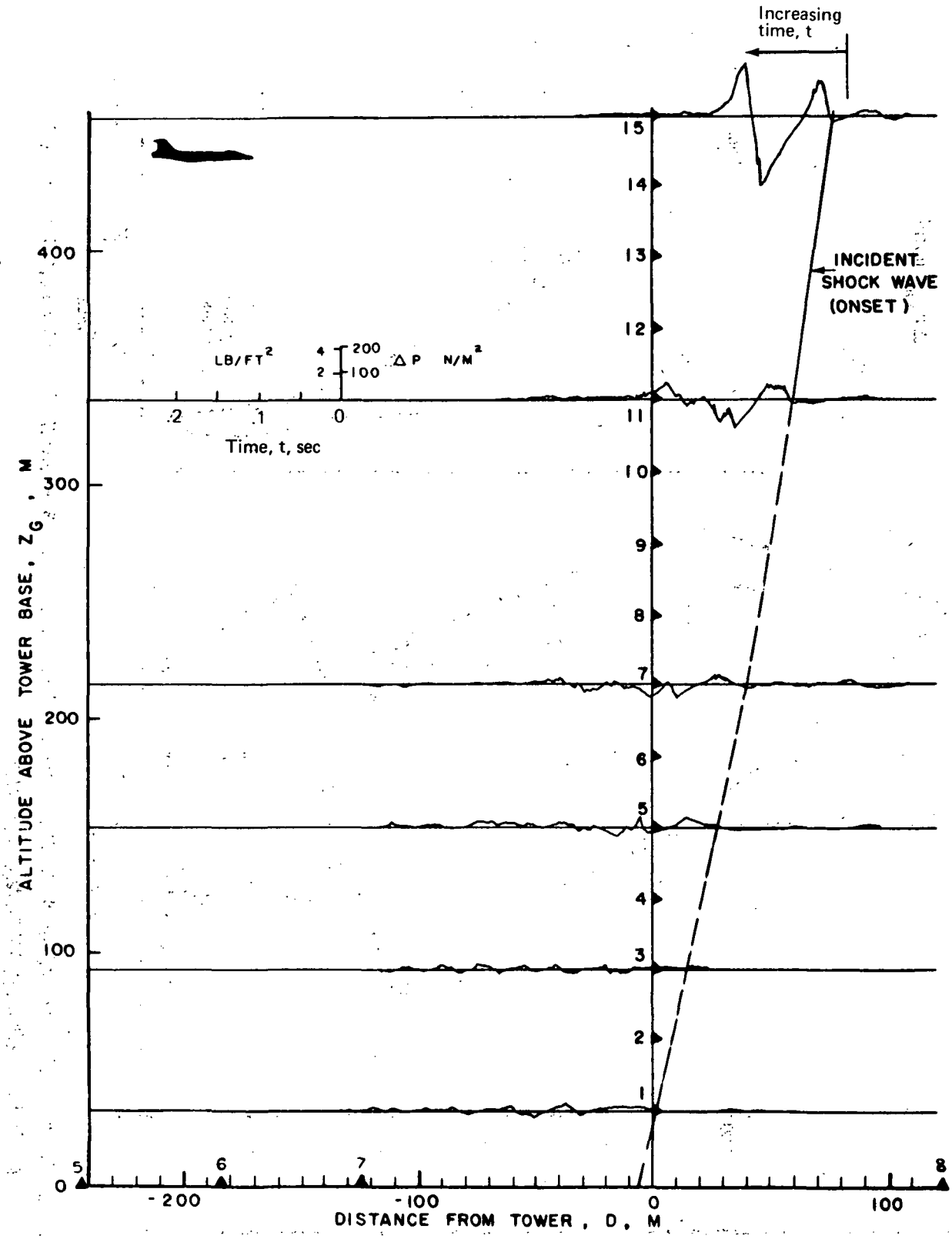

FIGURE 11.—SHOCK WAVE PROFILE AND TOWER PRESSURE SIGNATURES FOR PASS 074, M_O = 0.99, LOW-ALTITUDE NEAR-SONIC FLIGHT

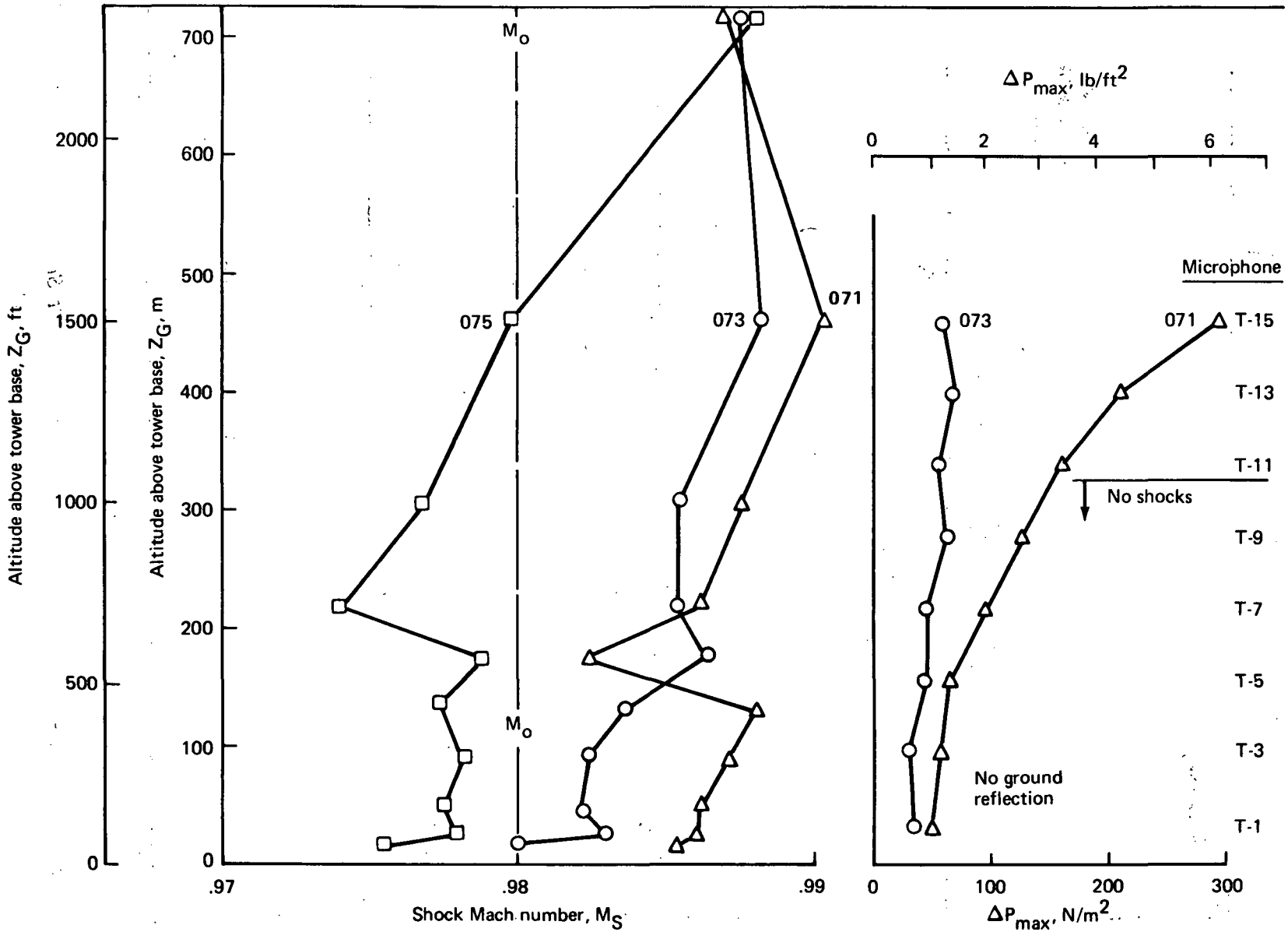

FIGURE 12.—SHOCK MACH NUMBER AND OVERPRESSURE PROFILES FOR PASSES 071, 073, and 075, M_O = 0.98, LOW-ALTITUDE NEAR-SONIC FLIGHT

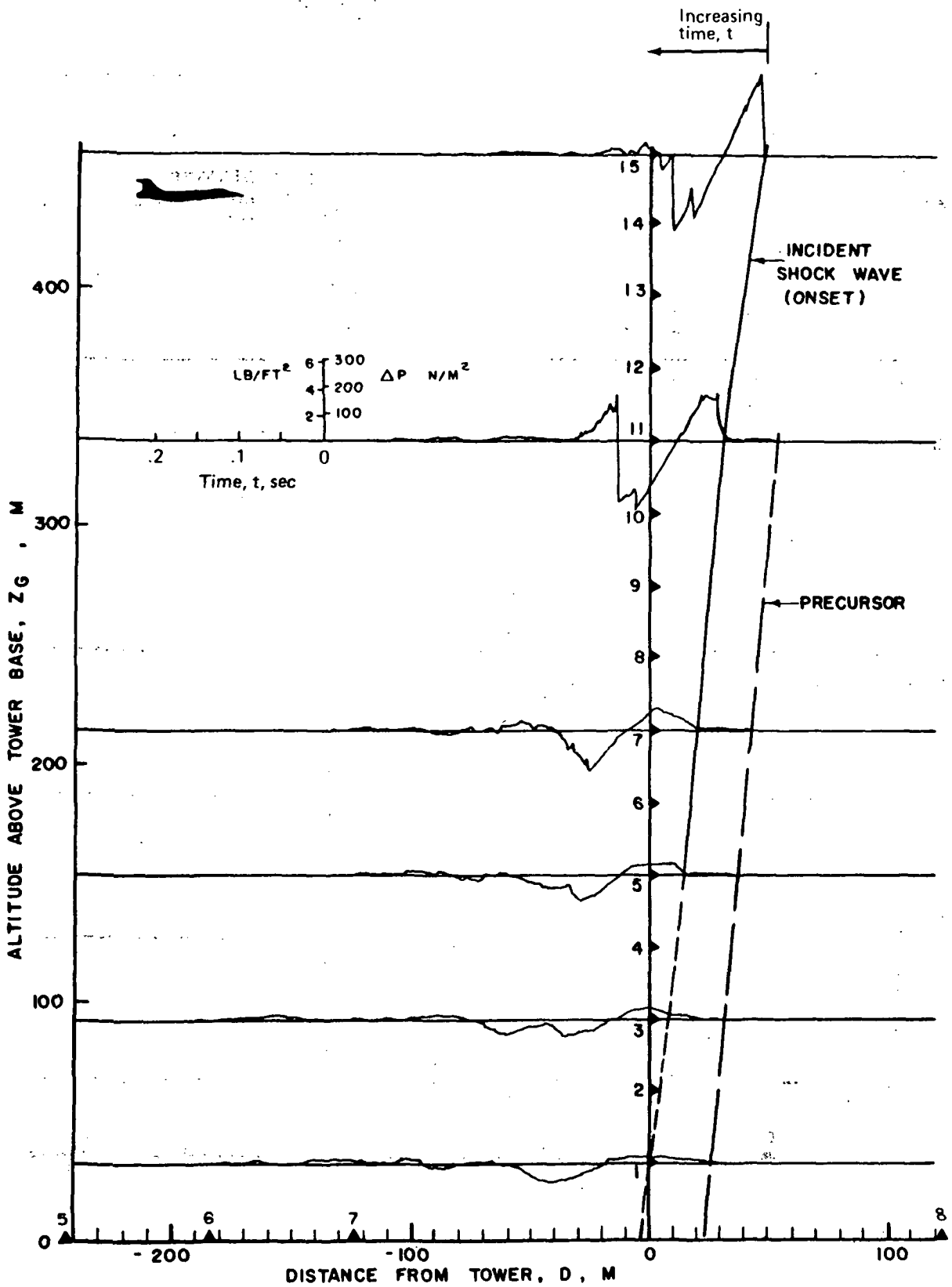

FIGURE 13.—SHOCK WAVE PROFILE AND TOWER PRESSURE SIGNATURES FOR PASS 071, M_0 = 0.98, LOW-ALTITUDE NEAR-SONIC FLIGHT

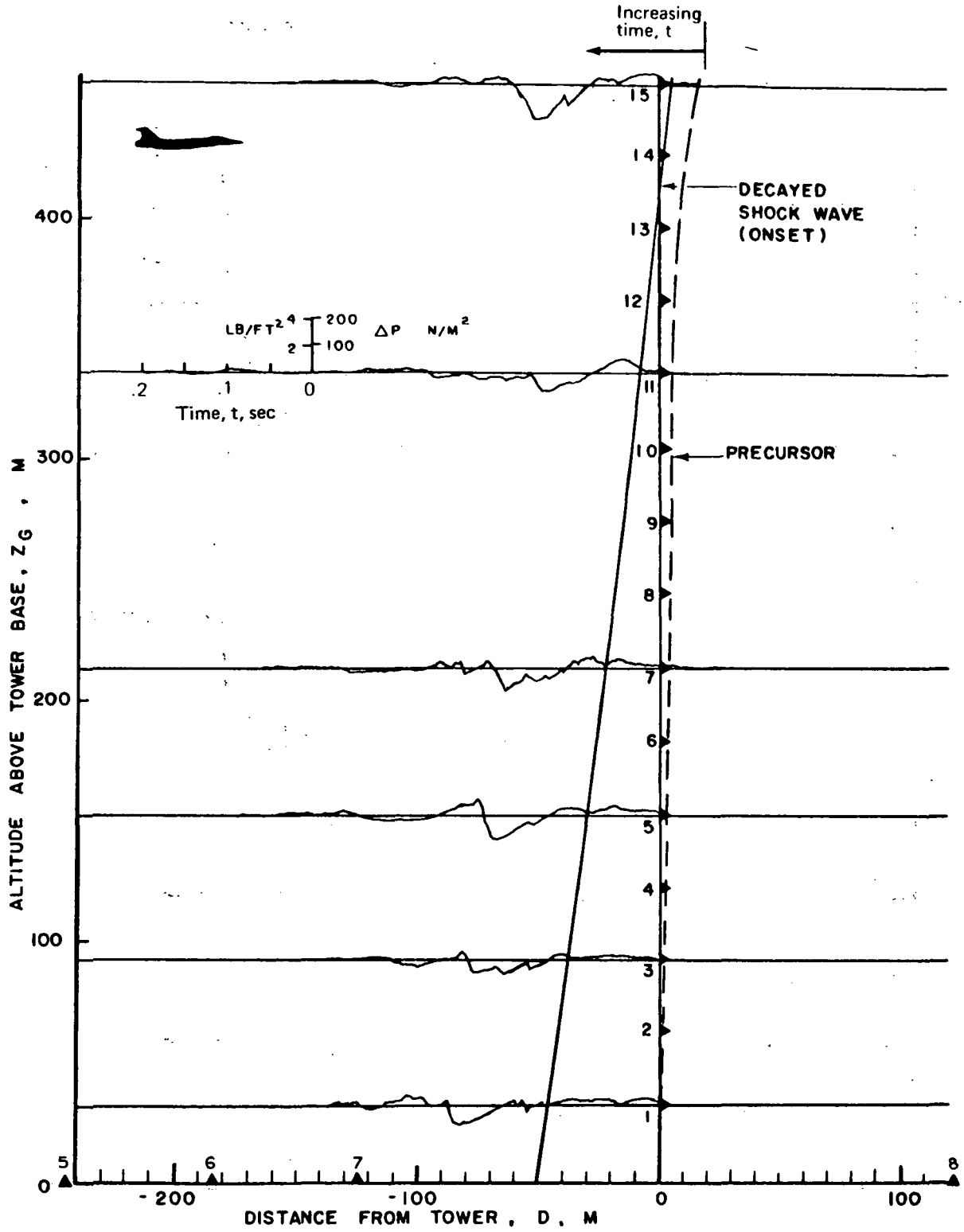

FIGURE 14.—SHOCK WAVE PROFILE AND TOWER PRESSURE SIGNATURES FOR PASS 073, M_O = 0.98, LOW-ALTITUDE NEAR-SONIC FLIGHT

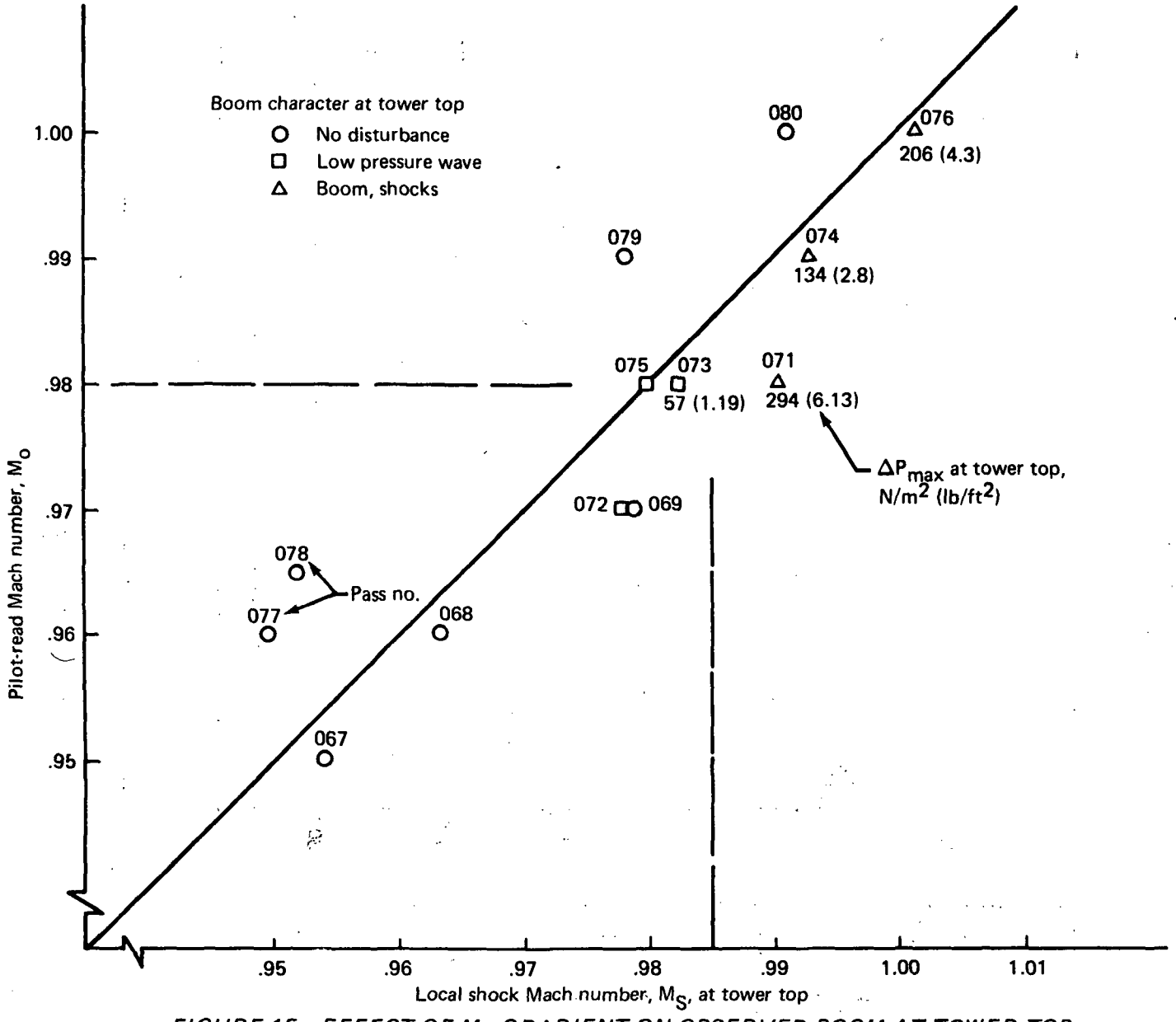

FIGURE 15.–EFFECT OF M_S GRADIENT ON OBSERVED BOOM AT TOWER TOP DURING LOW-ALTITUDE NEAR-SONIC FLIGHT

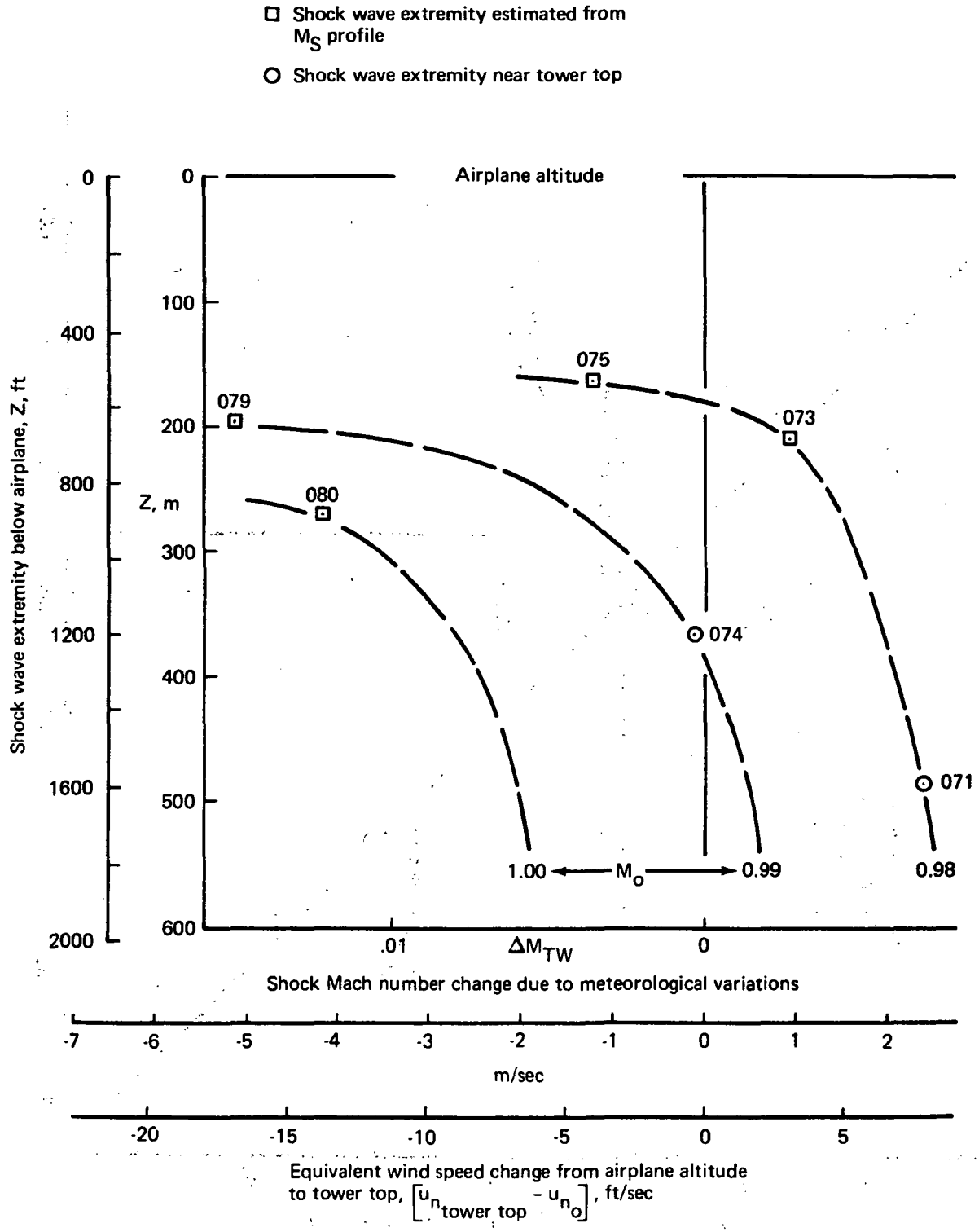

FIGURE 16.—EFFECT OF METEOROLOGICAL CONDITIONS ON SHOCK WAVE EXTREMITY OF ATTACHED SHOCKS DURING LOW-ALTITUDE NEAR-SONIC FLIGHT

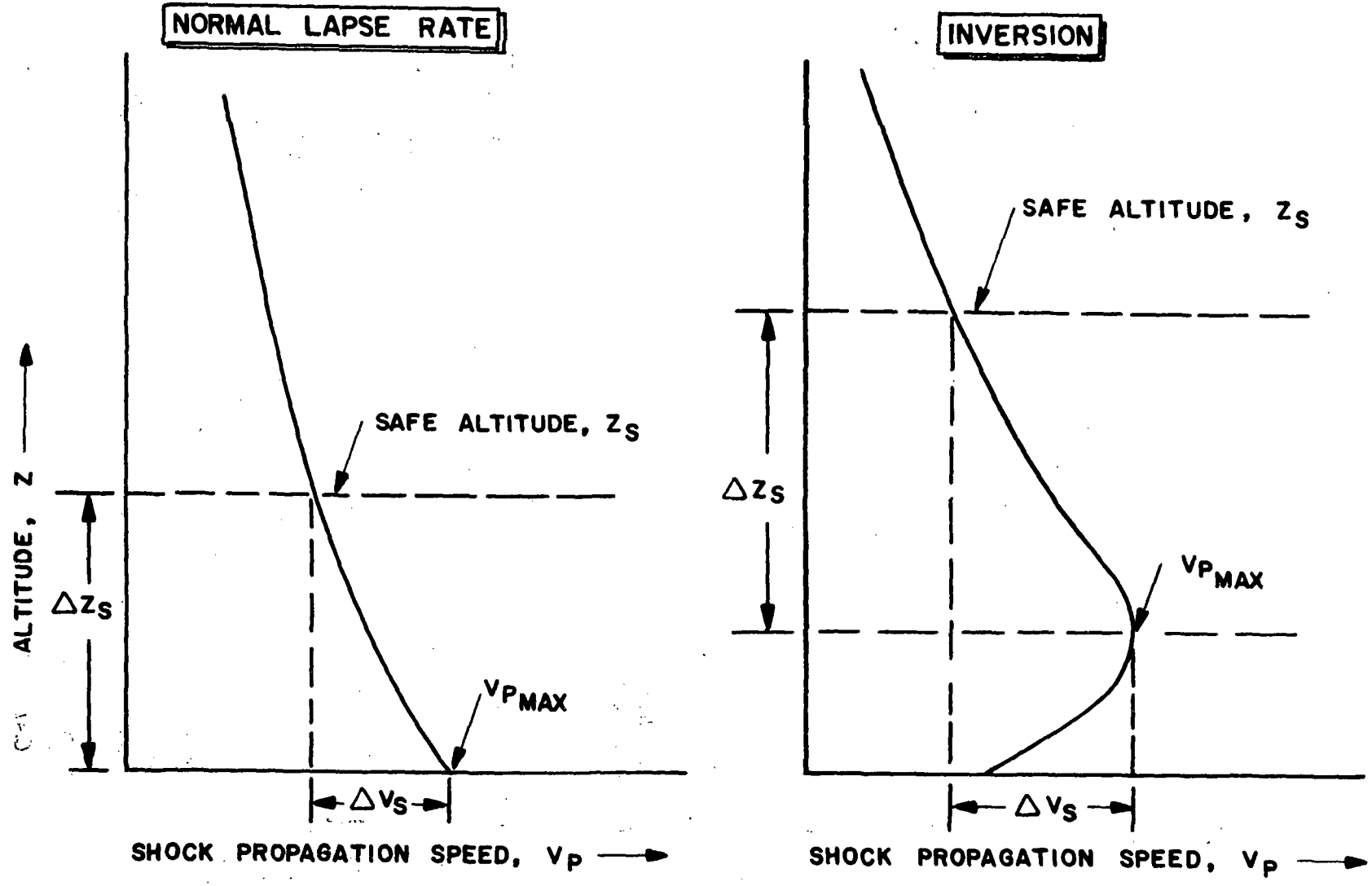

FIGURE 17.–RELATIONSHIP BETWEEN Z_S, ΔZ_S, ΔV_S, THRESHOLD MACH NUMBER FLIGHT

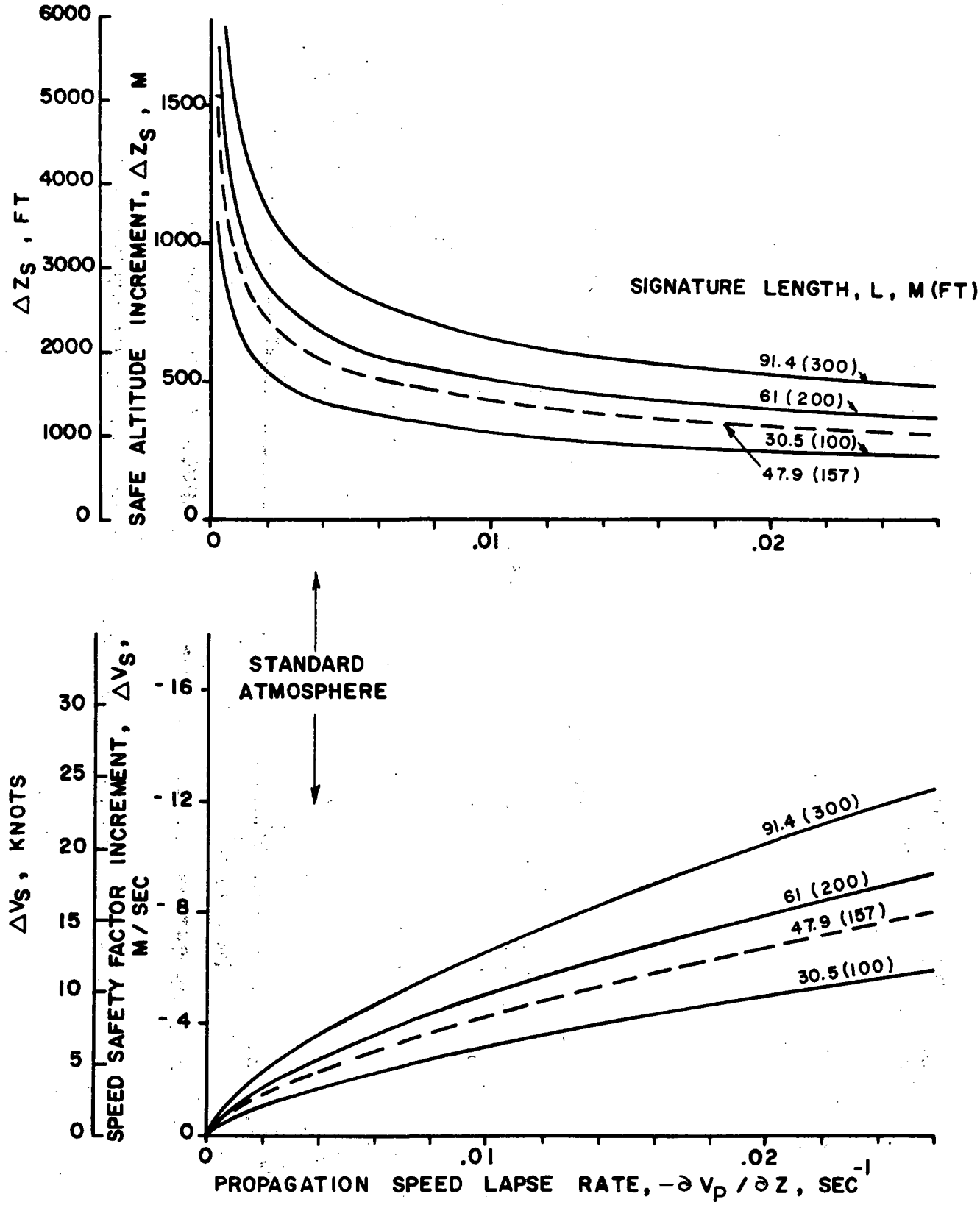

FIGURE 18.—THEORETICAL SPEED SAFETY FACTOR AND CORRESPONDING BUFFER ZONE DEPTH, THRESHOLD MACH NUMBER FLIGHT

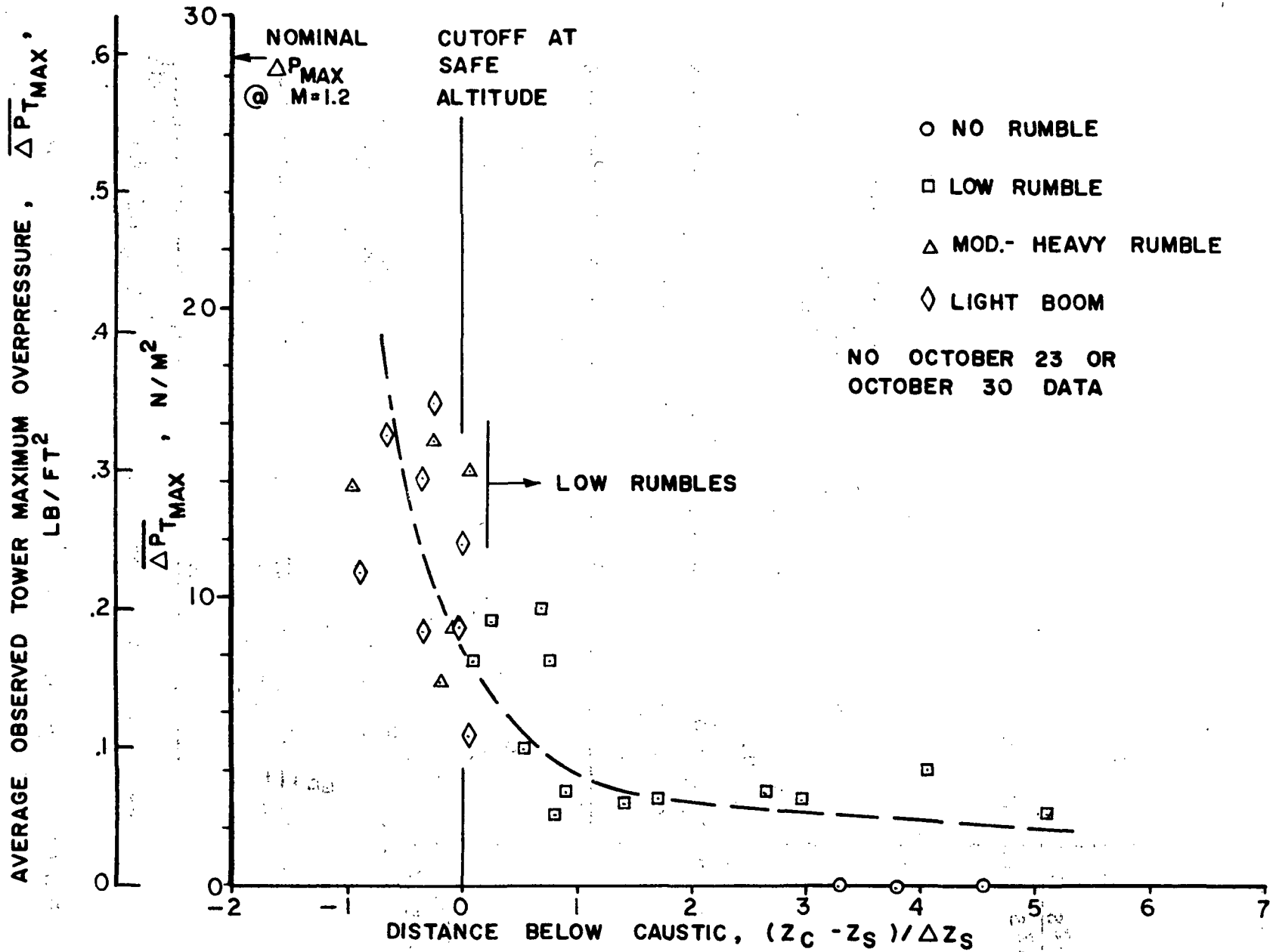

FIGURE 19.—OVERPRESSURE VARIATION WITH DISTANCE BELOW CAUSTIC FOR FLIGHT NEAR THE THRESHOLD MACH NUMBER

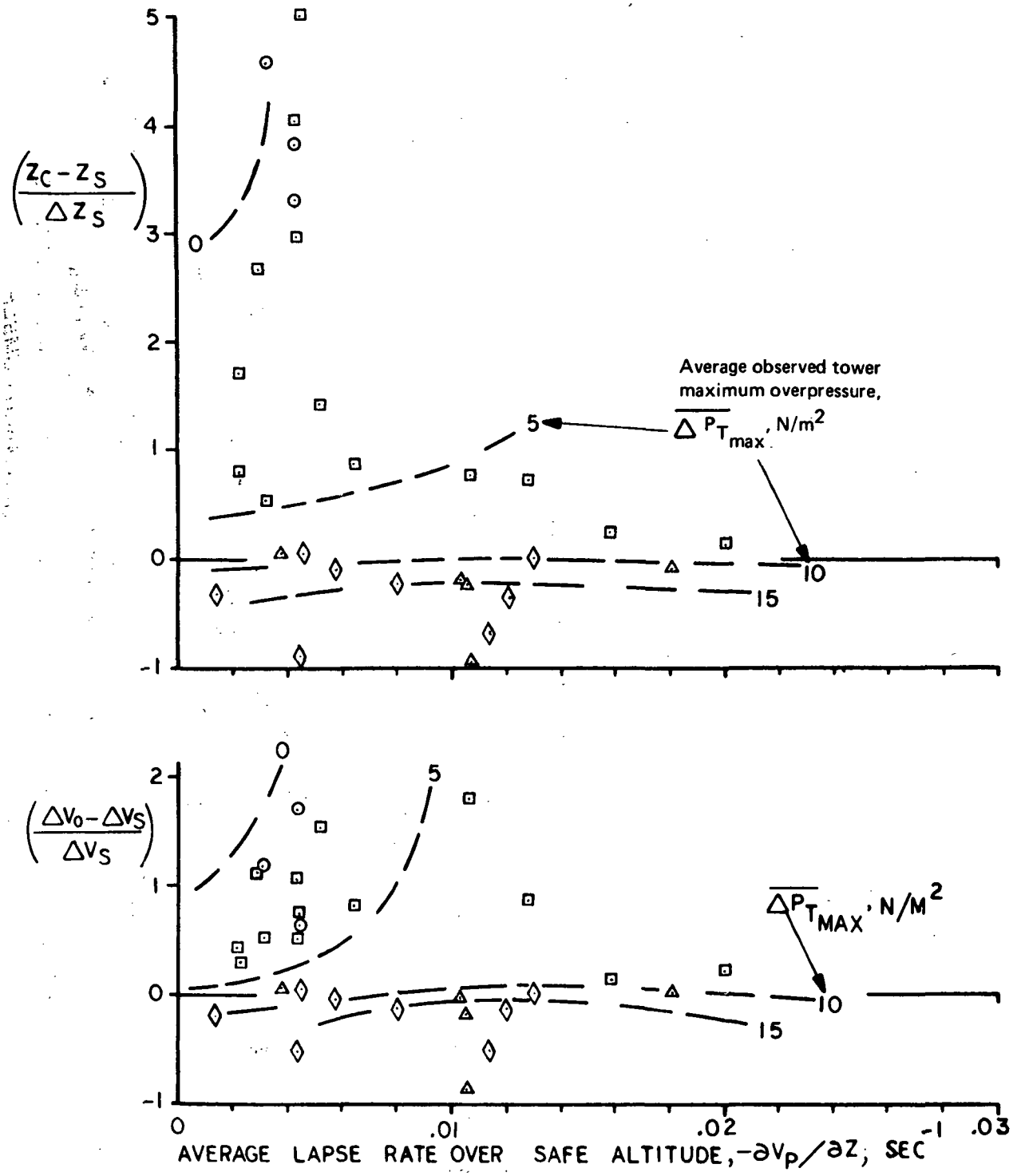

FIGURE 20.–EFFECT OF PROPAGATION SPEED LAPSE RATE ON BUFFER ZONE DEPTH AND SPEED SAFETY FACTOR, FLIGHT NEAR THE THRESHOLD MACH NUMBER

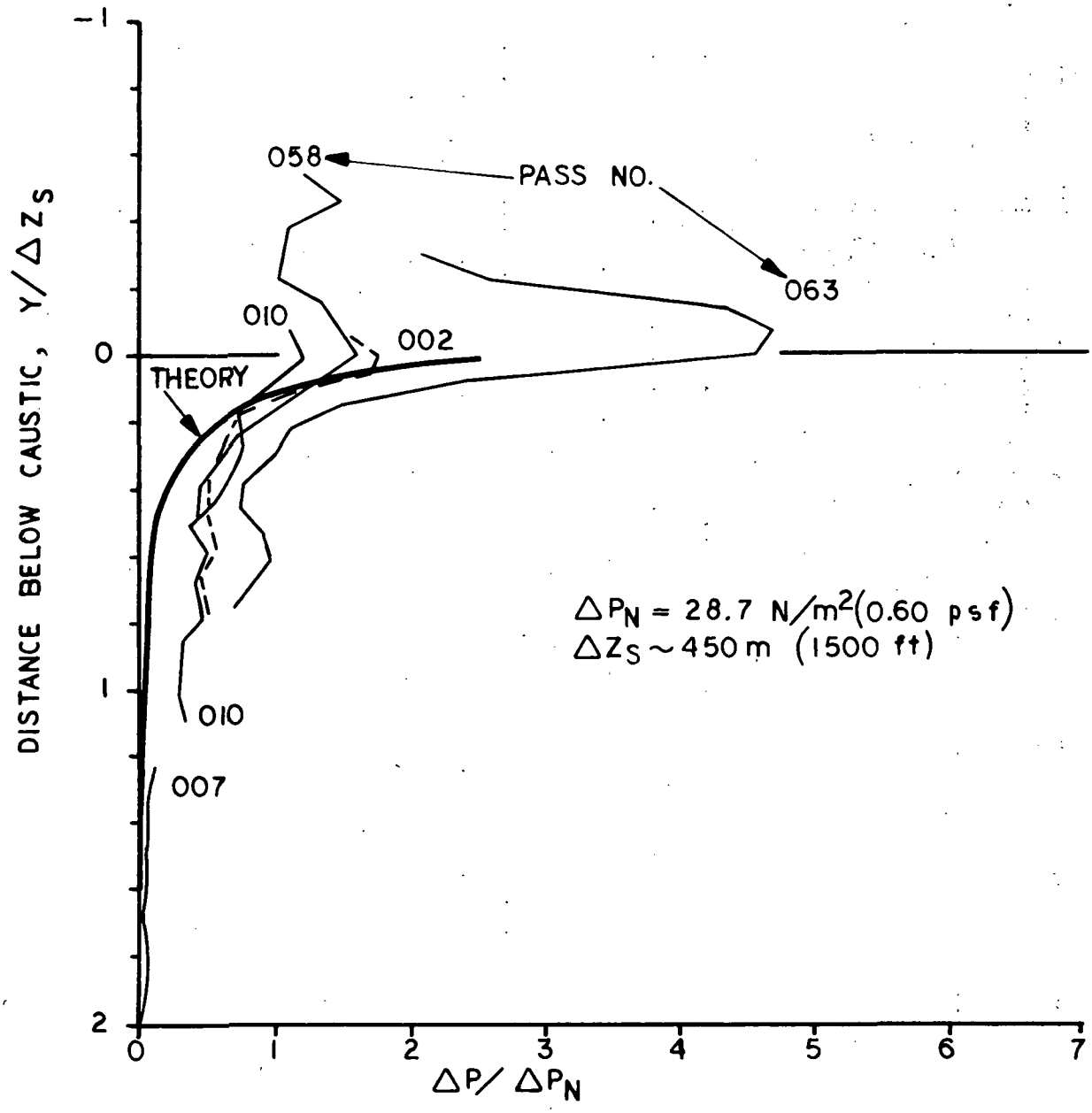

FIGURE 21:—ΔP_{max} NEAR CAUSTIC, THEORY AND EXPERIMENT, THRESHOLD MACH NUMBER FLIGHT

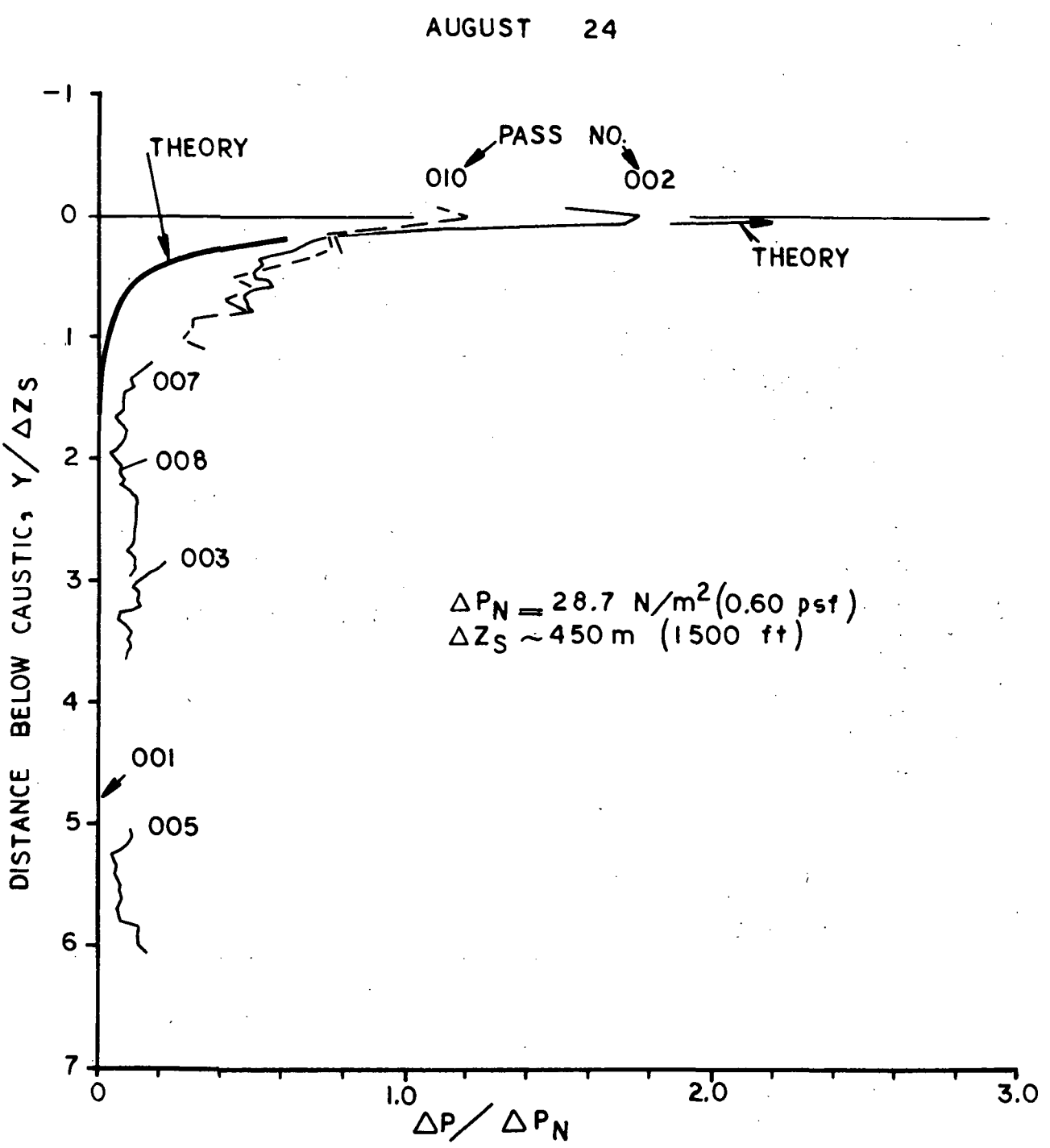

FIGURE 22.—ΔP_{max} NEAR CAUSTIC, AUGUST 24 DATA, THRESHOLD MACH NUMBER FLIGHT

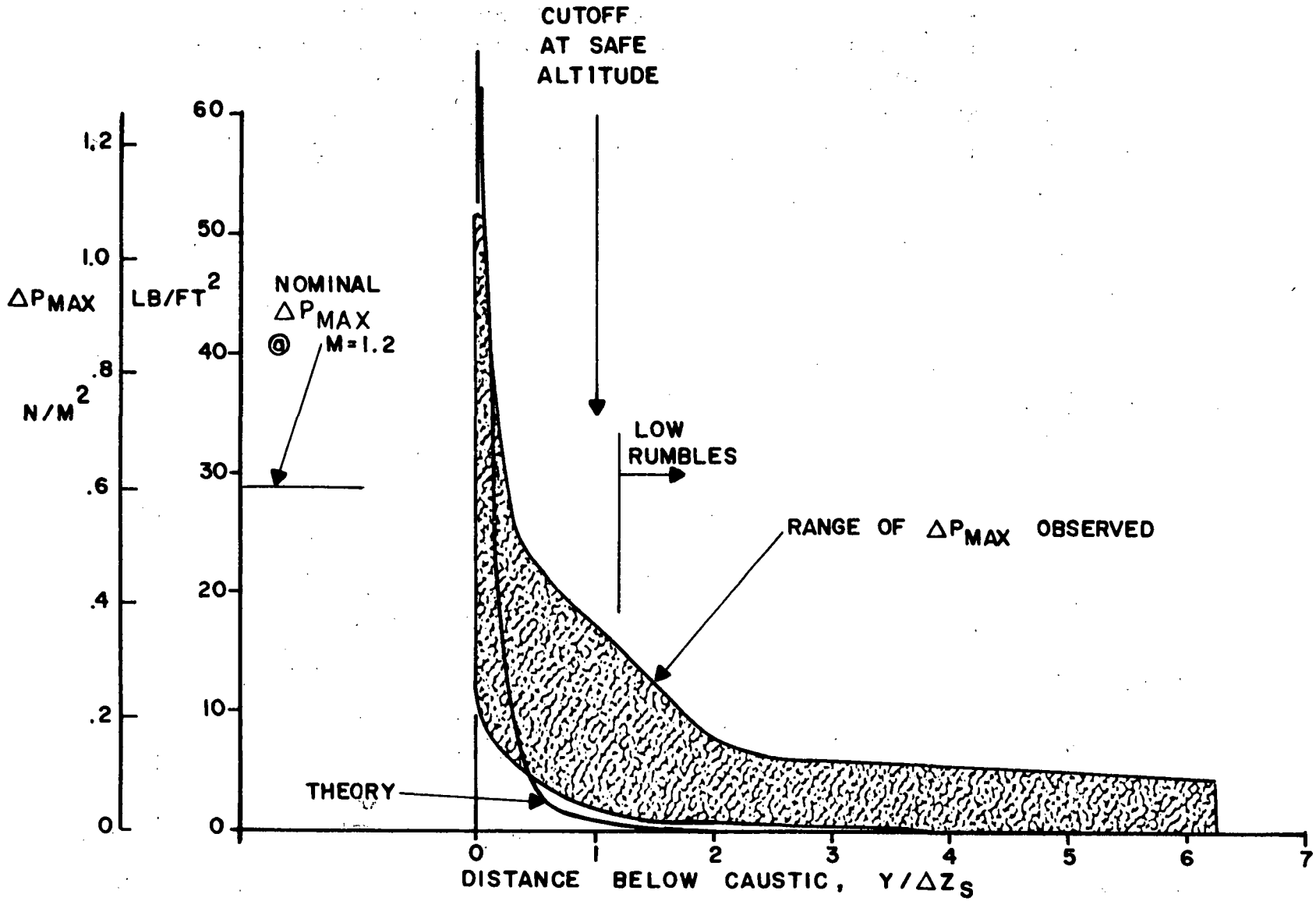

FIGURE 23.—ΔP_{max} BELOW CAUSTIC, THEORY AND EXPERIMENT, THRESHOLD MACH NUMBER FLIGHT

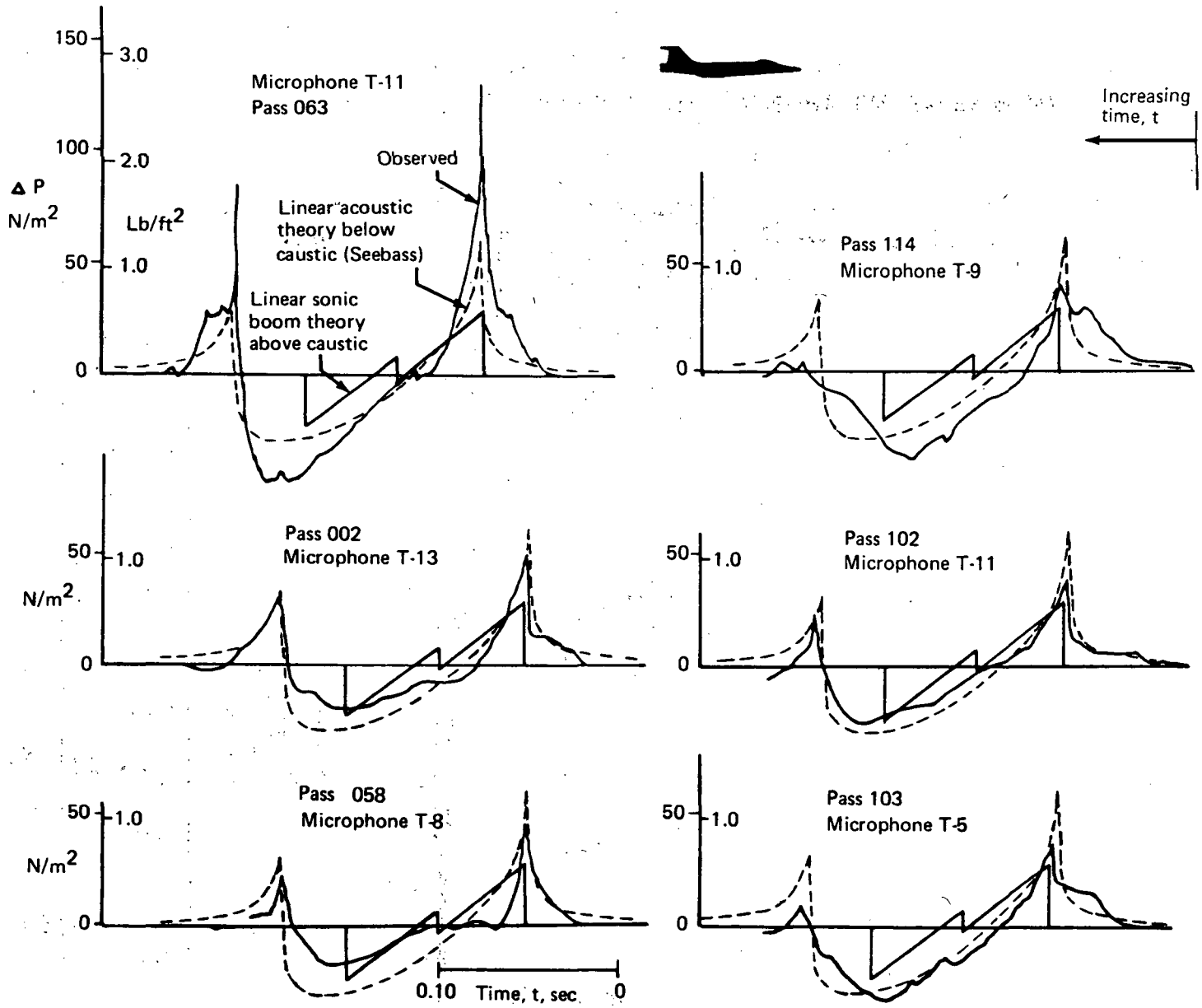

FIGURE 24.–COMPARISON BETWEEN THEORY AND EXPERIMENT NEAR CAUSTICS, THRESHOLD MACH NUMBER FLIGHT

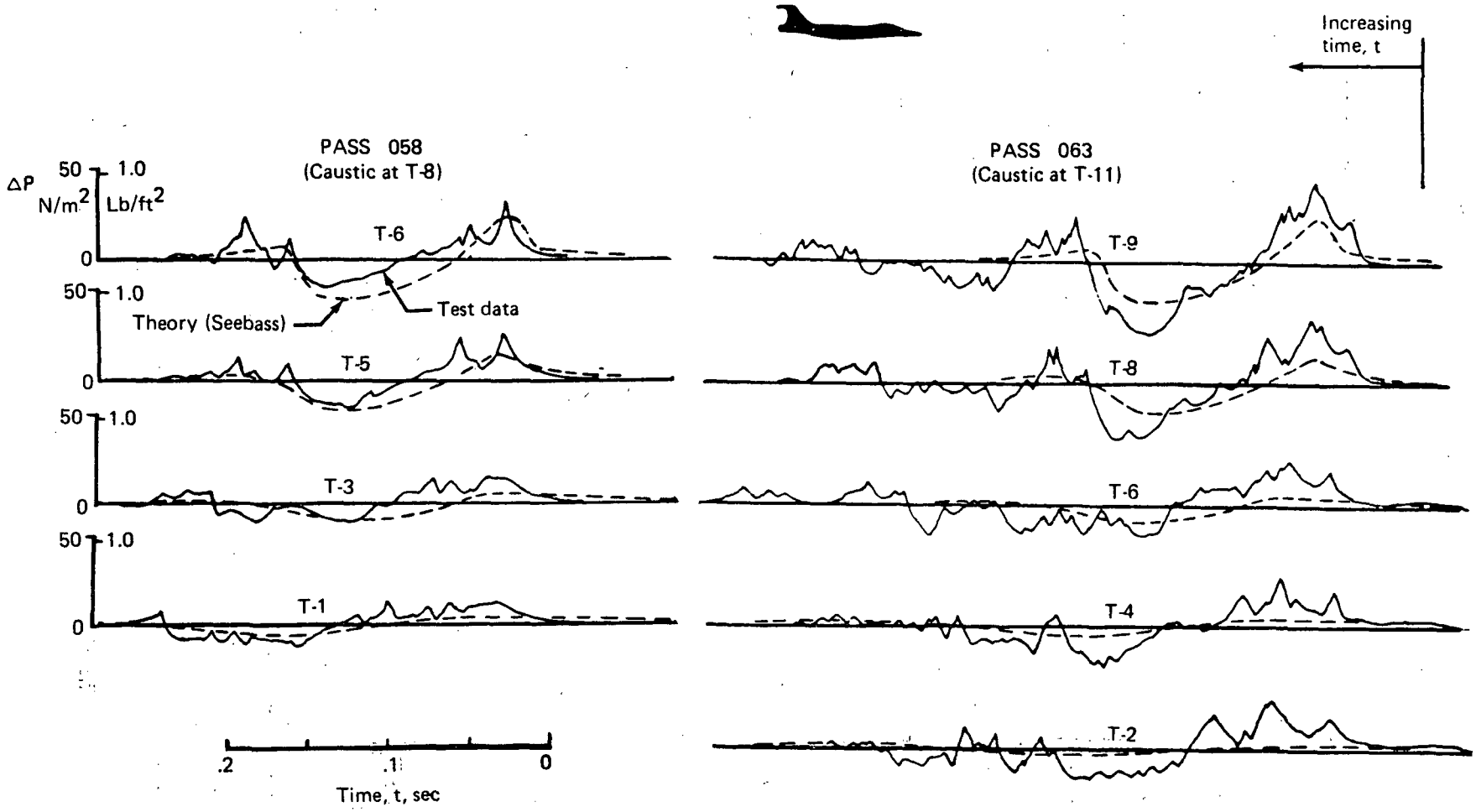

FIGURE 25.—COMPARISON BETWEEN THEORY AND EXPERIMENT AWAY FROM CAUSTIC, THRESHOLD MACH NUMBER FLIGHT

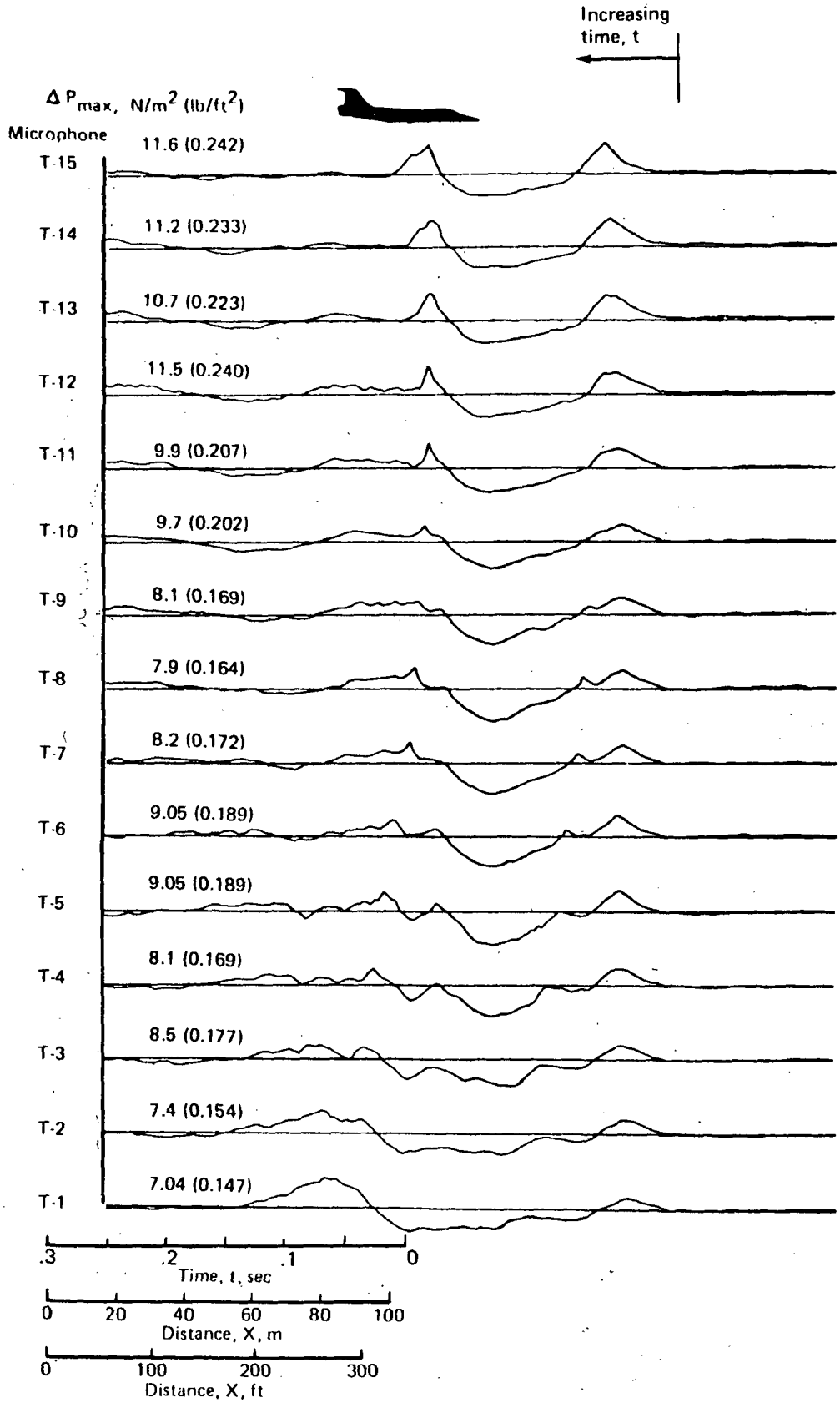

FIGURE 26.—TOWER PRESSURE SIGNATURES FOR PASS III, THRESHOLD MACH NUMBER FLIGHT

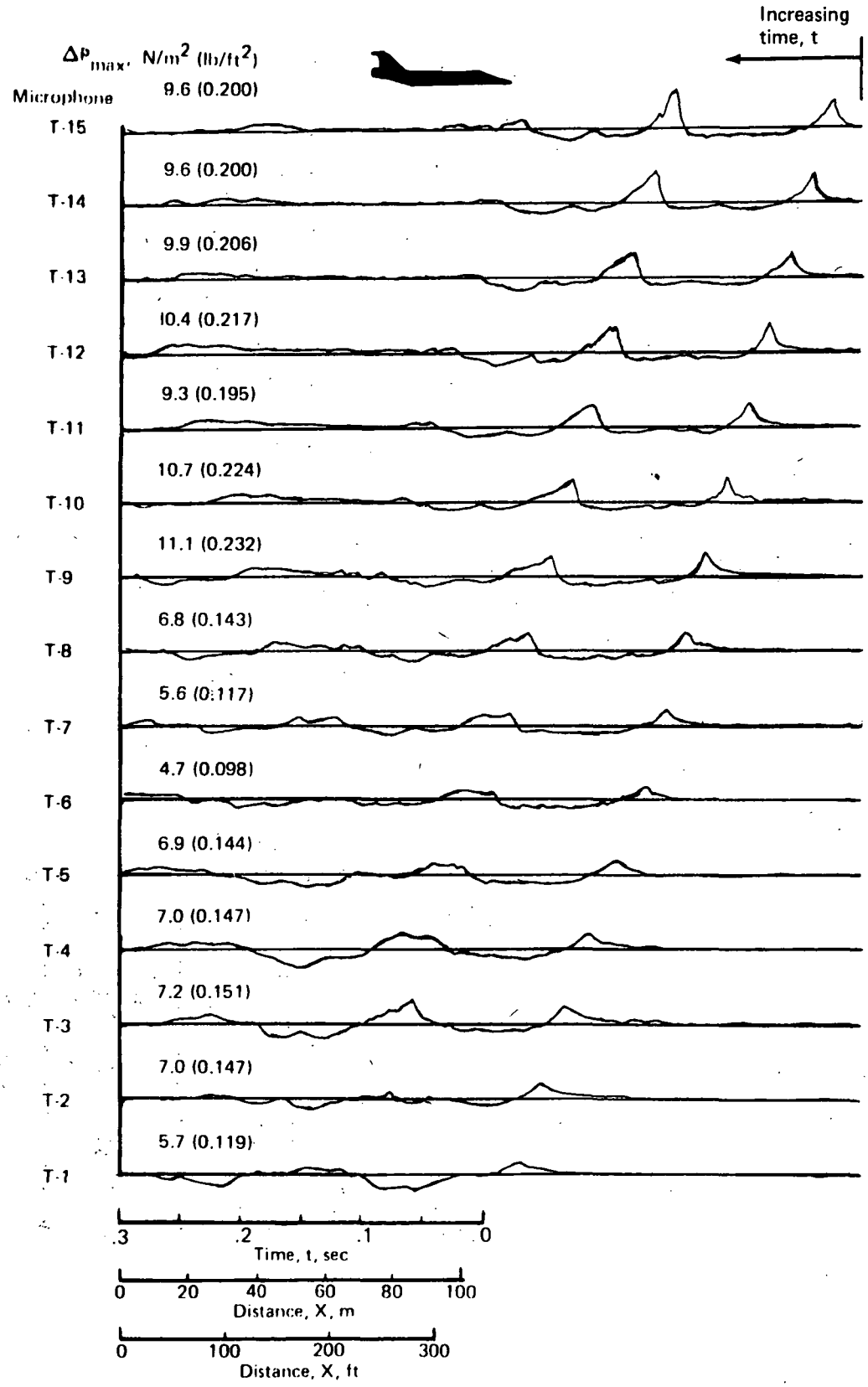

FIGURE 27.—TOWER PRESSURE SIGNATURES FOR PASS 085, THRESHOLD MACH NUMBER FLIGHT

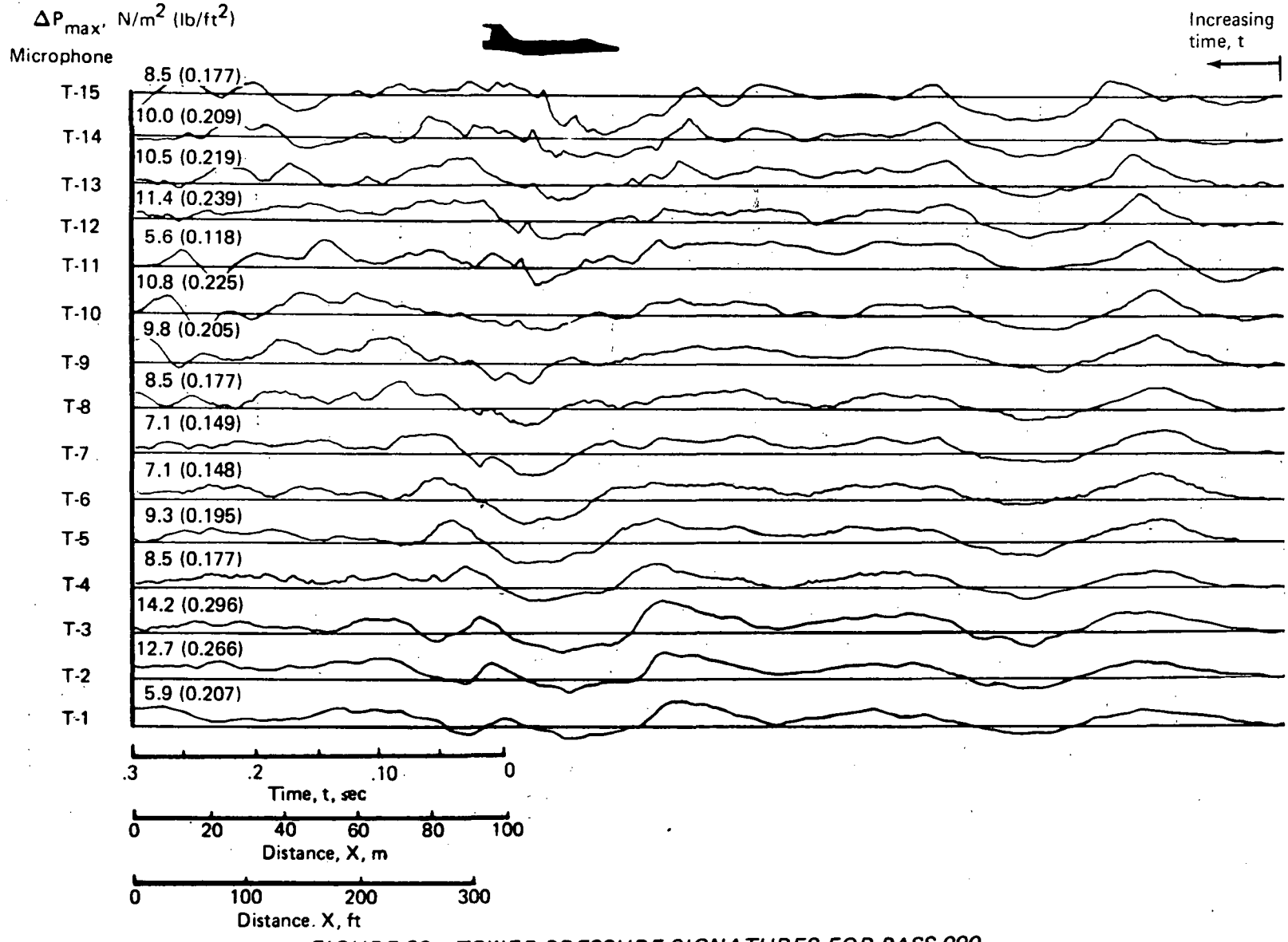

FIGURE 28.—TOWER PRESSURE SIGNATURES FOR PASS 090, THRESHOLD MACH NUMBER FLIGHT

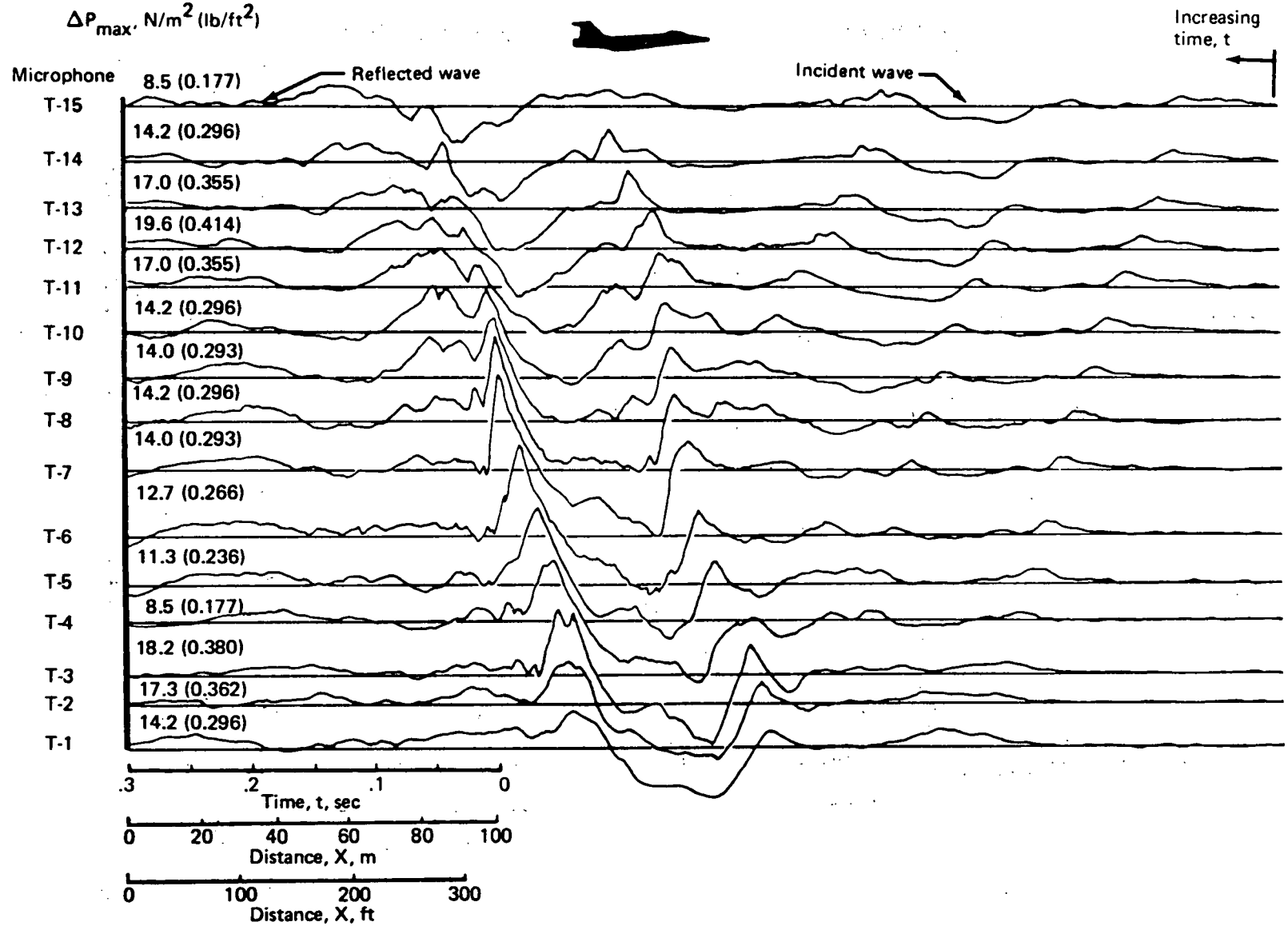

FIGURE 29.—TOWER PRESSURE SIGNATURES FOR PASS 097, THRESHOLD MACH NUMBER FLIGHT

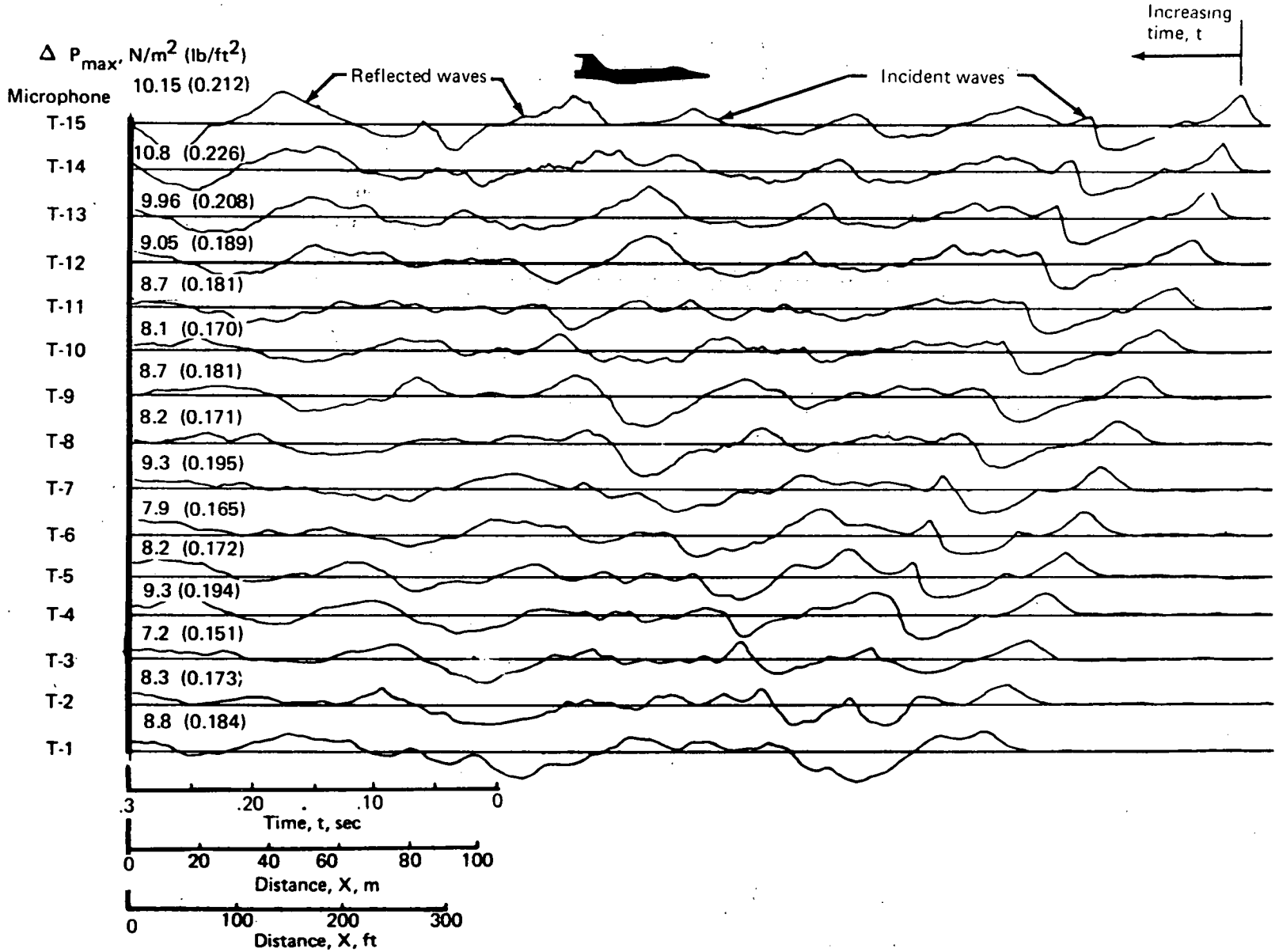

FIGURE 30.—TOWER PRESSURE SIGNATURES FOR PASS 122

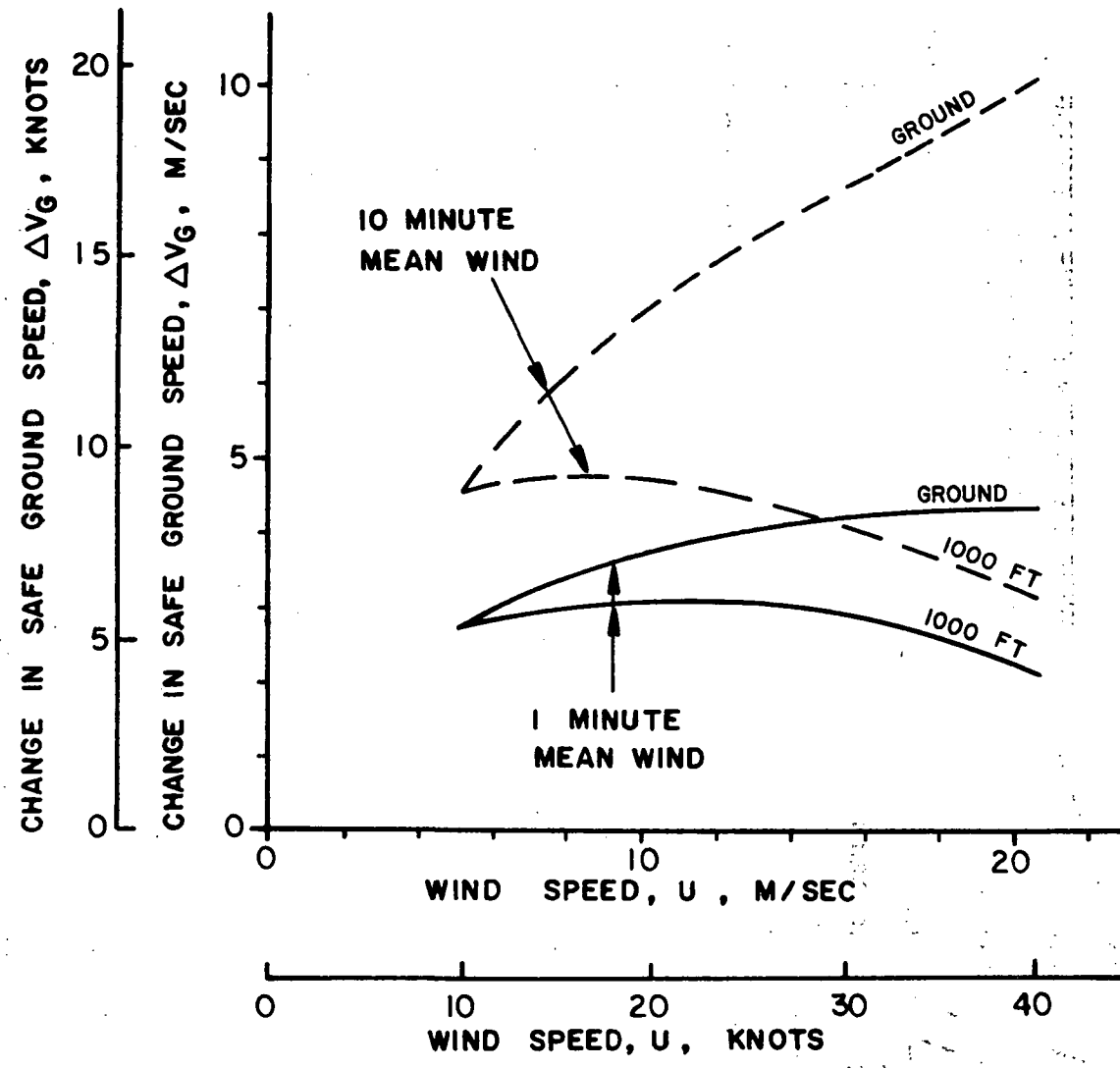

FIGURE 31.—EFFECT OF WIND GUSTS ON ALLOWABLE GROUND SPEED, THRESHOLD MACH NUMBER FLIGHT

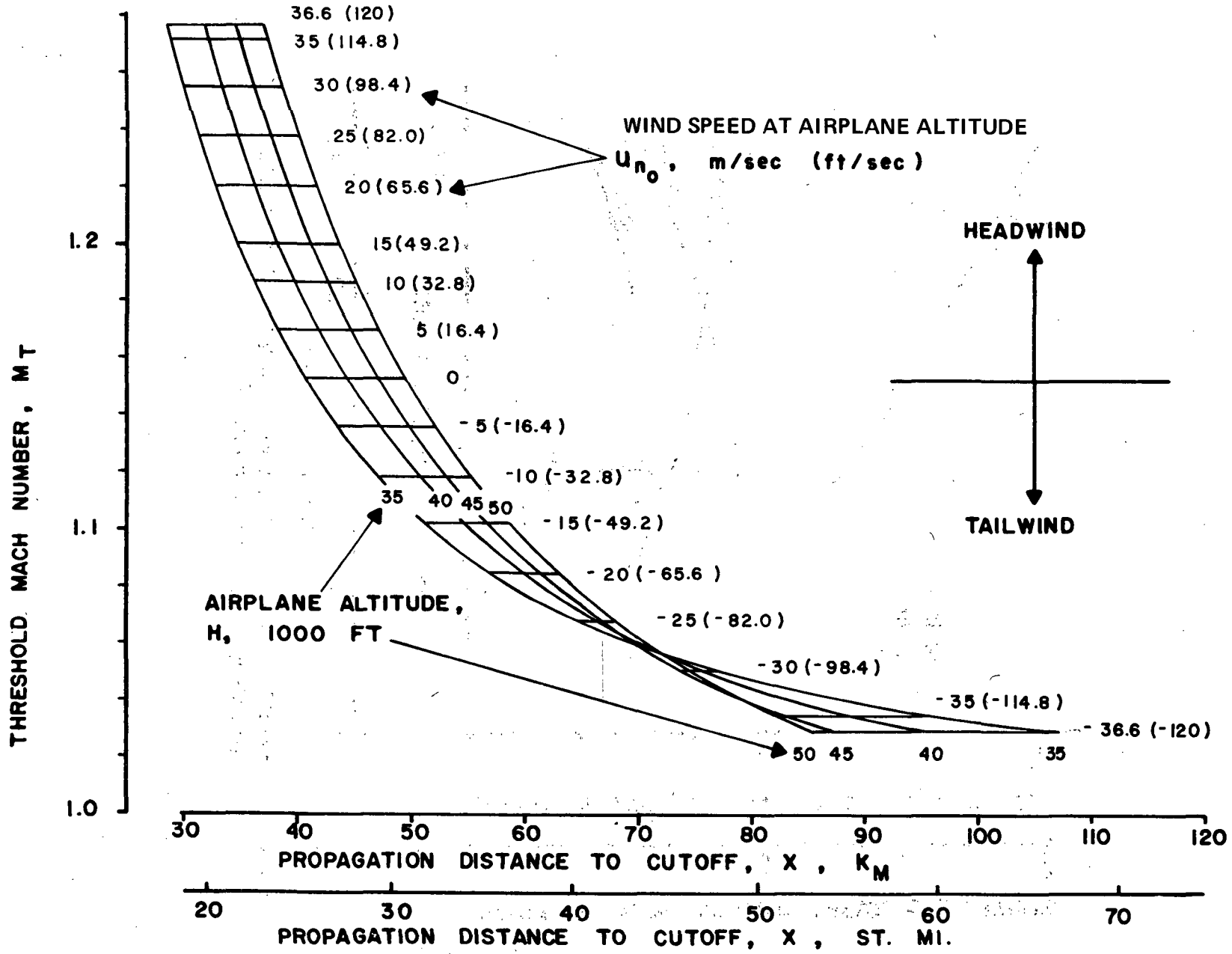

FIGURE 32.–EFFECT OF WIND ON PROPAGATION DISTANCE OF CUTOFF RAY AND THRESHOLD MACH NUMBER

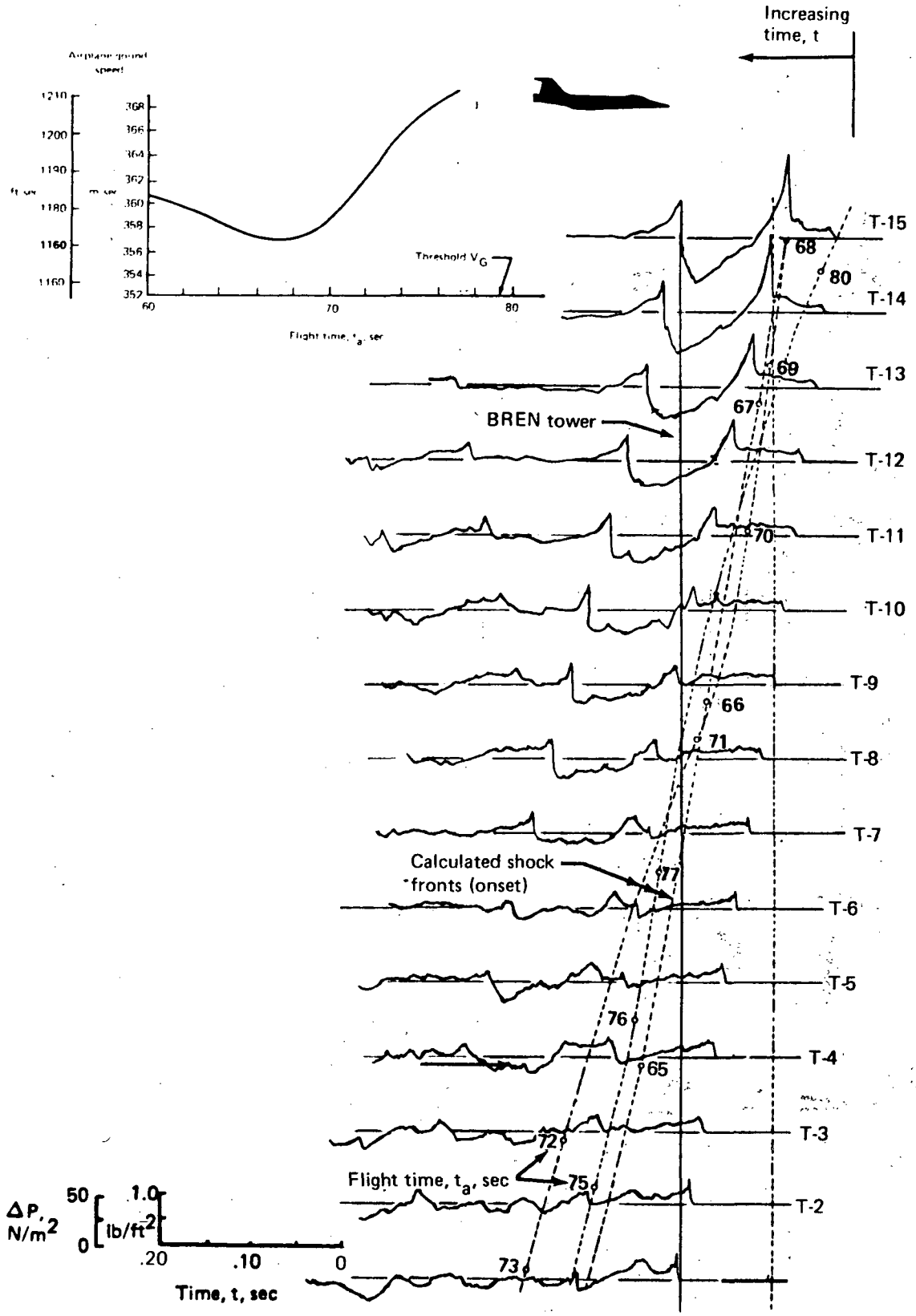

FIGURE 33.–TOWER PRESSURE SIGNATURES AND CALCULATED SHOCK FRONTS FOR PASS 017, FLIGHT NEAR THRESHOLD MACH NUMBER

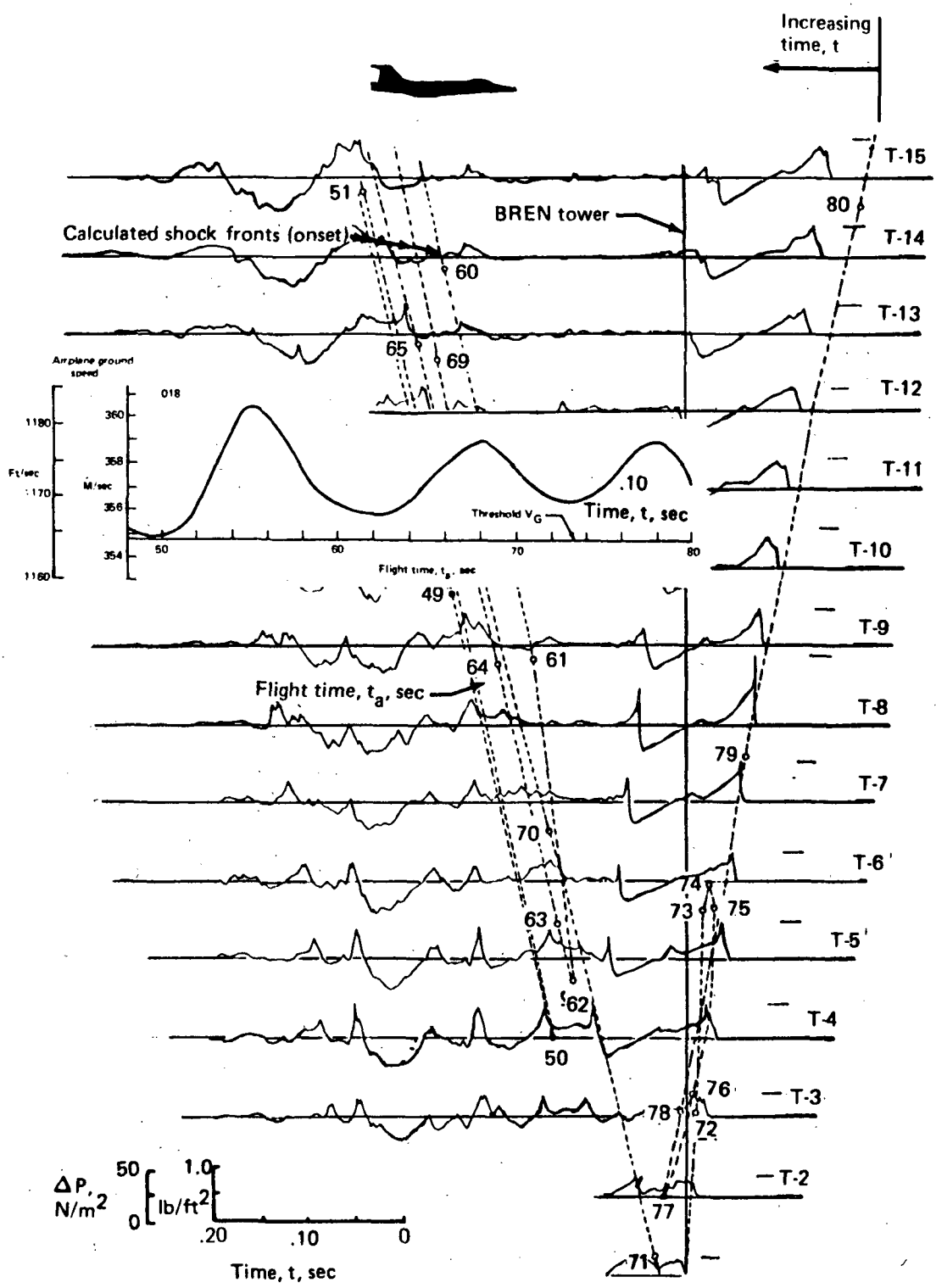

FIGURE 34.—TOWER PRESSURE SIGNATURES AND CALCULATED SHOCK FRONTS FOR PASS 018, FLIGHT NEAR THRESHOLD MACH NUMBER

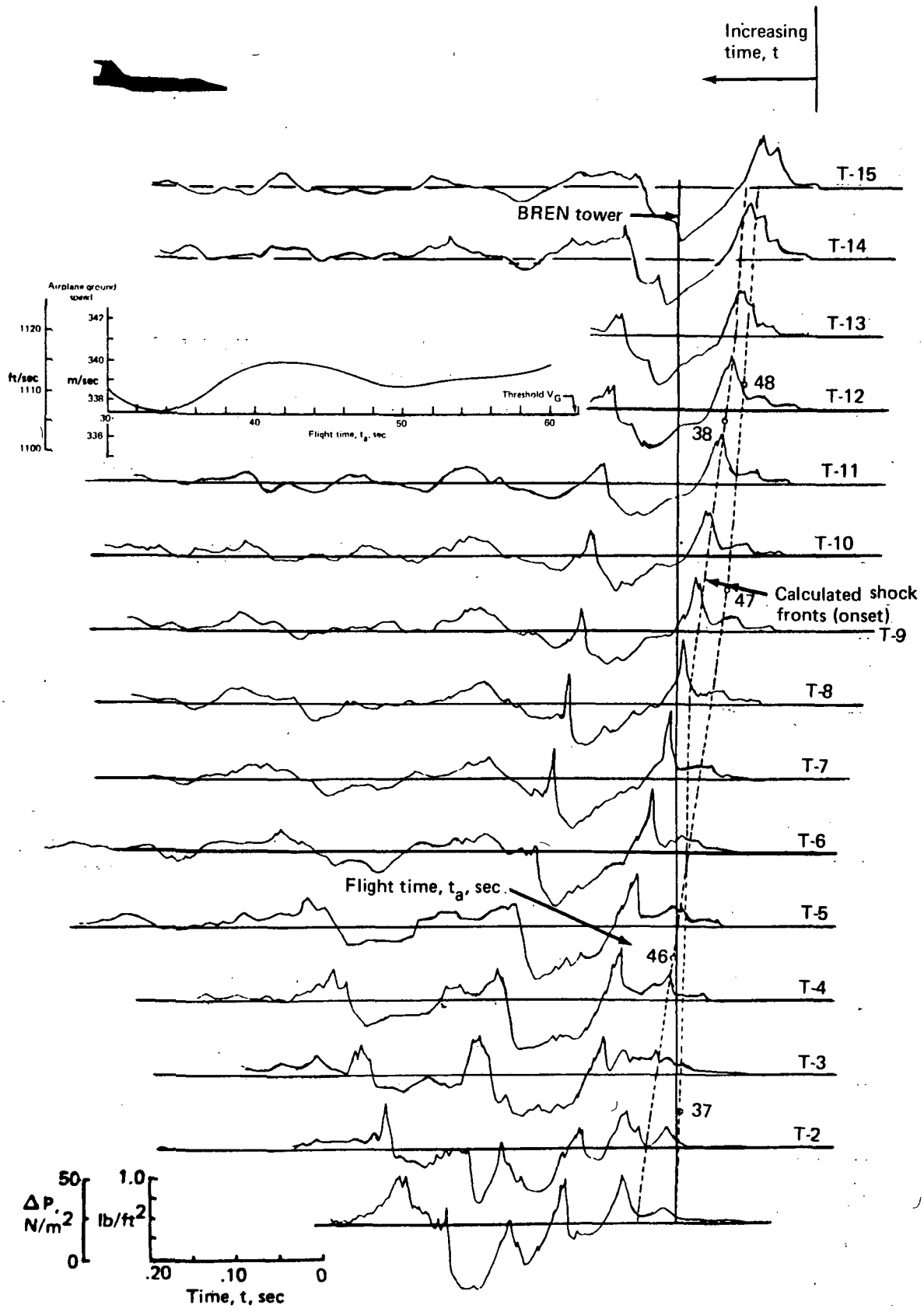

FIGURE 35.—TOWER PRESSURE SIGNATURES AND CALCULATED SHOCK FRONTS FOR PASS 106, FLIGHT NEAR THRESHOLD MACH NUMBER

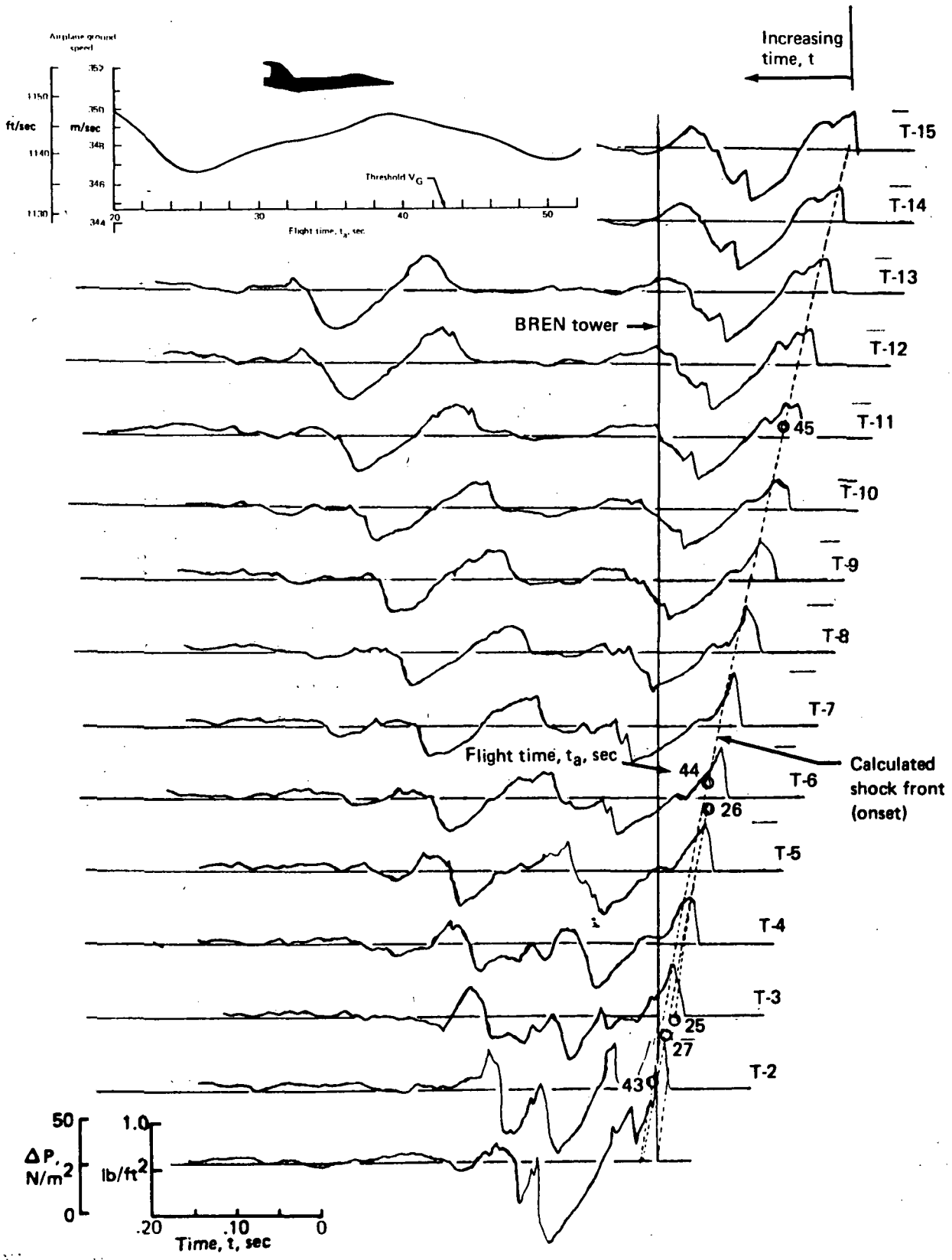

FIGURE 36.—TOWER PRESSURE SIGNATURES AND CALCULATED SHOCK FRONTS FOR PASS 116, FLIGHT NEAR THRESHOLD MACH NUMBER

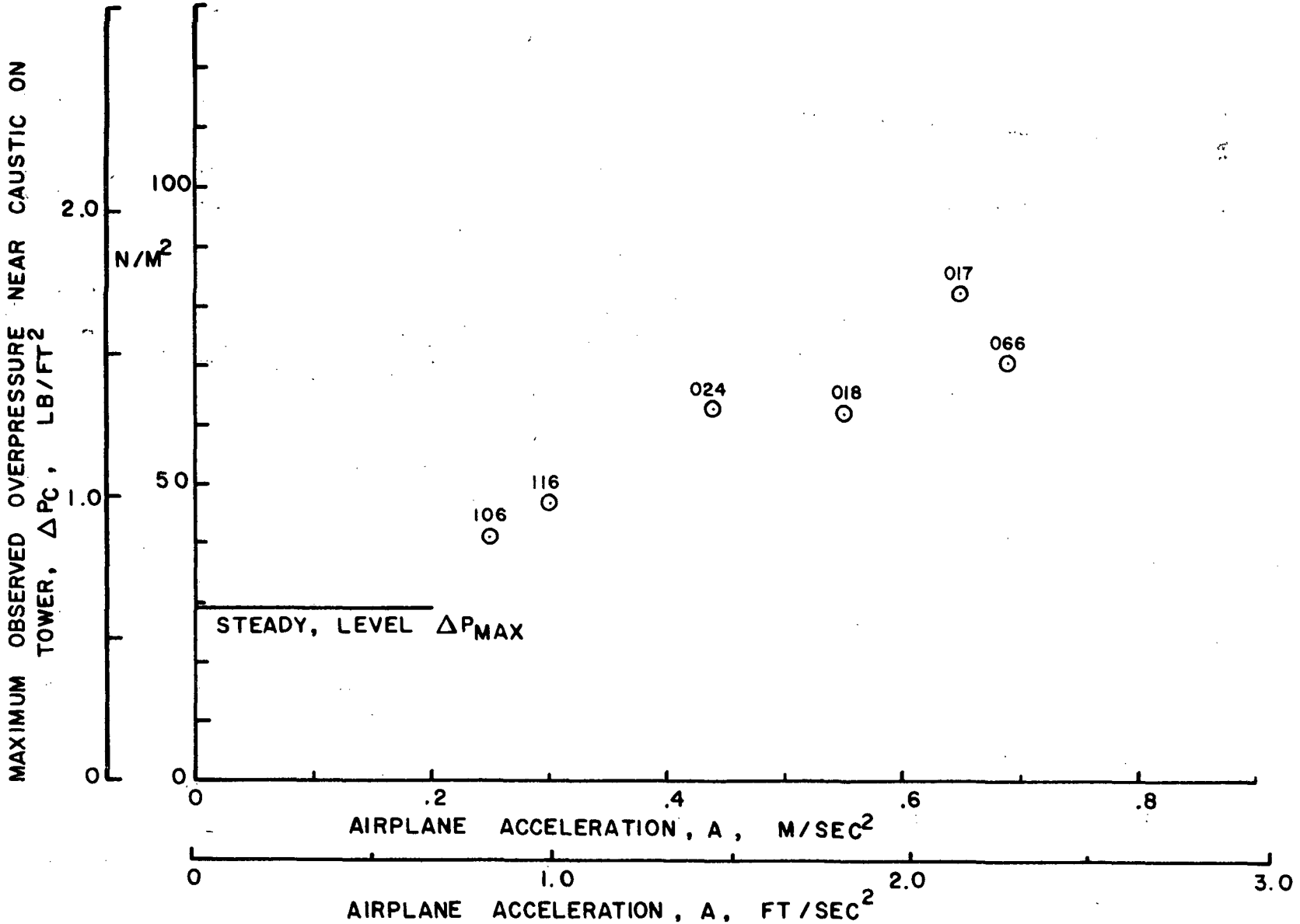

FIGURE 37.–EFFECT OF ACCELERATION MAGNITUDE ON CAUSTIC INTENSITY–THRESHOLD MACH NUMBER FLIGHTS

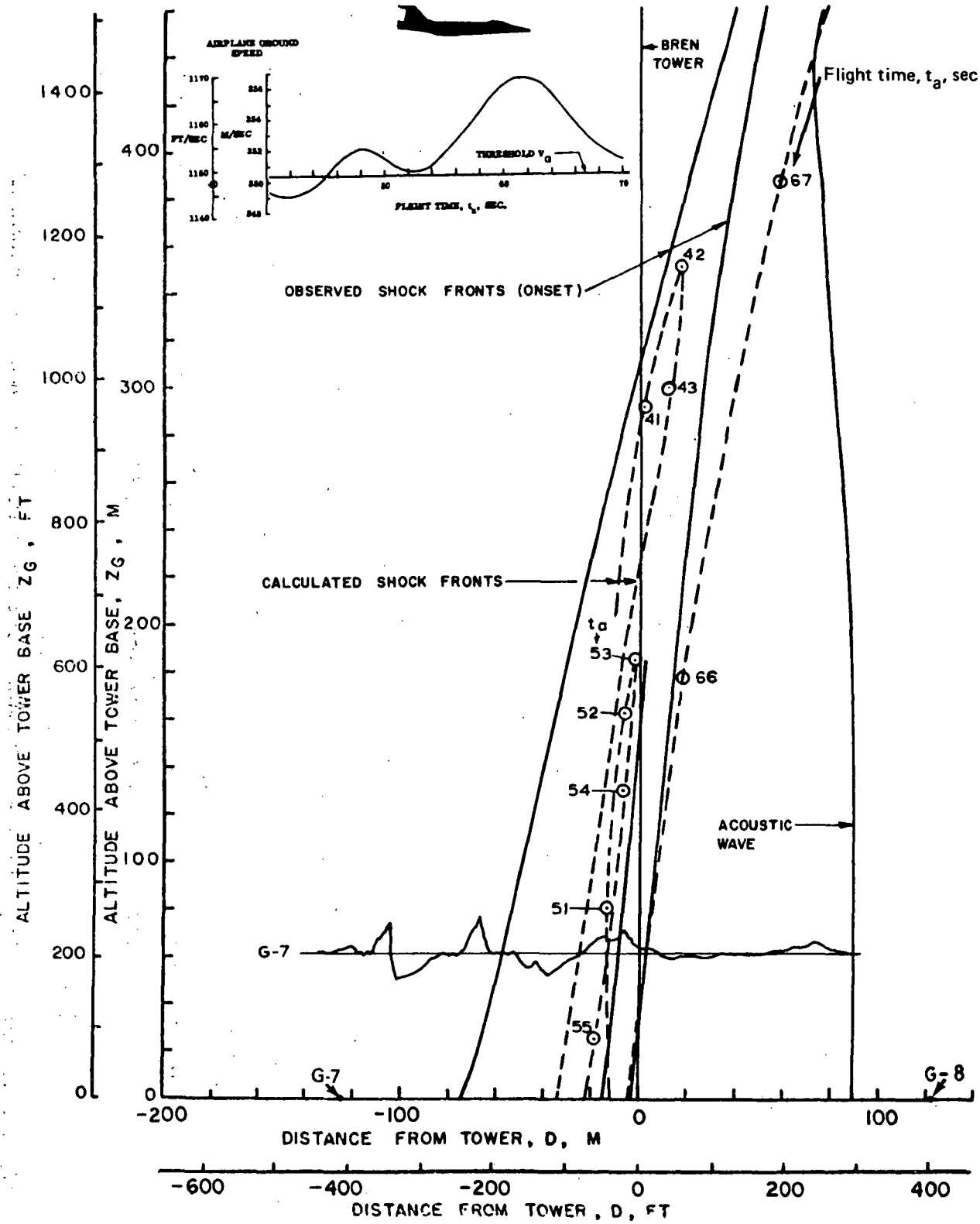

FIGURE 38.–OBSERVED AND CALCULATED BOW SHOCK WAVE PROFILES FOR PASS 004, FLIGHT NEAR THRESHOLD MACH NUMBER

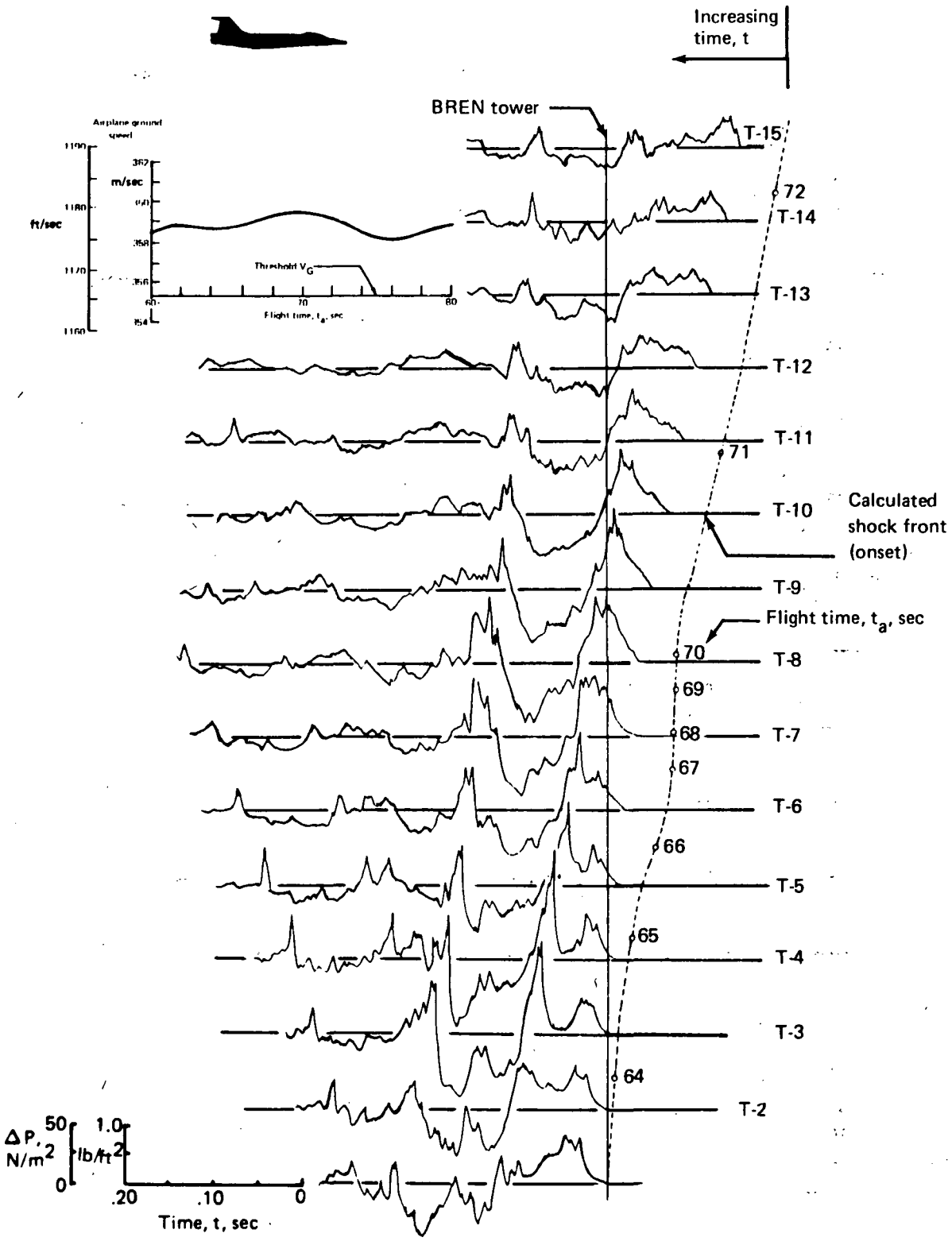

FIGURE 39.–TOWER PRESSURE SIGNATURES AND CALCULATED SHOCK FRONTS FOR PASS 028, FLIGHT NEAR THRESHOLD MACH NUMBER

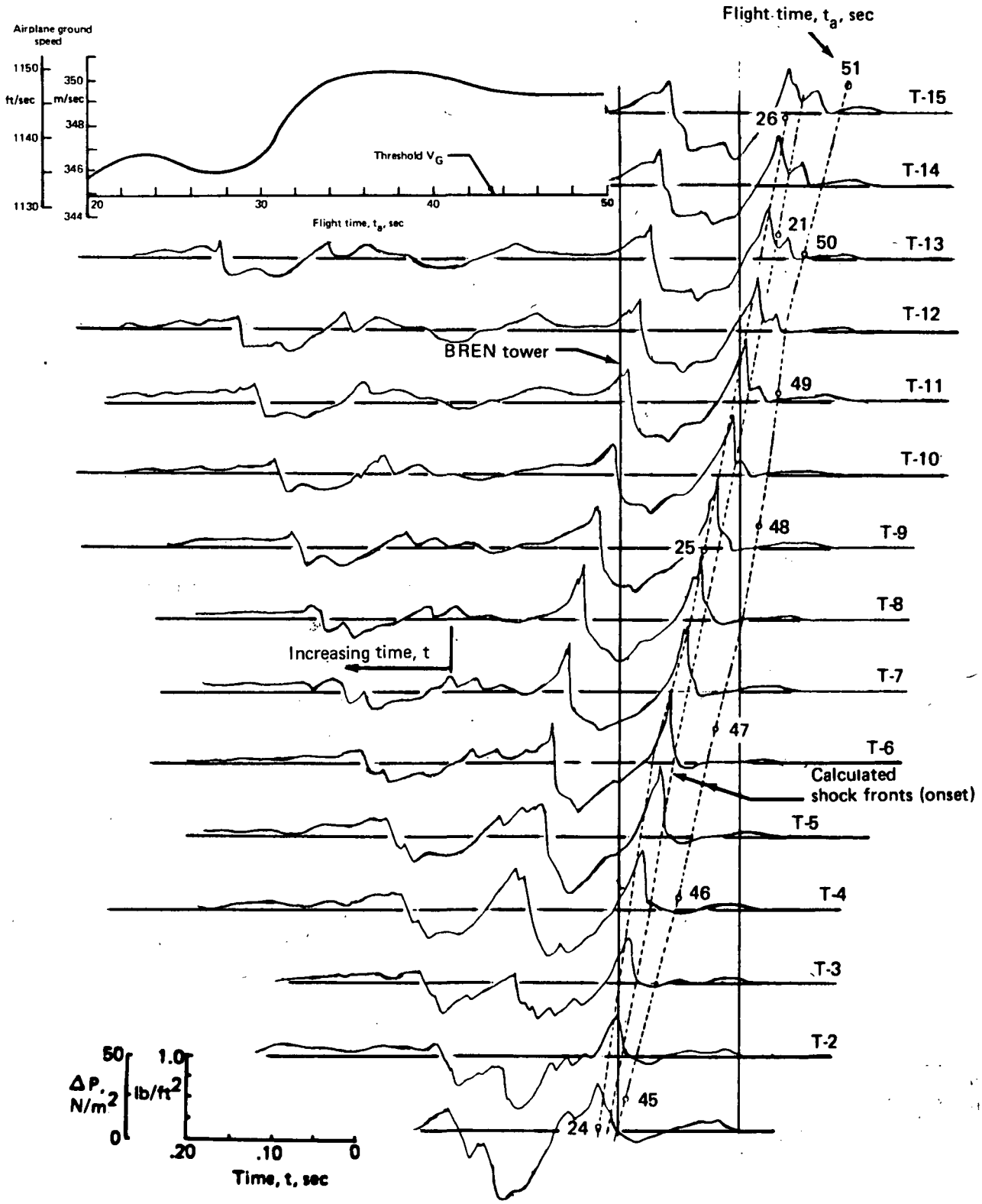

FIGURE 40.–TOWER PRESSURE SIGNATURES AND CALCULATED SHOCK FRONTS FOR PASS 117, FLIGHT NEAR THRESHOLD MACH NUMBER

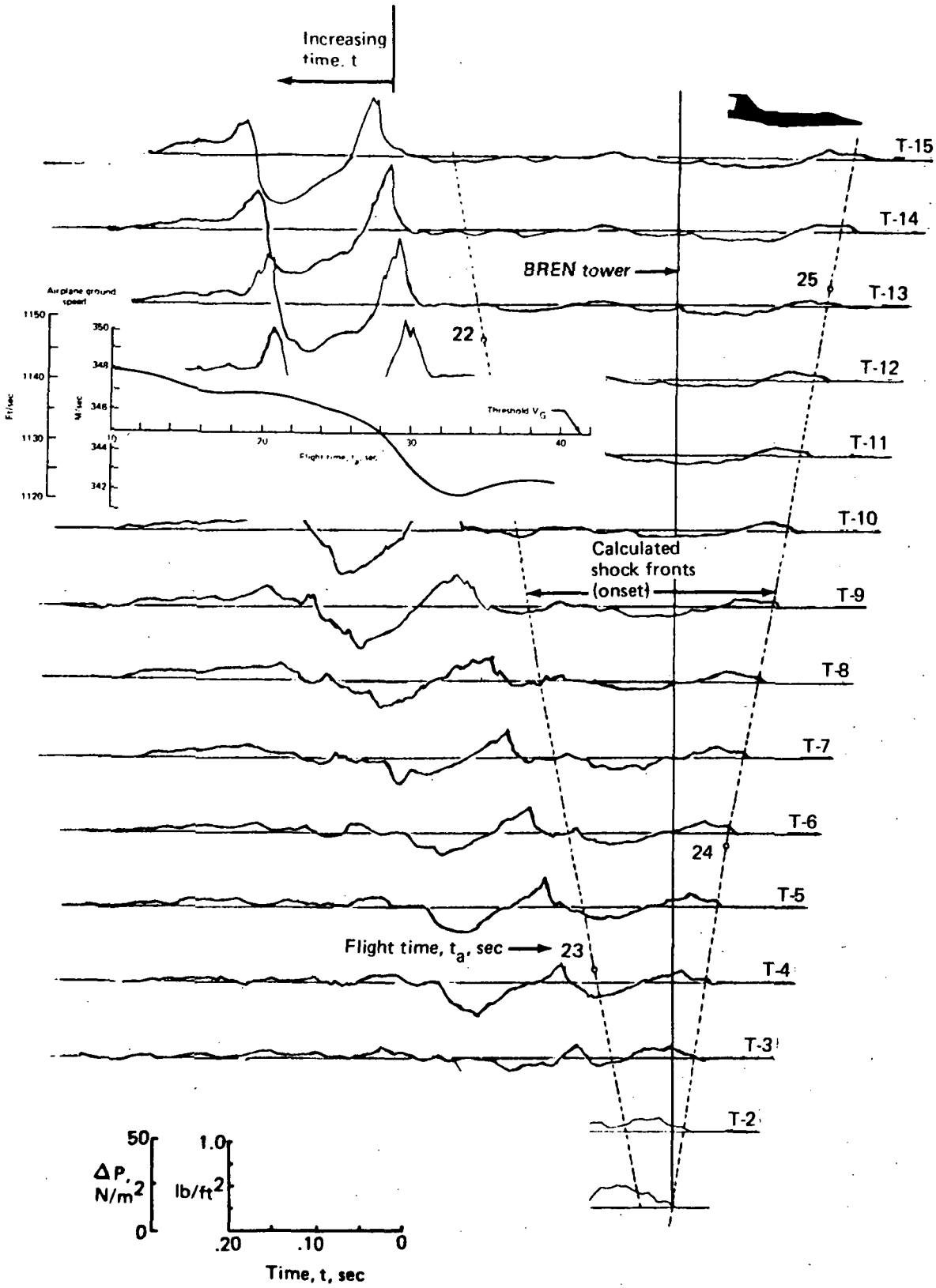

FIGURE 41.–TOWER PRESSURE SIGNATURES AND CALCULATED SHOCK FRONTS FOR PASS 119, FLIGHT NEAR THRESHOLD MACH NUMBER

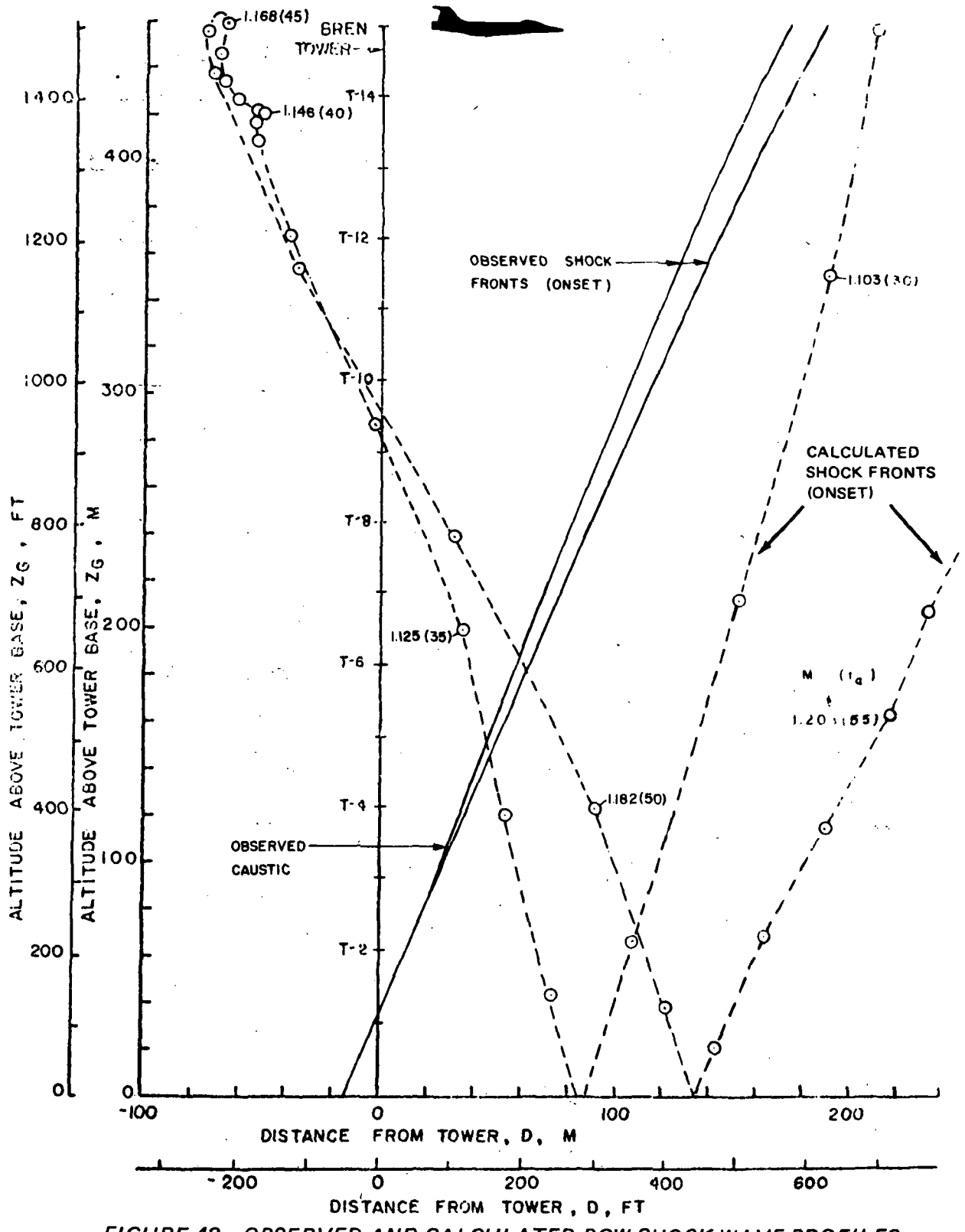

FIGURE 42.—OBSERVED AND CALCULATED BOW SHOCK WAVE PROFILES FOR PASS 045, LONGITUDINAL ACCELERATION

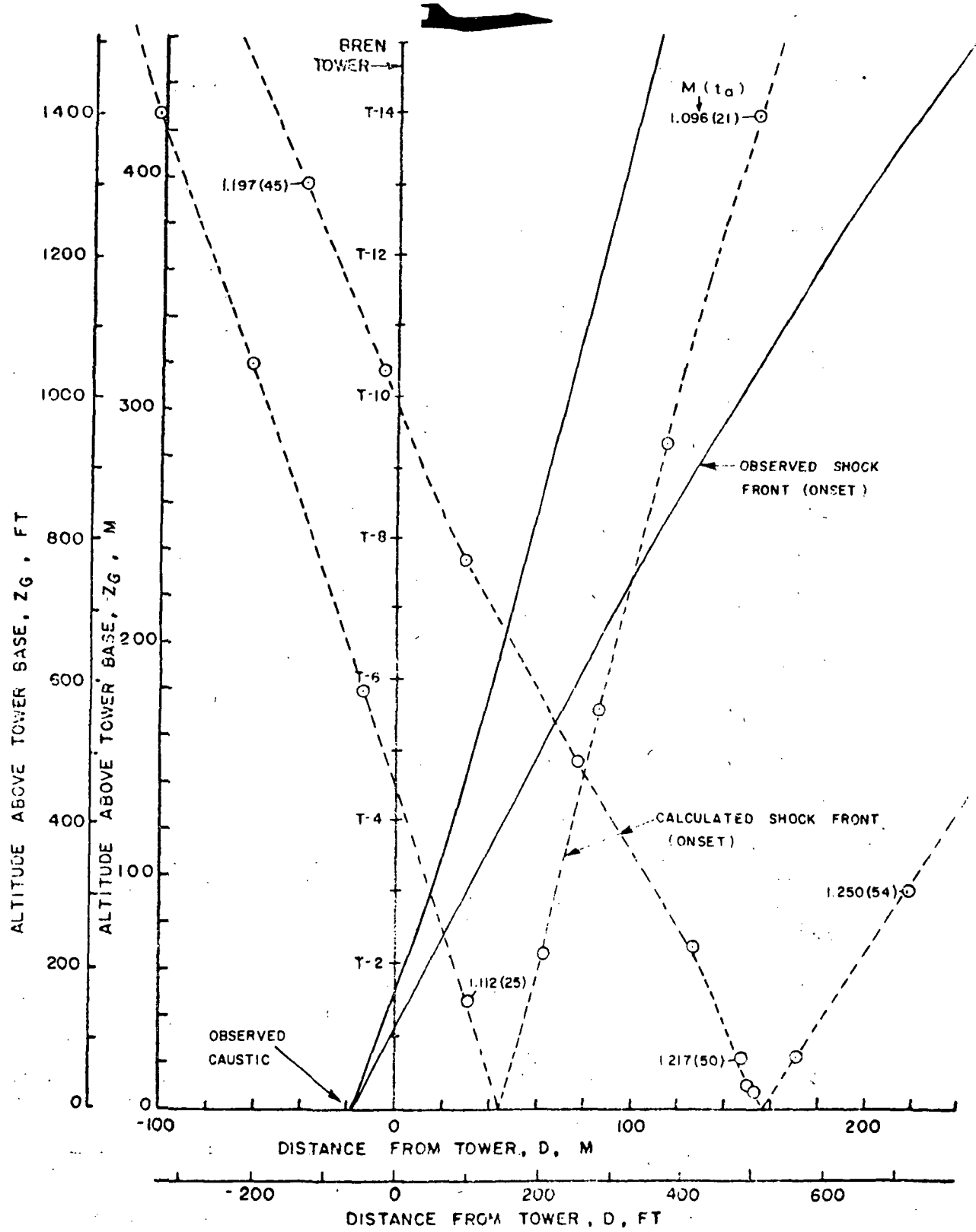

FIGURE 43.—OBSERVED AND CALCULATED BOW SHOCK WAVE PROFILES FOR PASS 046, LONGITUDINAL ACCELERATION

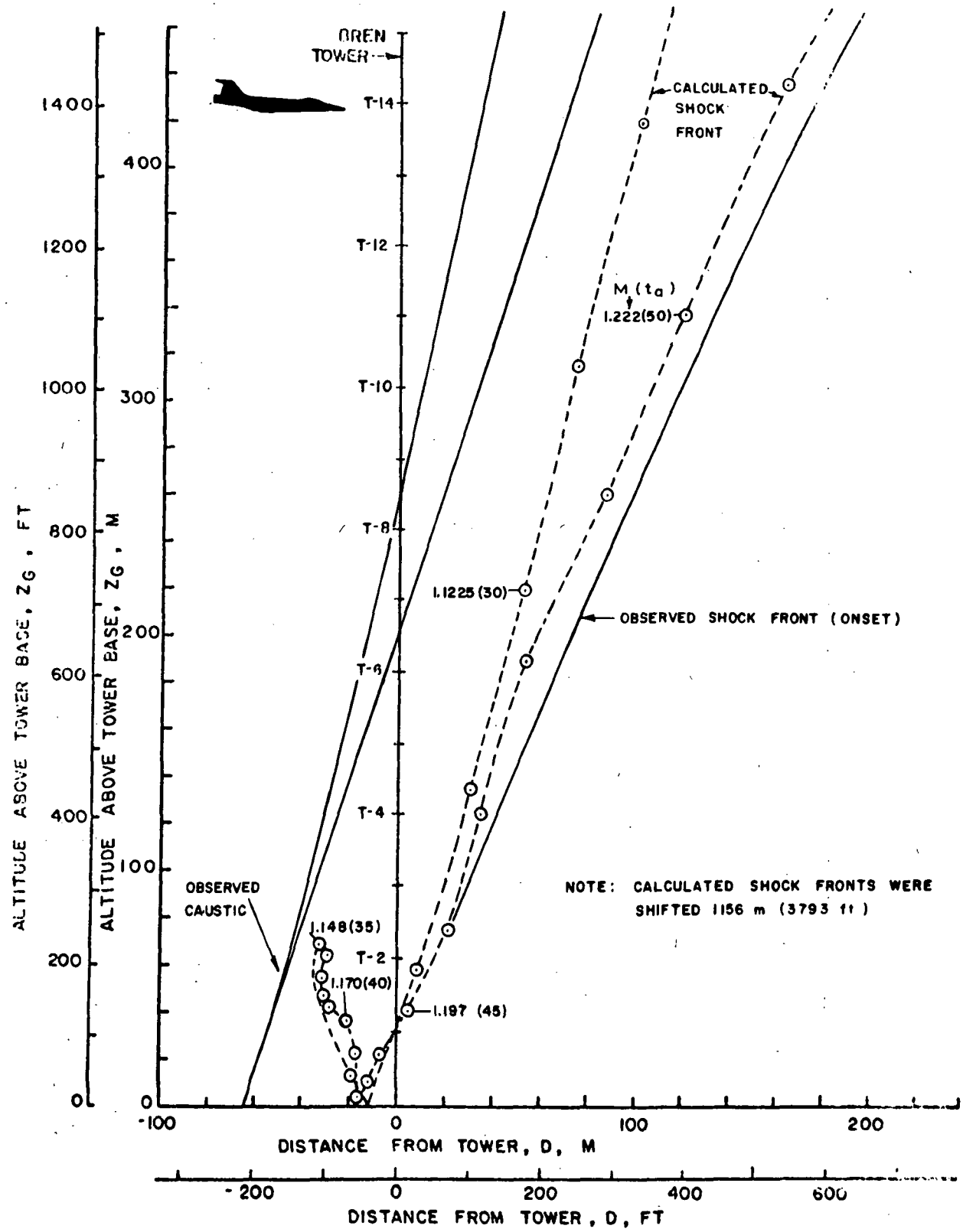

FIGURE 44.—OBSERVED AND CALCULATED BOW SHOCK WAVE PROFILES FOR PASS 088, LONGITUDINAL ACCELERATION

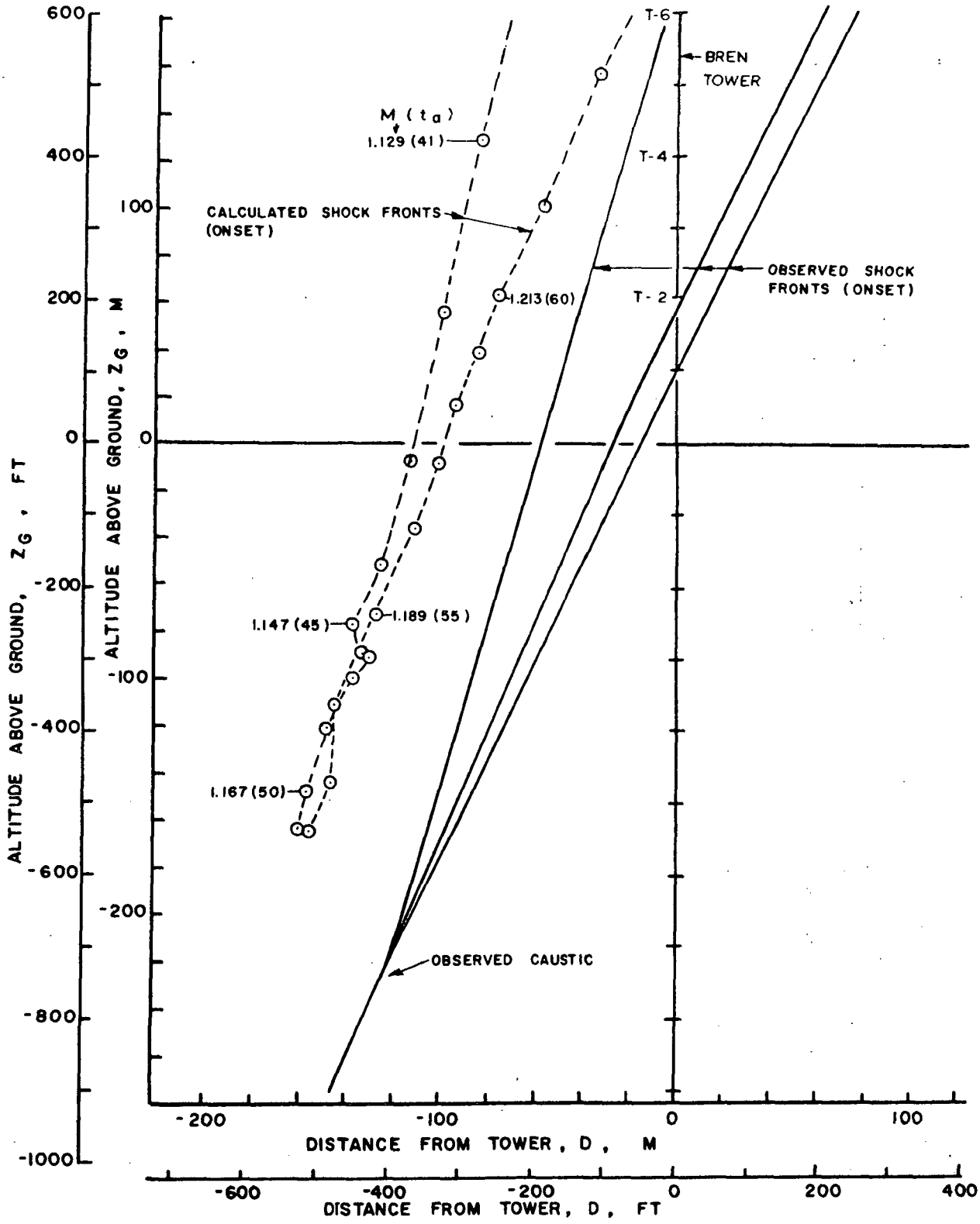

FIGURE 45.—OBSERVED AND CALCULATED BOW SHOCK WAVE PROFILES FOR PASS 092, LONGITUDINAL ACCELERATION

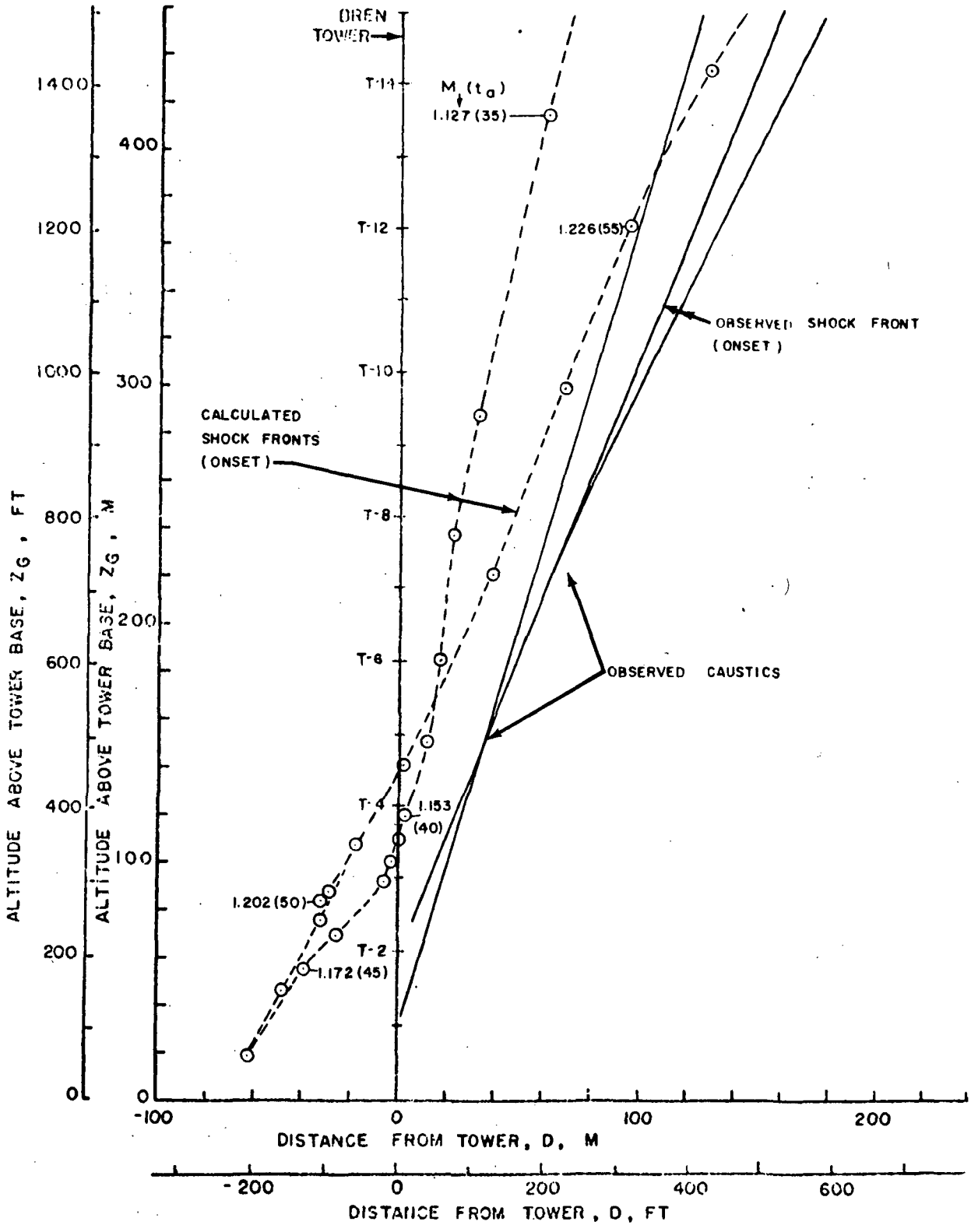

FIGURE 46.—OBSERVED AND CALCULATED BOW SHOCK WAVE PROFILES FOR PASS 093, LONGITUDINAL ACCELERATION

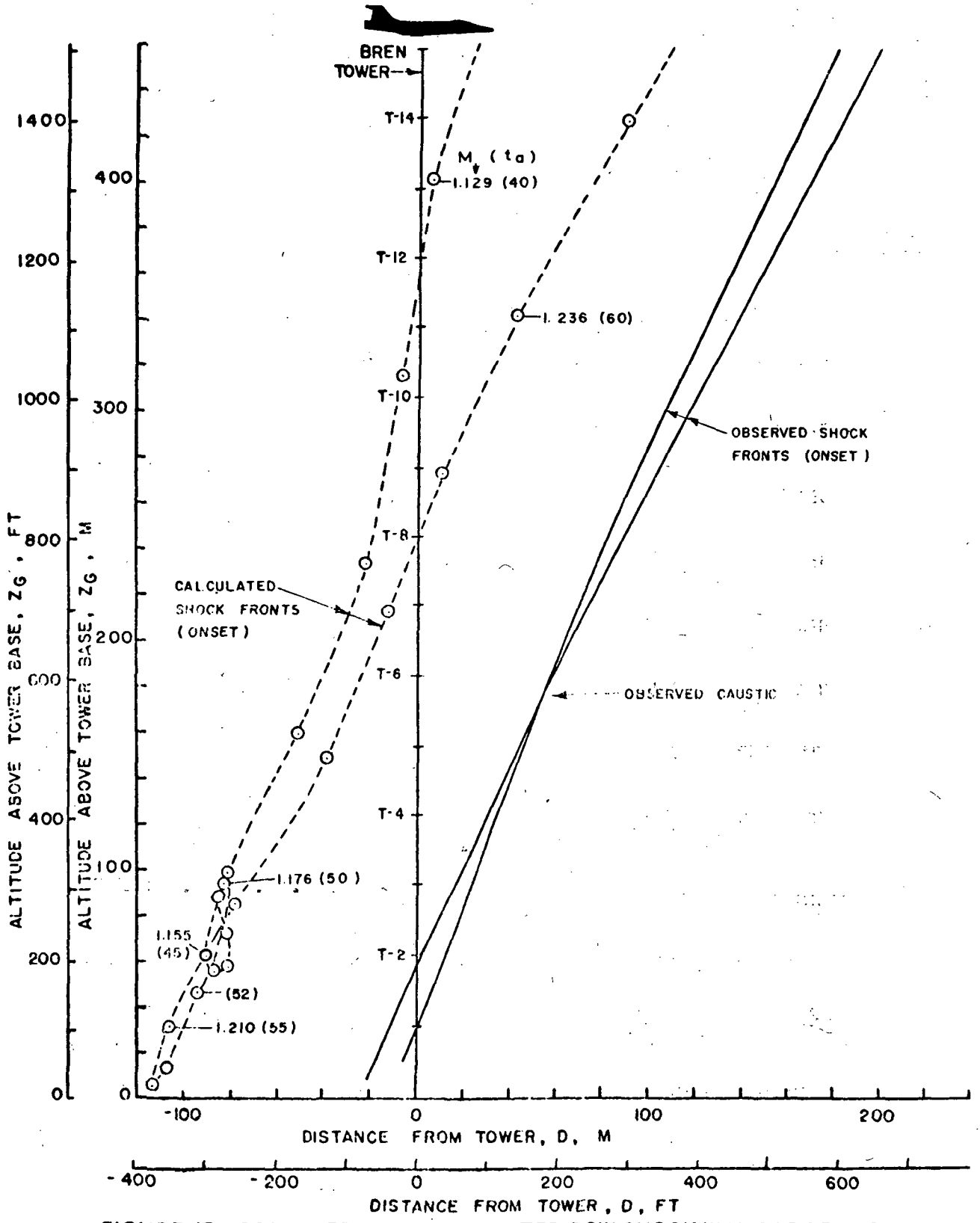

FIGURE 47.—OBSERVED AND CALCULATED BOW SHOCK WAVE PROFILES FOR PASS 094, LONGITUDINAL ACCELERATION

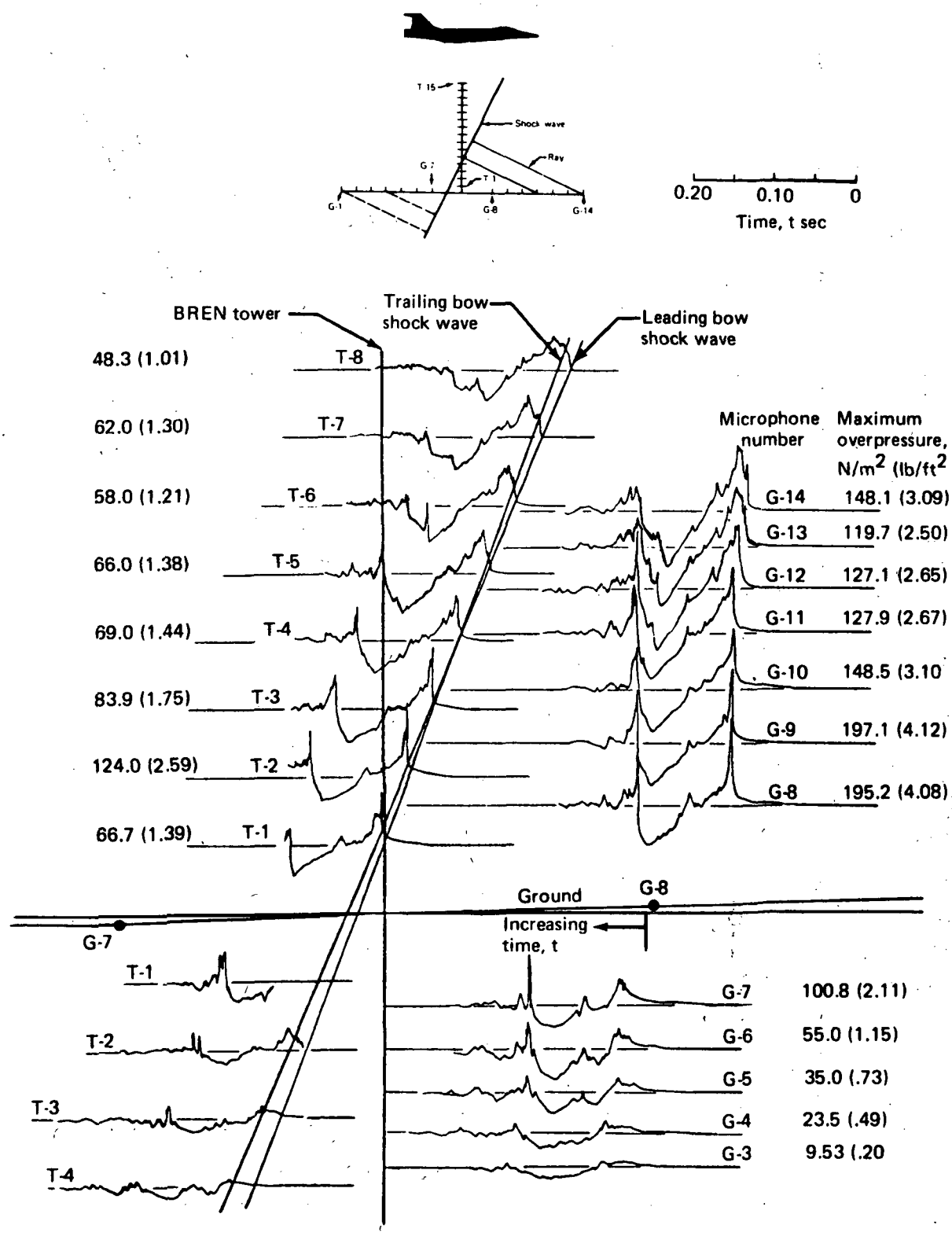

FIGURE 48.–OBSERVED PRESSURE SIGNATURES FOR PASS 045, LONGITUDINAL ACCELERATION

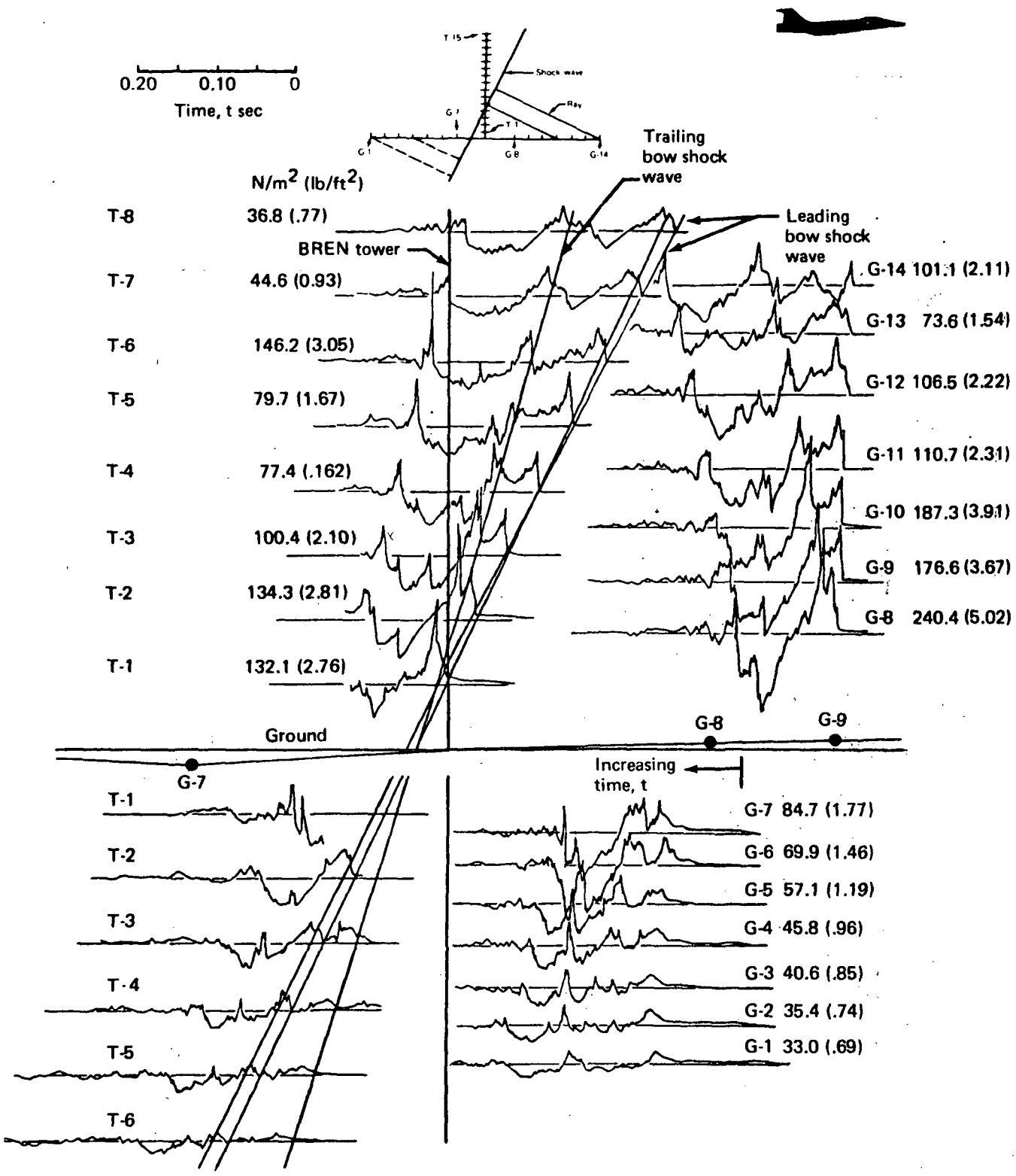

FIGURE 49.—OBSERVED PRESSURE SIGNATURES FOR PASS 046, LONGITUDINAL ACCELERATION

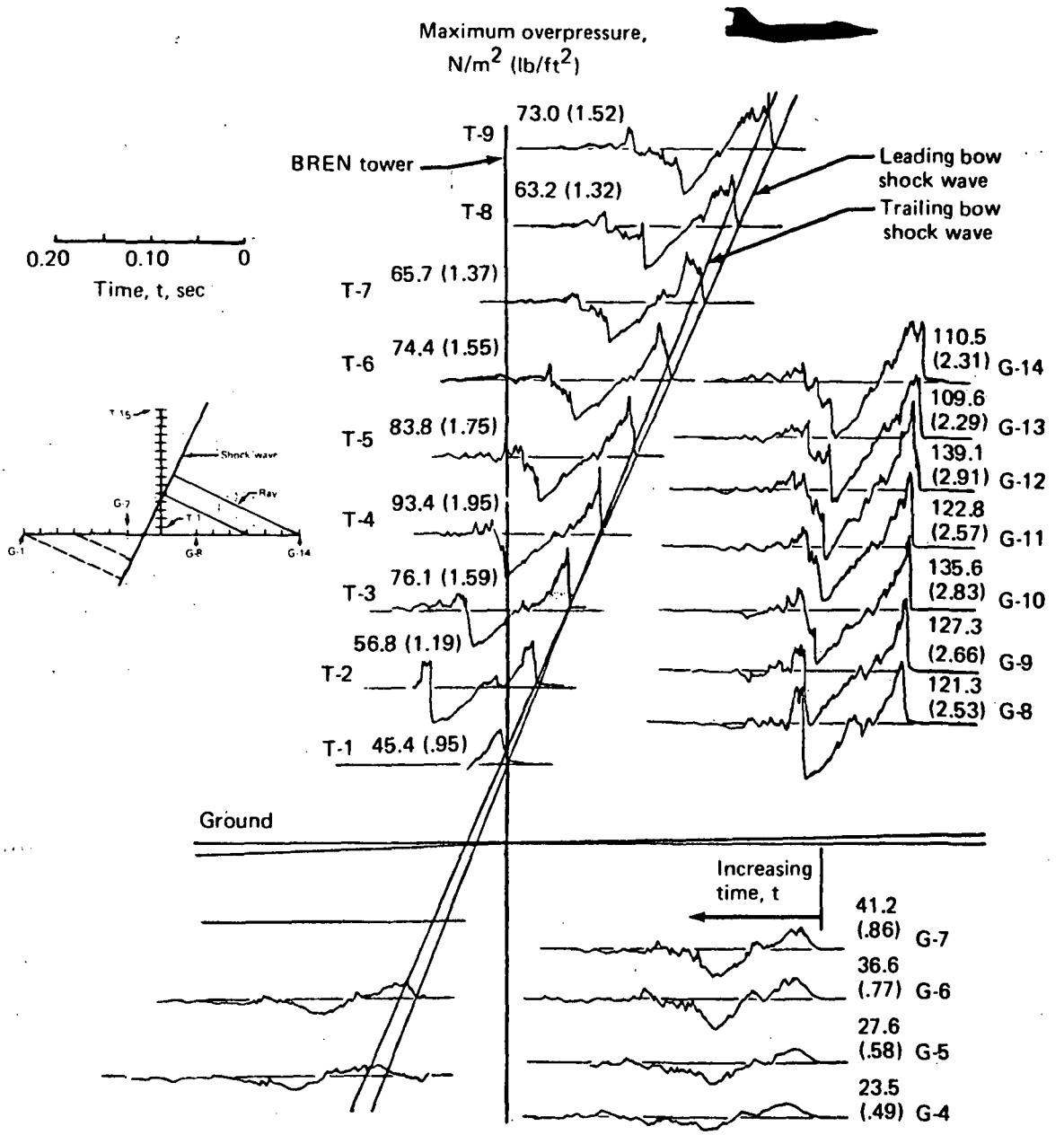

FIGURE 50.–OBSERVED PRESSURE SIGNATURES FOR PASS 047, LONGITUDINAL ACCELERATION

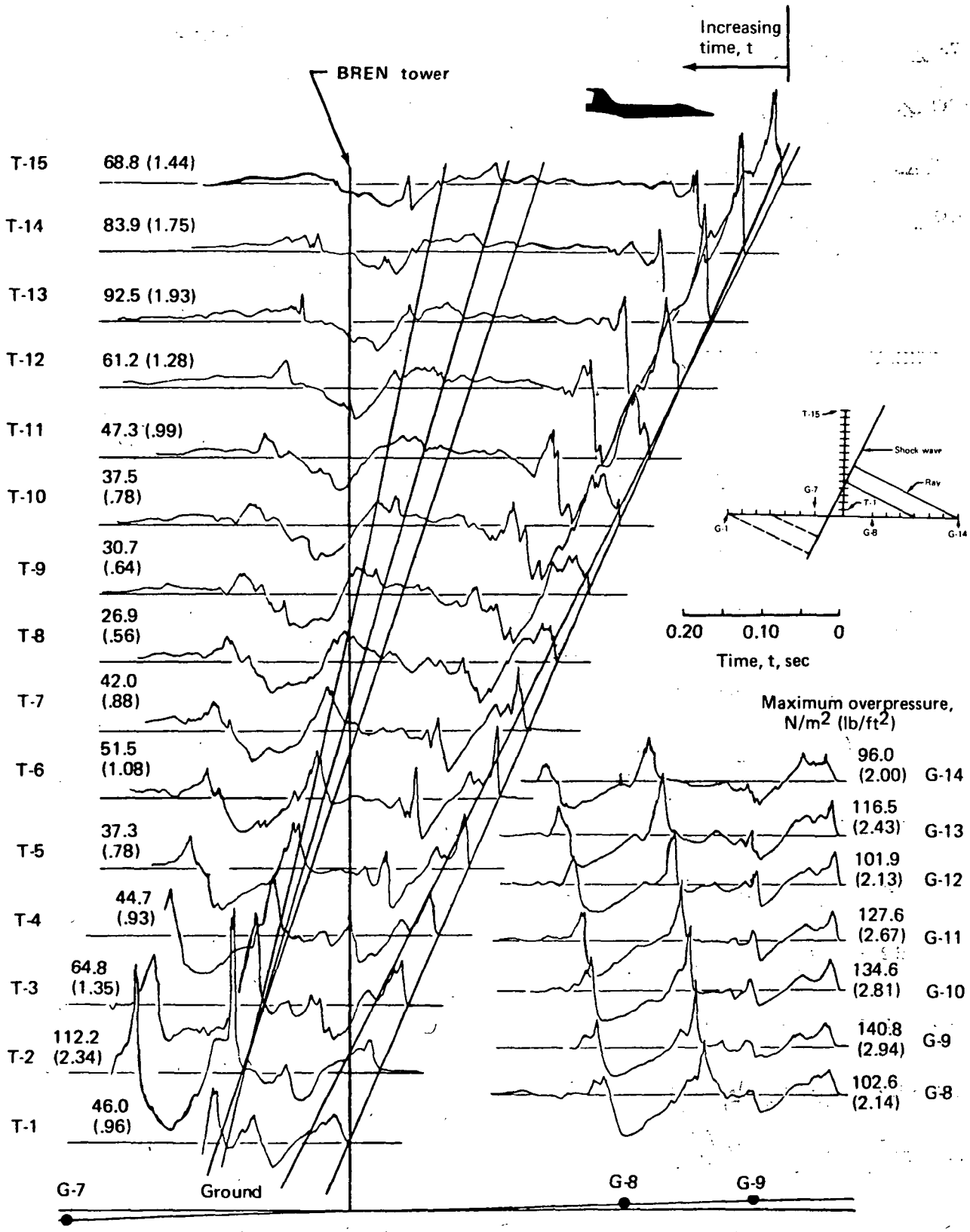

FIGURE 51.—OBSERVED PRESSURE SIGNATURES FOR PASS 088, LONGITUDINAL ACCELERATION

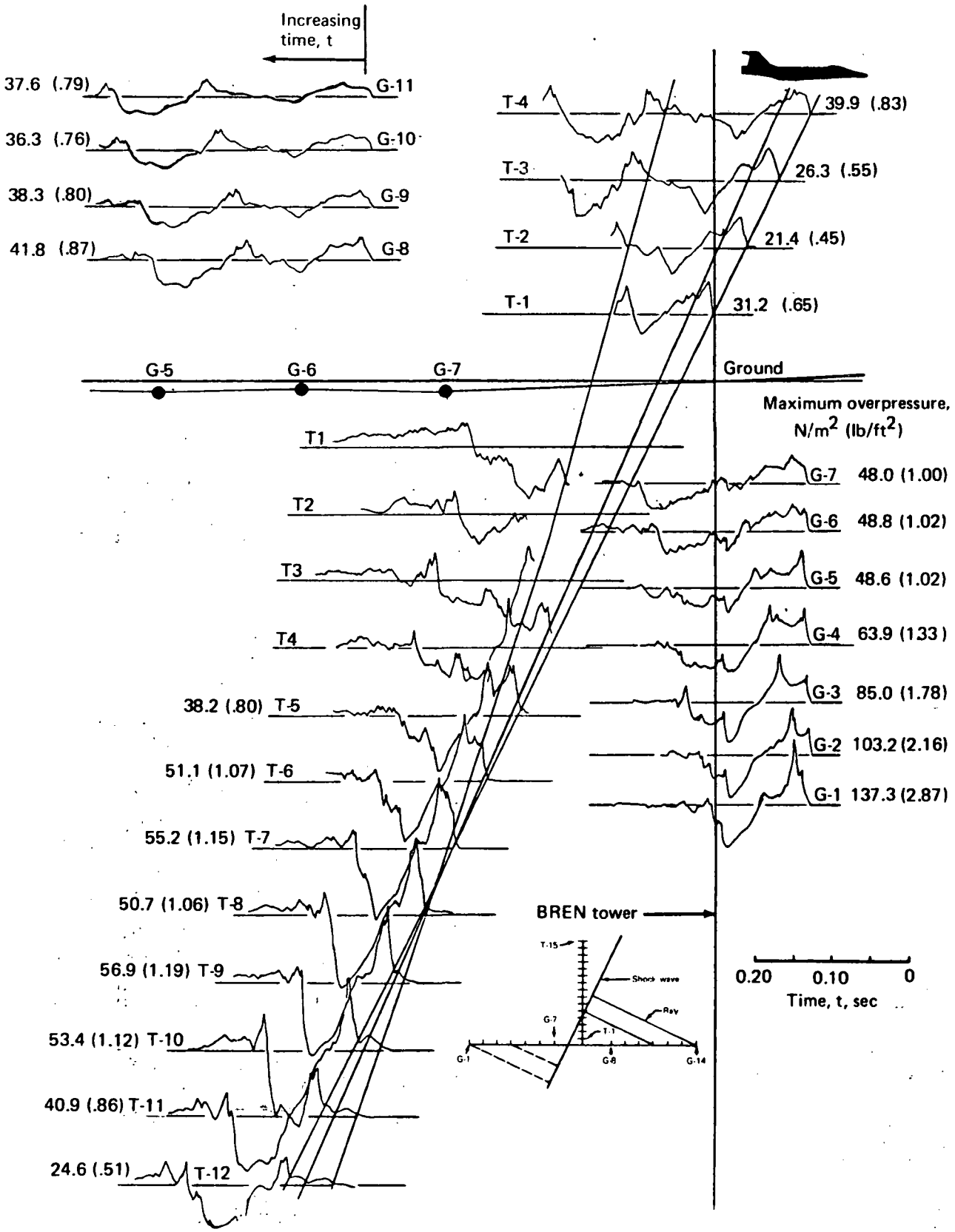

FIGURE 52.—OBSERVED PRESSURE SIGNATURES FOR PASS 092, LONGITUDINAL ACCELERATION

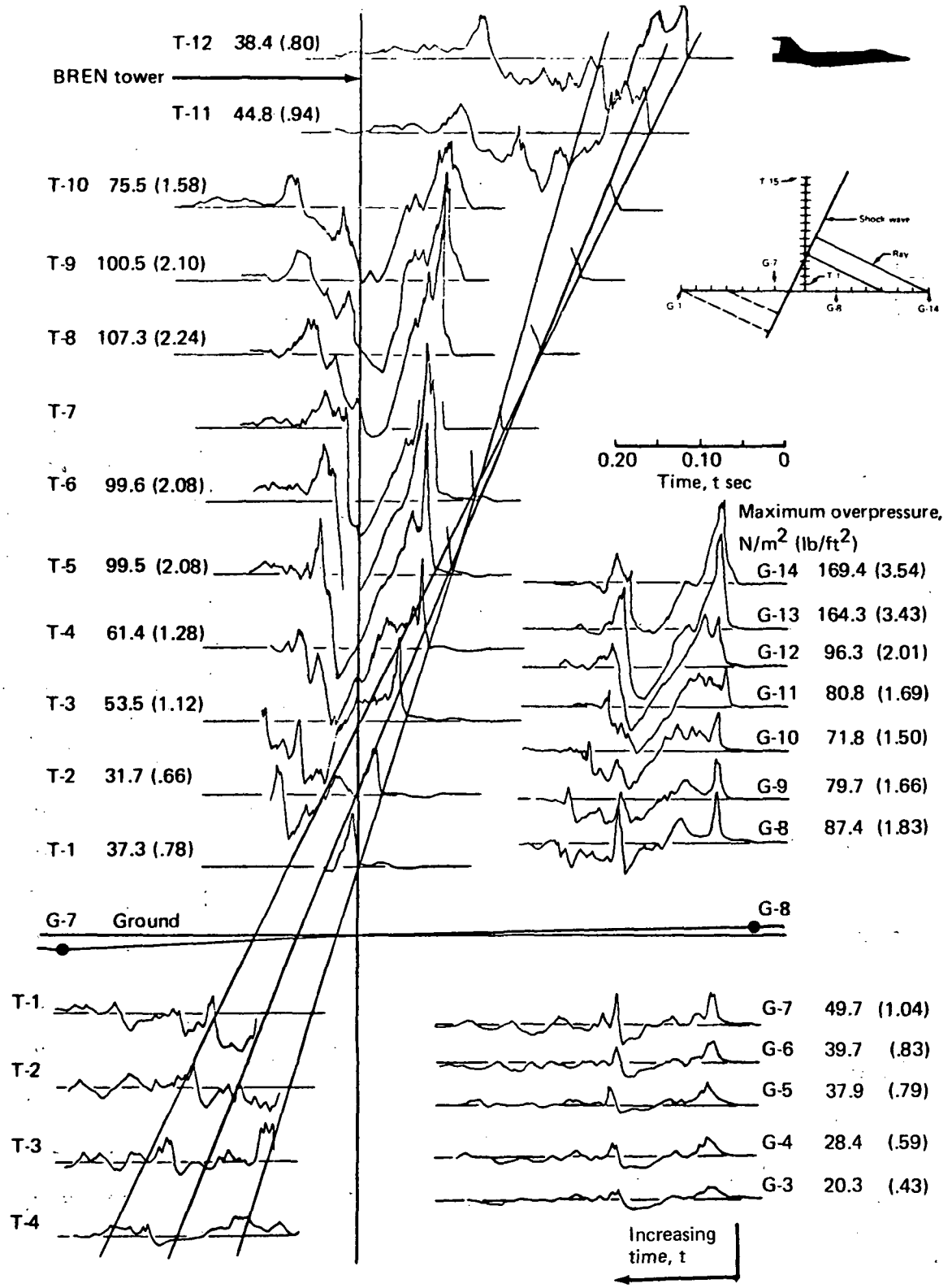

FIGURE 53.–OVSERVED PRESSURE SIGNATURES FOR PASS 093, LONGITUDINAL ACCELERATION

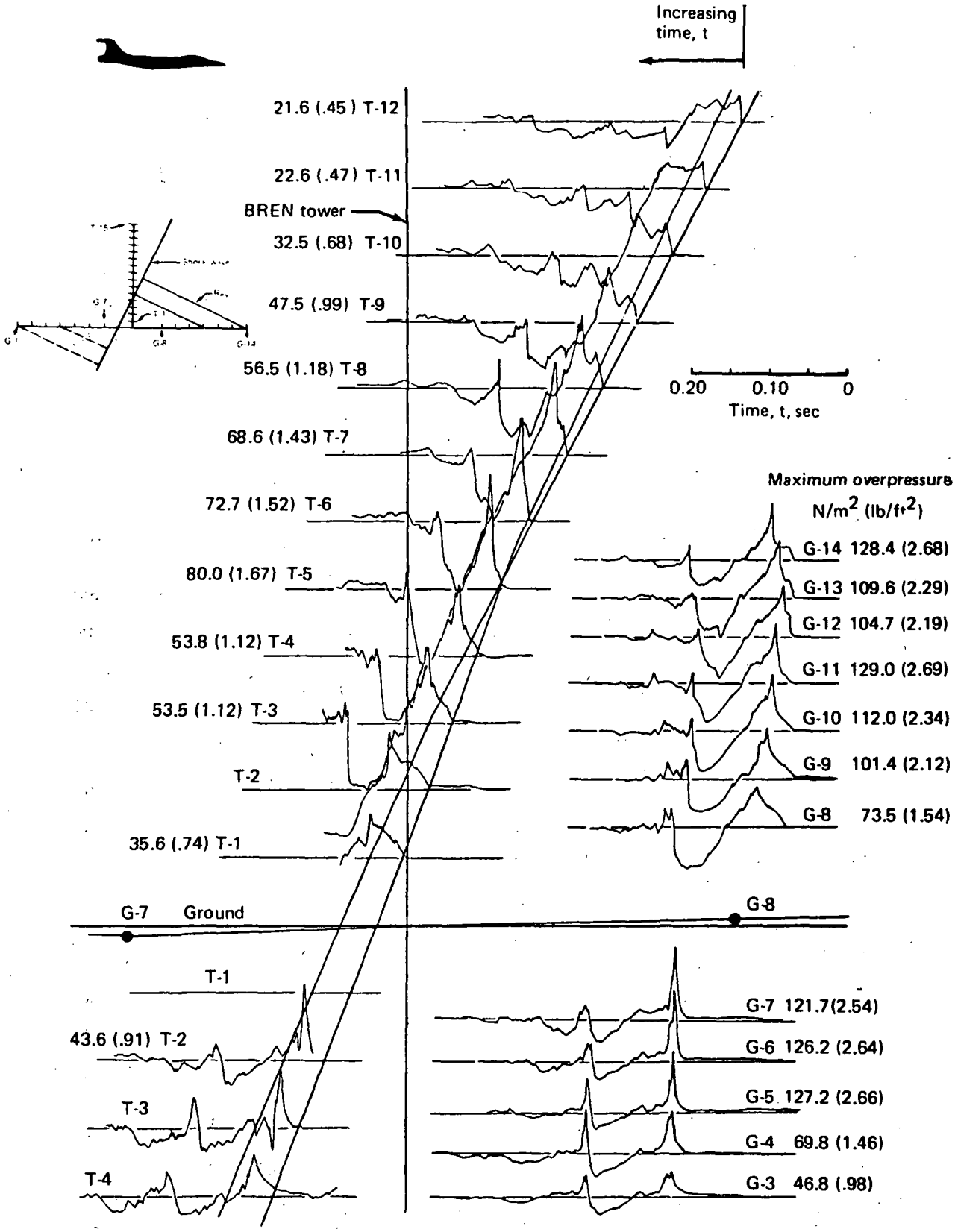

FIGURE 54.—OBSERVED PRESSURE SIGNATURES FOR PASS 094, LONGITUDINAL ACCELERATION

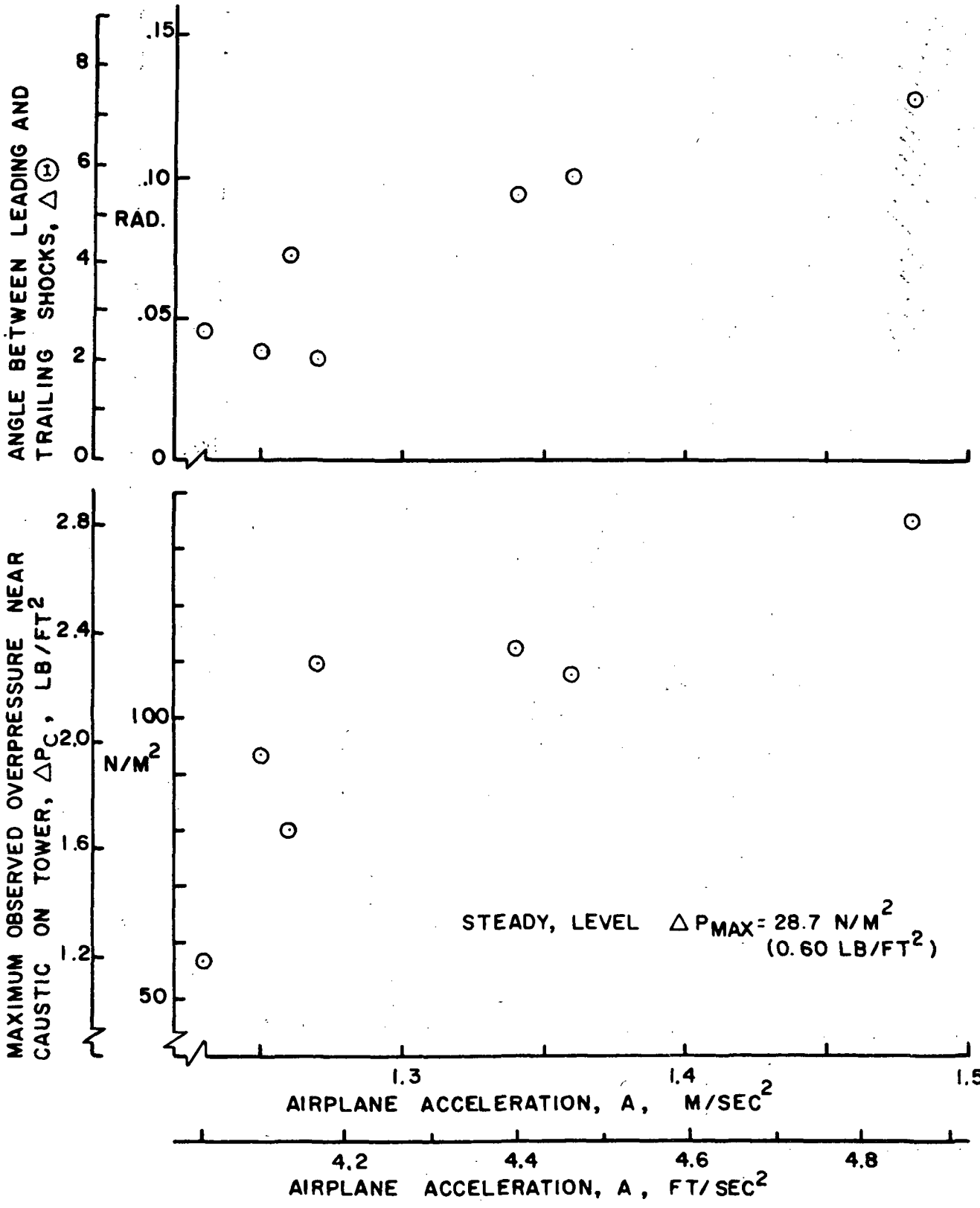

FIGURE 55.–EFFECT OF ACCELERATION MAGNITUDE ON CAUSTIC STRENGTH AND INCIDENCE ANGLES–LONGITUDINAL ACCELERATION FLIGHTS

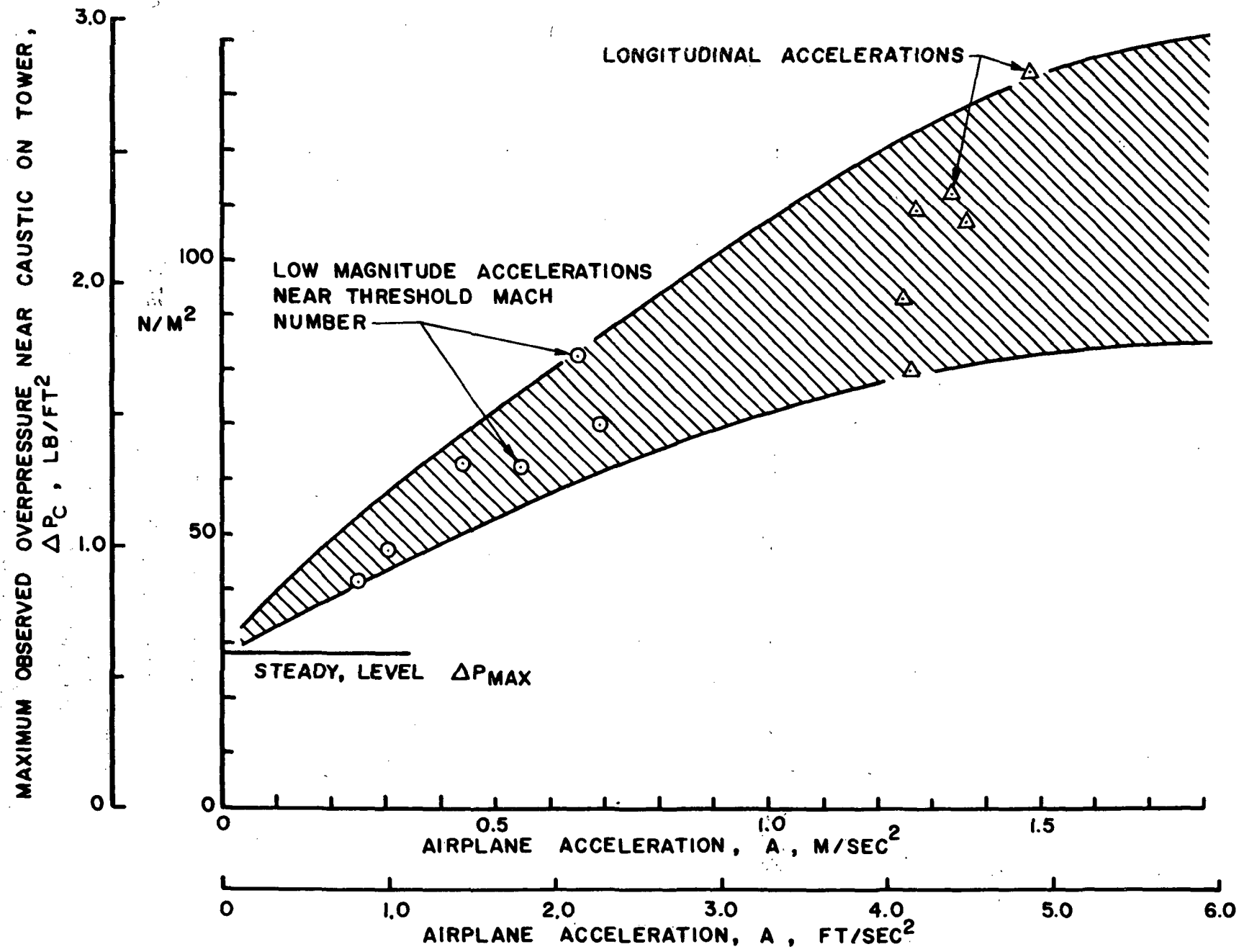

FIGURE 56.–COMPARISON OF THE EFFECT OF SLOW AND FAST ACCELERATIONS ON CAUSTIC INTENSITY

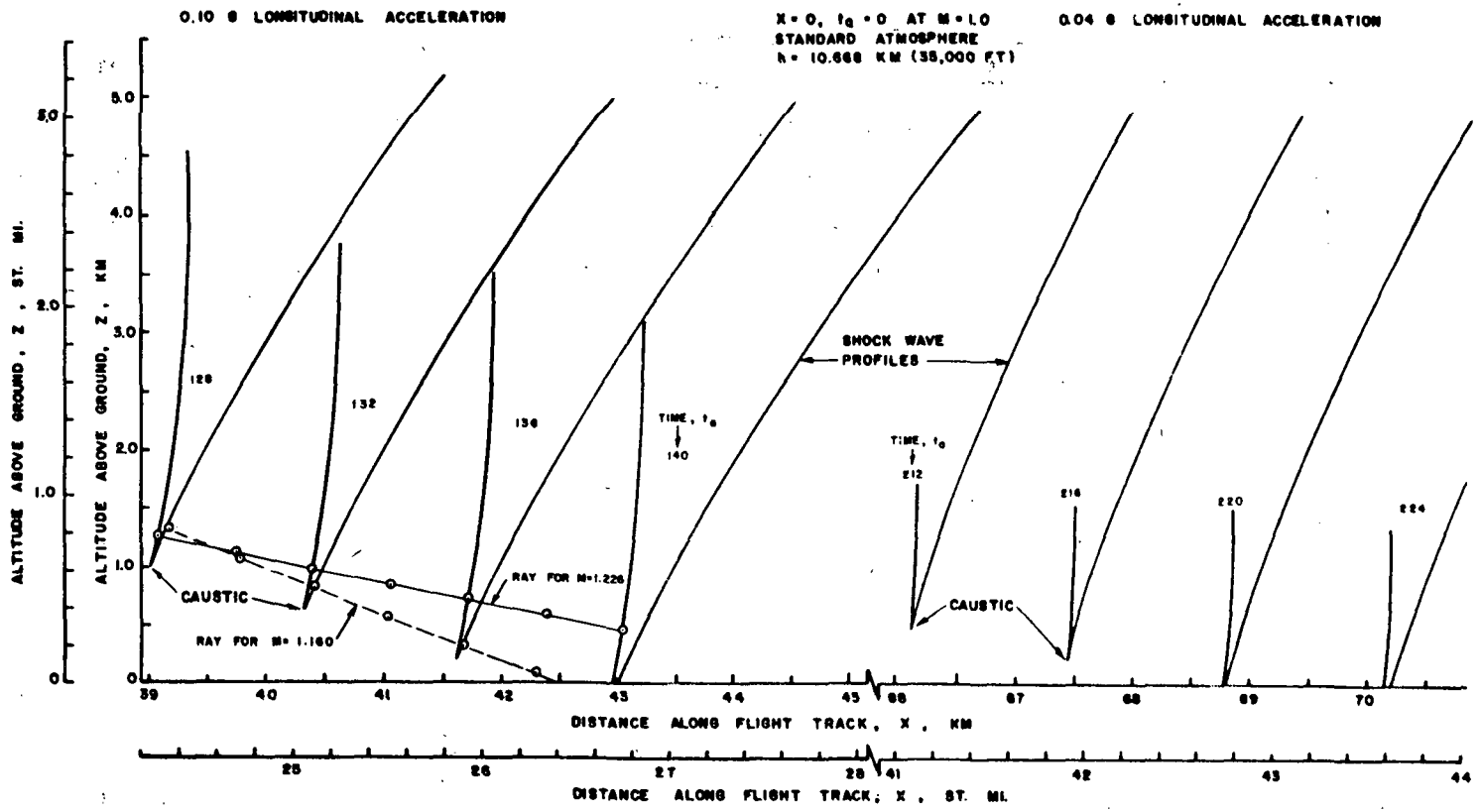

FIGURE 57.—SHOCK WAVE PROFILES PRODUCED BY 0.10 g and 0.04 g LONGITUDINAL ACCELERATIONS

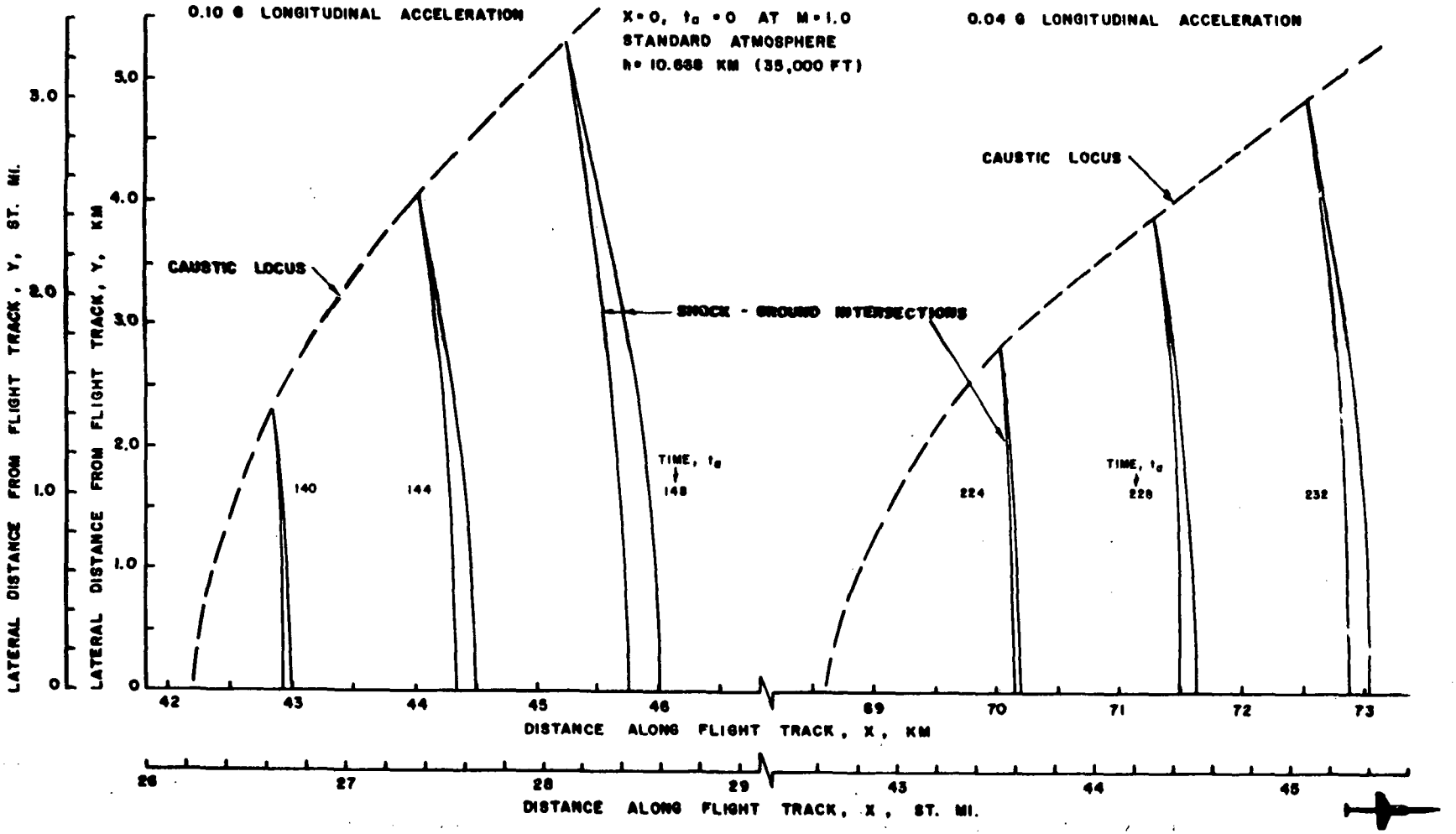

FIGURE 58.—SHOCK-GROUND INTERSECTIONS PRODUCED BY 0.10 g AND 0.04 g LONGITUDINAL ACCELERATIONS

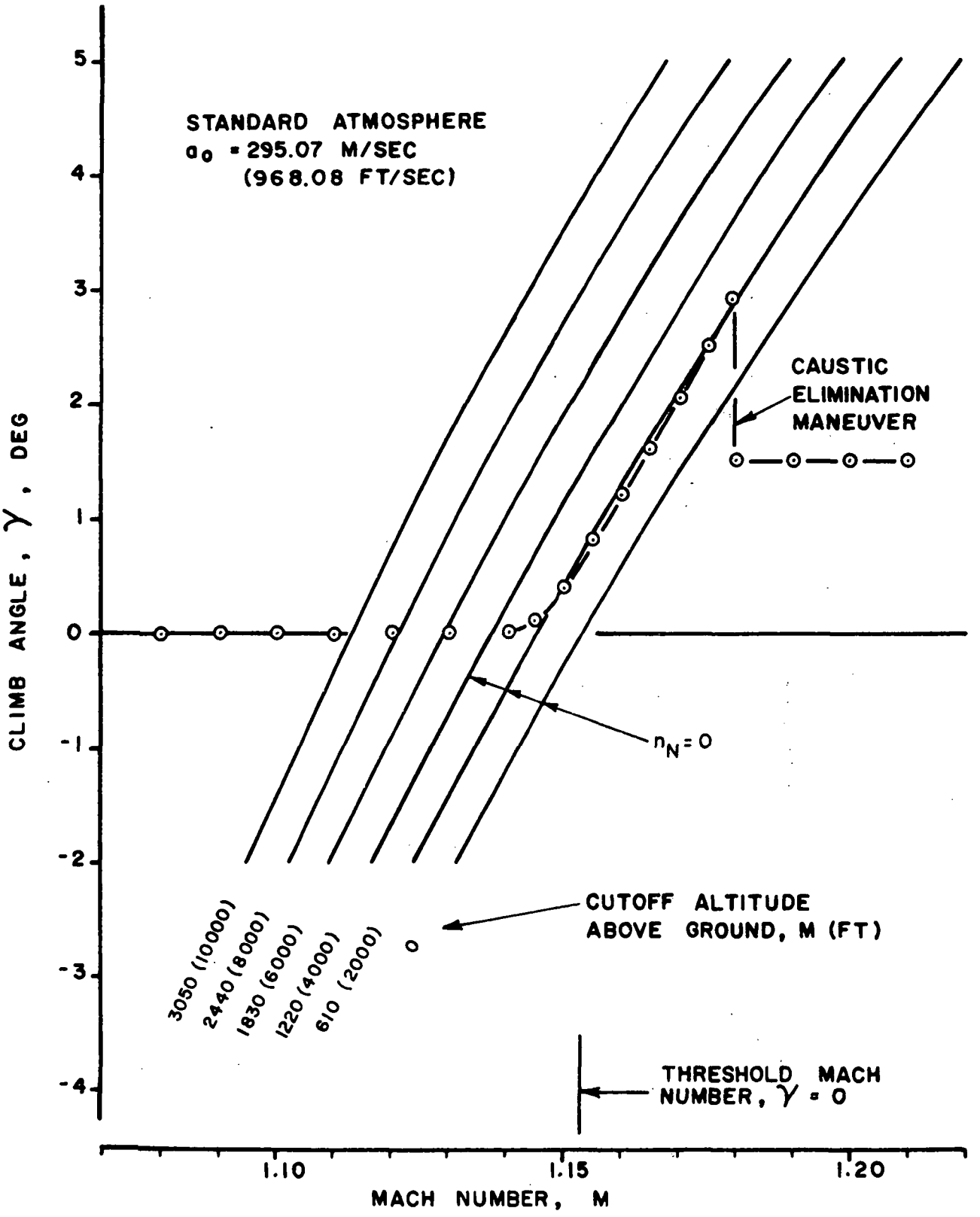

FIGURE 59.—CAUSTIC-ELIMINATION MANEUVER AND M, γ RELATIONSHIP FOR CUTOFF ABOVE GROUND

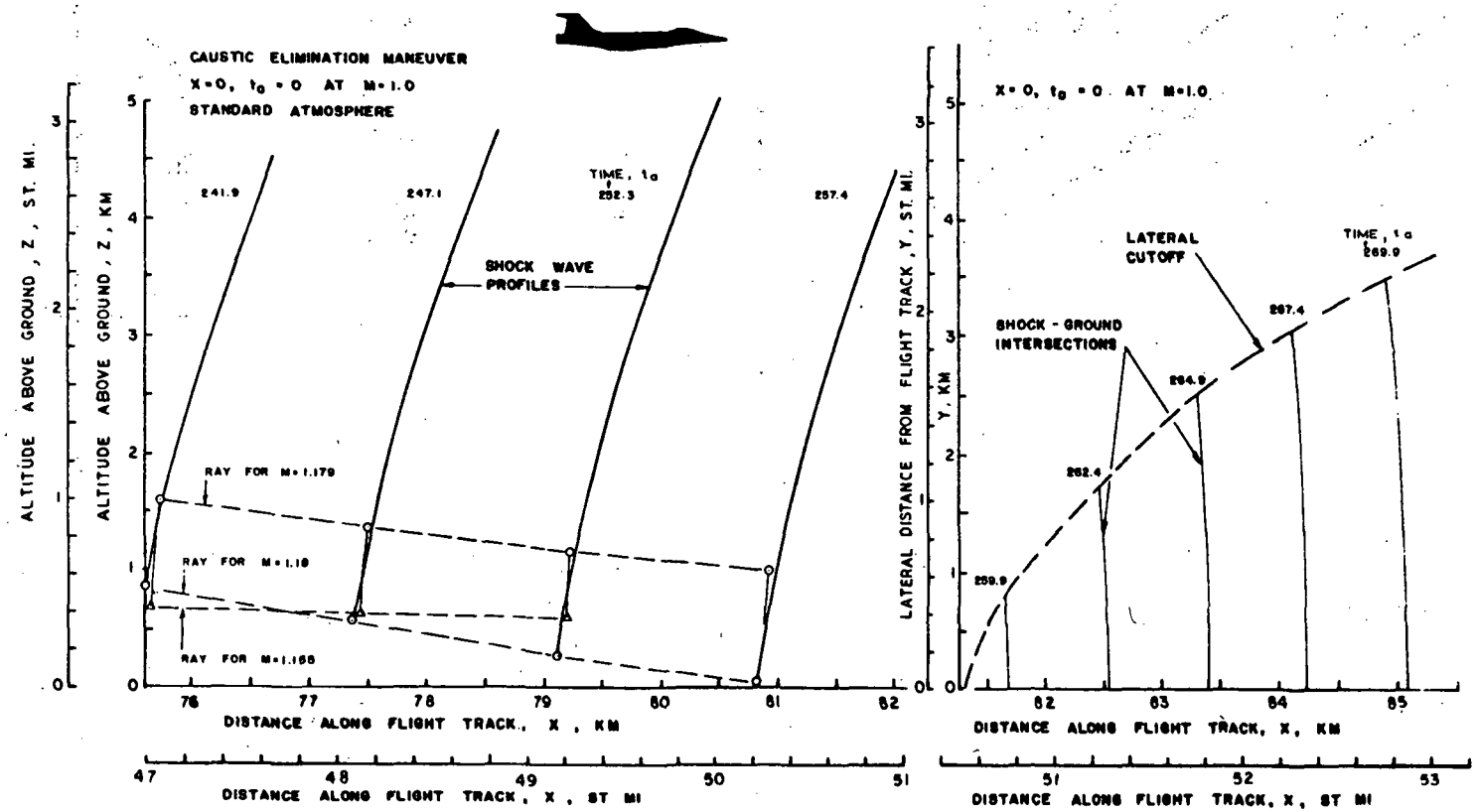

FIGURE 60.–SHOCK WAVE PATTERNS PRODUCED BY CAUSTIC-ELIMINATION MANEUVER

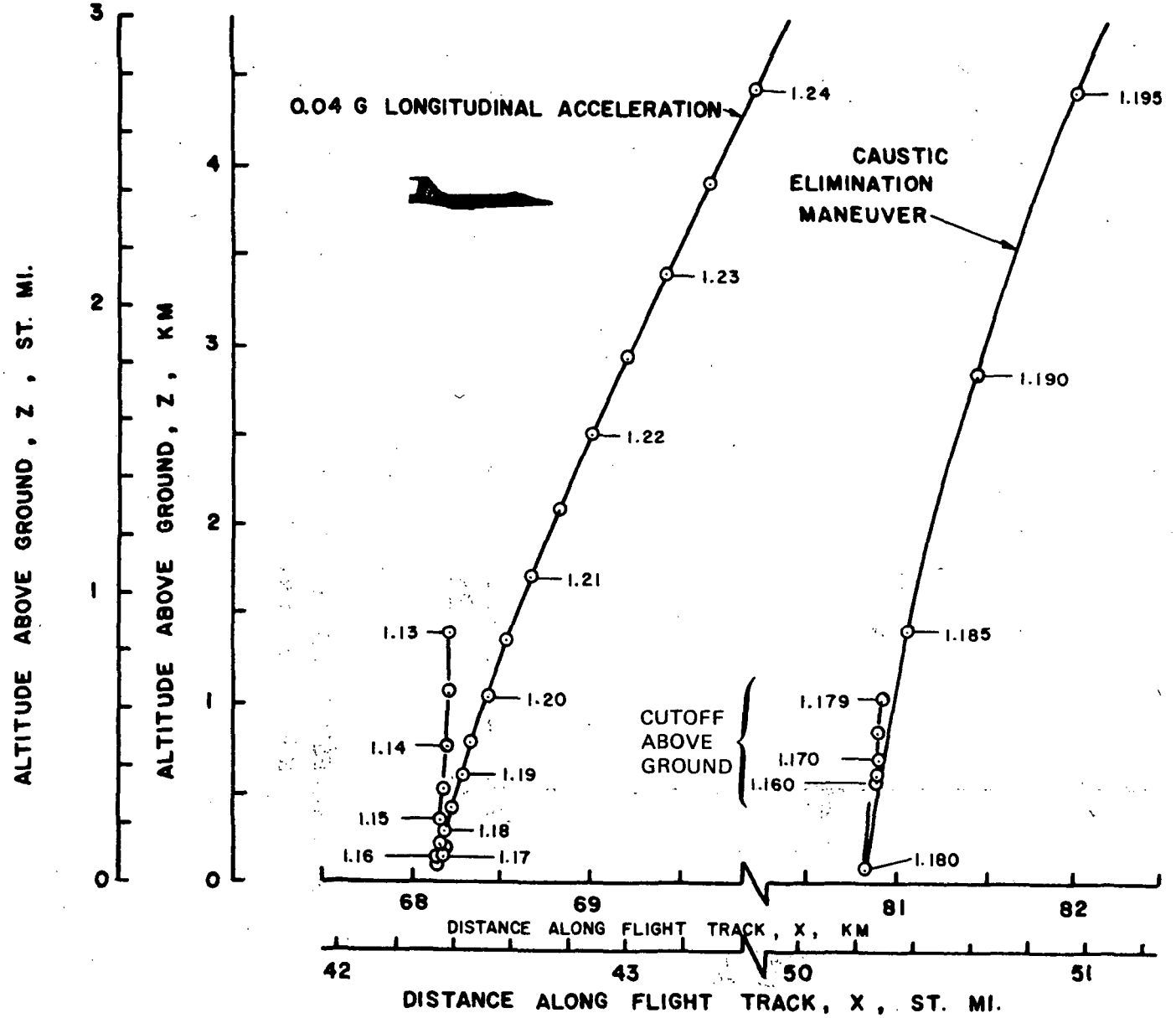

FIGURE 61.—COMPARISON OF NORMAL ACCELERATION CAUSTIC AND CAUSTIC-ELIMINATION MANEUVER SHOCK FRONTS

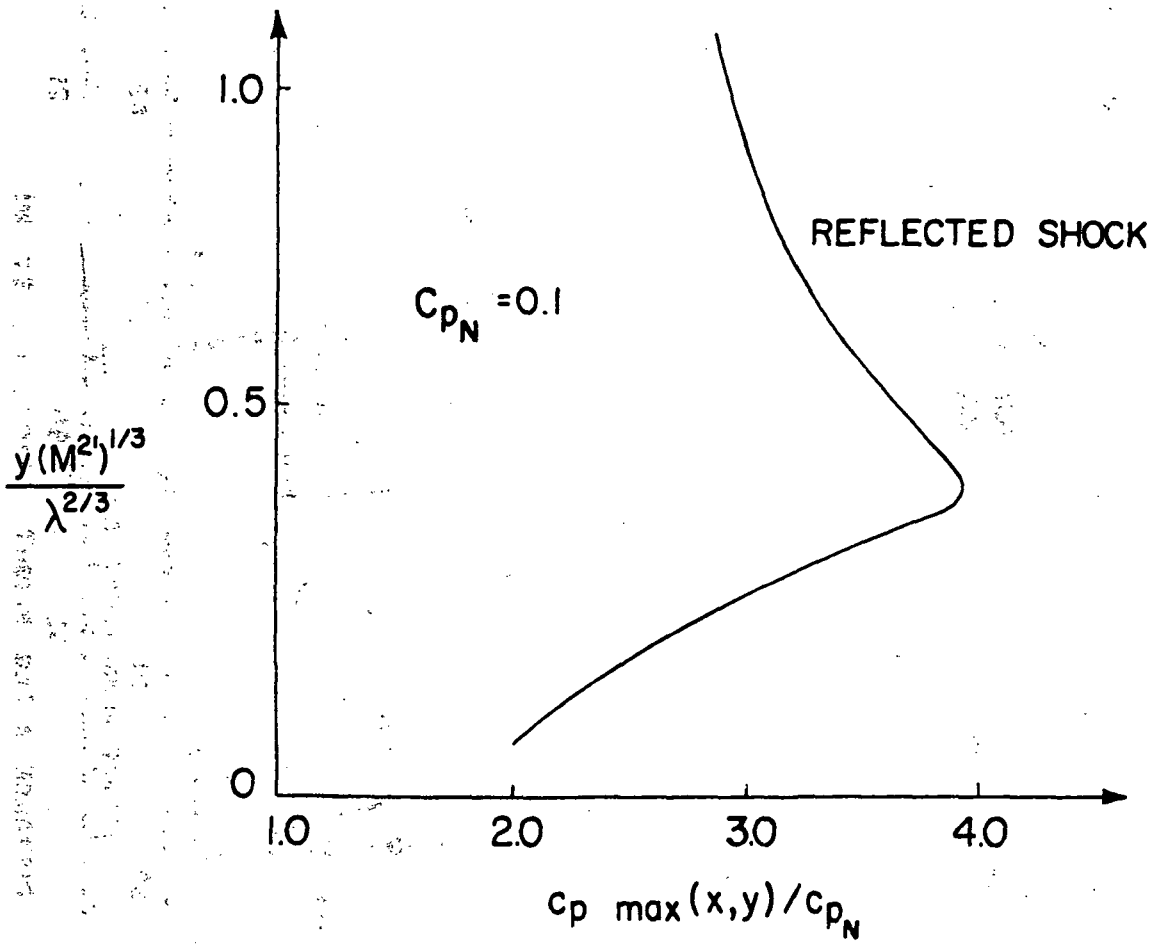

FIGURE 62.–ESTIMATED VARIATION OF STRENGTH OF REFLECTED SHOCK (FROM REF. 19)–THRESHOLD MACH NUMBER FLIGHT

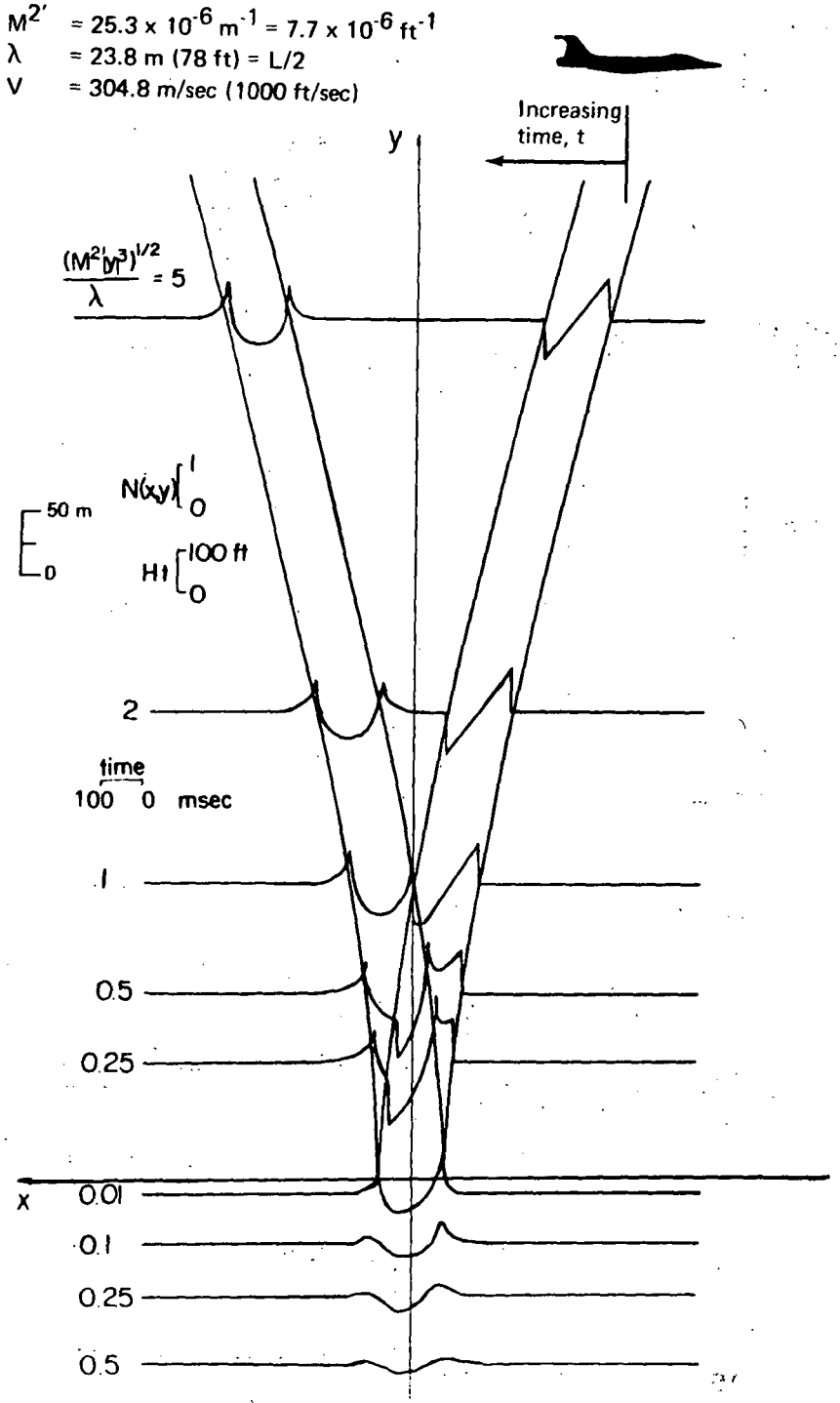

FIGURE 63.—LINEAR SOLUTION IN PHYSICAL COORDINATES FOR $M^{2'}\lambda = 6 \times 10^{-4}$, THRESHOLD MACH NUMBER FLIGHT

$M^{2'}$ = 25.3 x 10^{-6} m^{-1} (7.7 x 10^{-6} ft^{-1})
λ = 45.7 m (150 ft) = L/2
V = 304.8 m/sec (1000 ft/sec)

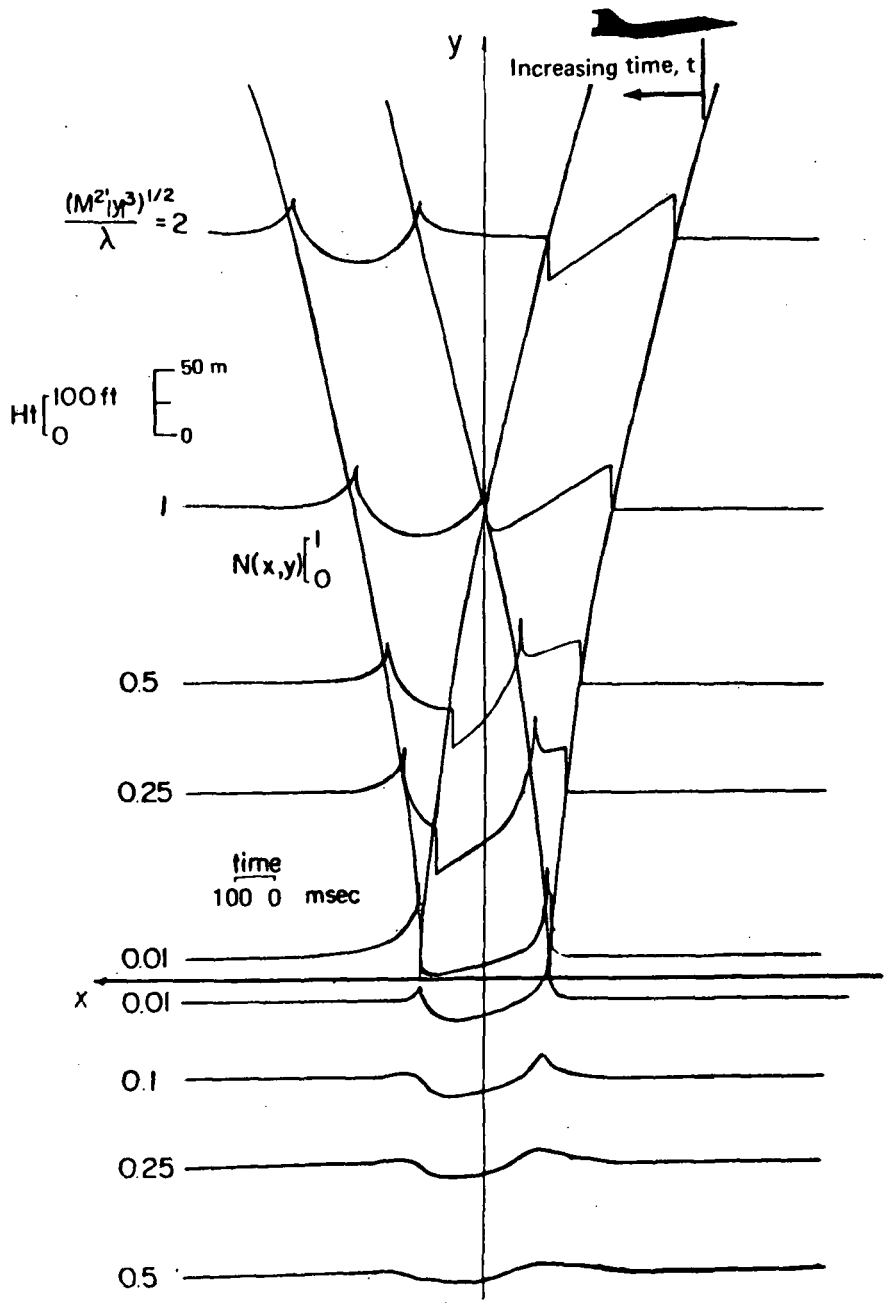

FIGURE 64.–LINEAR SOLUTION IN PHYSICAL COORDINATES FOR $M^{2'}\lambda = 11.6 \times 10^{-4}$, THRESHOLD MACH NUMBER FLIGHT

$M^{2'}$ = 3.28 x 10^{-5} m^{-1} (10^{-5} ft^{-1})
λ = 23.8 m (78 ft)
V = 304.8 m/sec (1000 ft/sec)

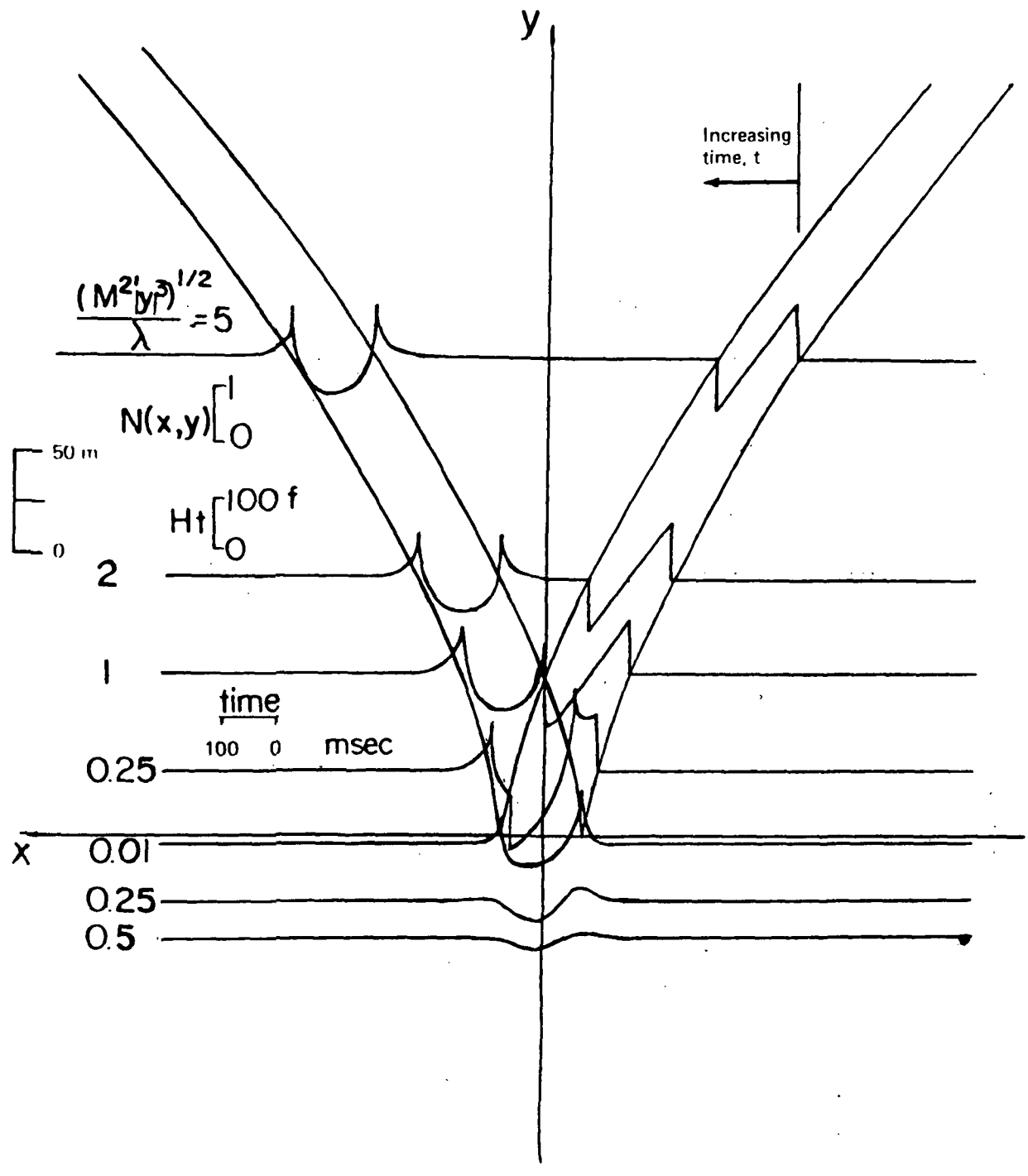

FIGURE 65.—LINEAR SOLUTION IN PHYSICAL COORDINATES FOR $M^{2'}\lambda = 7.8 \times 10^{-4}$, THESHOLD MACH NUMBER FLIGHT

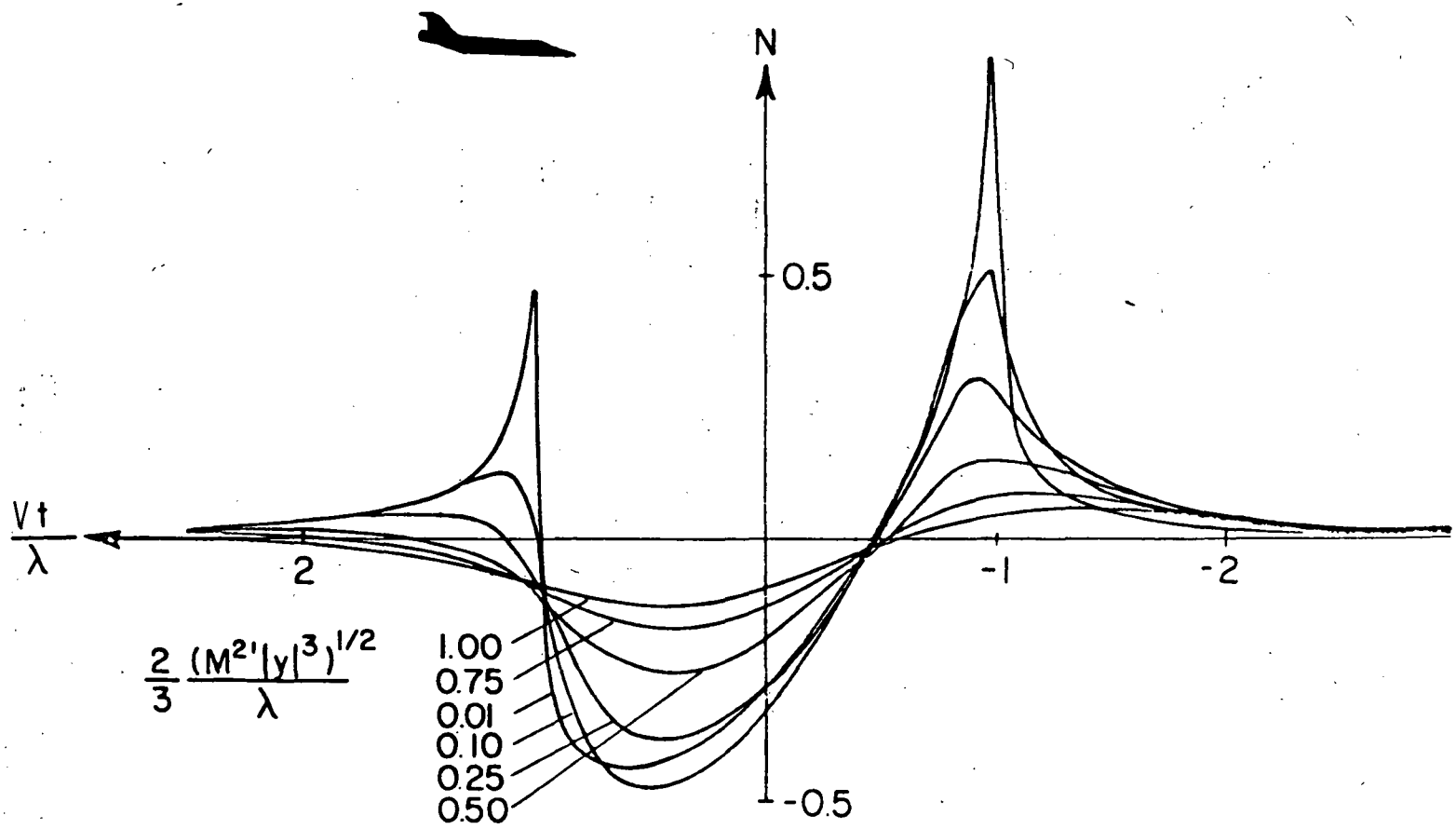

FIGURE 66.—BEHAVIOR OF PRESSURE SIGNATURE BELOW CAUSTIC FOR A STATIONARY OBSERVER, THRESHOLD MACH NUMBER FLIGHT

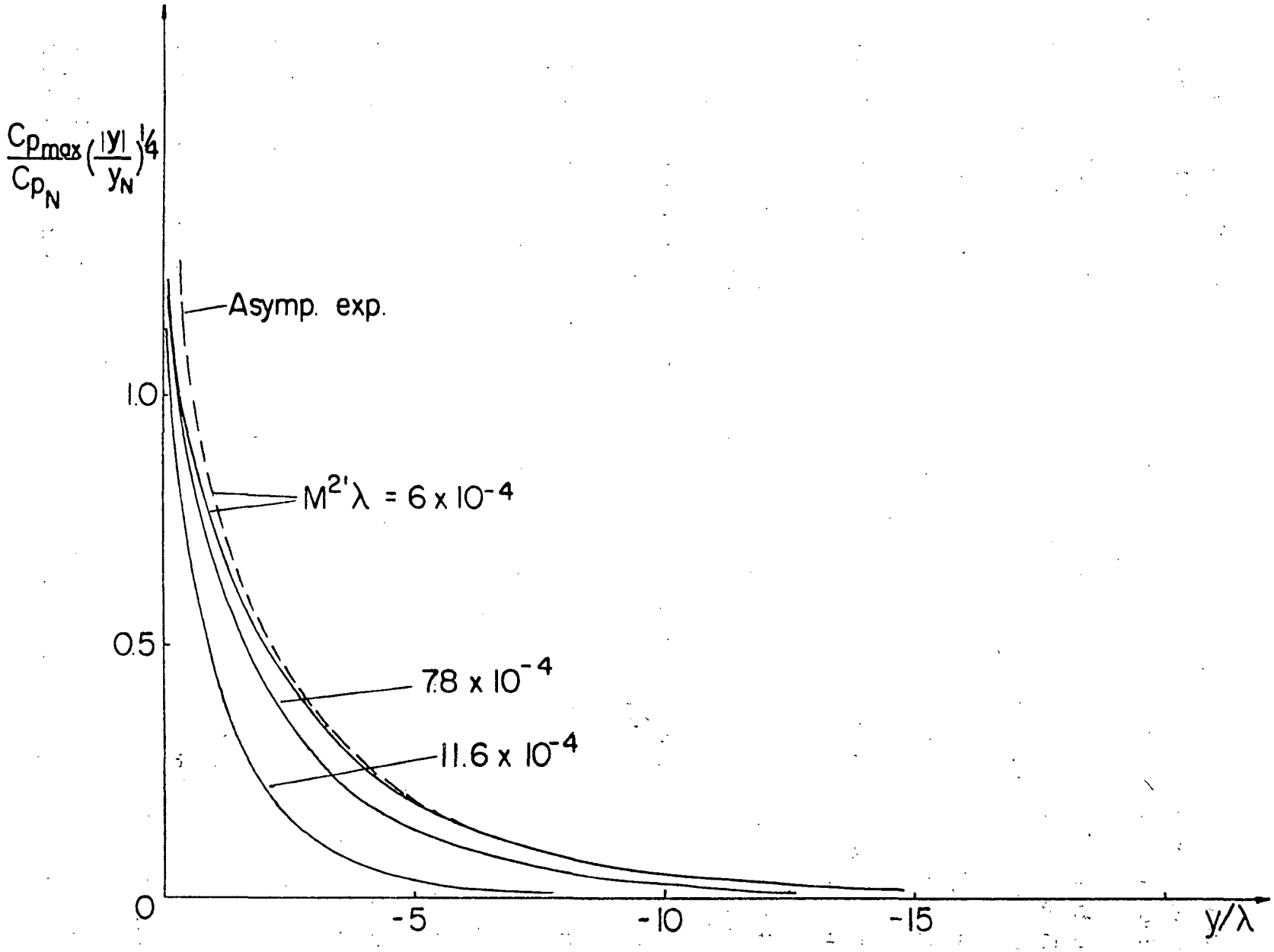

FIGURE 67.–MAXIMUM PRESSURE IN SIGNATURE AS A FUNCTION OF DISTANCE BELOW THE CAUSTIC, THRESHOLD MACH NUMBER FLIGHT

REFERENCES

1. Maglieri, D. J.; Hilton, D. A.; Huckel, V.; Henderson, H. R.; and McLeod, N. J.: Measurements of Sonic Boom Signatures From Flights at Cutoff Mach Number. Third Conference on Sonic Boom Research, NASA SP-255, 1971, pp. 243-254.

2. Hubbard, Harvey H.; Maglieri, Domenic J.; and Huckel, Vera: Variability of Sonic Boom Signatures With Emphasis on the Extremities of the Ground Exposure Patterns. Third Conference on Sonic Boom Research, NASA SP-255, 1971, pp. 351-360.

3. Haglund, G. T.; and Kane, E. J.: Flight Test Measurements and Analysis of Sonic Boom Phenomena Near the Shock Wave Extremity. NASA CR-2167, 1973.

4. Barger, Raymond L.: Sonic Booms Attributed to Subsonic Flight. J. AIAA, Vol. 5, No. 5, May 1967, pp. 1042-1043.

5. Goodmanson, Lloyd T.: Transonic Transports. Paper No. 72-18 presented at 12th Anglo-American Aero. Conf., Can. Aeronautics and Space Inst. (Calgary, Alberta), July 1971.

6. Hayes, Wallace D.; Haefeli, Rudolph C.; and Kulsrud, H. E.: Sonic Boom Propagation in a Stratified Atmosphere with Computer Program. NASA CR-1299, 1969.

7. Parker, L. W.; and Zalosh, R. G.: Godunov Method and Computer Program to Determine the Pressure and Flow Field Associated with a Sonic Boom Focus. NASA CR-2127, 1973.

8. Whitham, G. B.: A New Approach to Problems of Shock Dynamics, Part I, Two Dimensional Problems. J. Fluid Mech., Vol. 2, 1957, pp. 145-171.

9. Guiraud, J. P.: Acoustique Géométrique, Bruit Ballistique des Avions Supersoniques et Focalisation. J. de Mécanique, Vol. 4, 1965, pp. 215-267.

10. Hayes, W. D.: Similarity Rules for Nonlinear Acoustic Propagation Through a Caustic. Second Conference on Sonic Boom Research, NASA SP-180, 1969, pp. 165-171.

11. Seebass, A. R.: Nonlinear Acoustic Behavior at a Caustic. Third Conference on Sonic Boom Research, NASA SP-255, 1971, pp. 87-120.

12. Seebass, R.; Murman, E. M.; and Krupp, J. A.: Finite Difference Calculation of the Behavior of a Discontinuous Signal Near a Caustic. Third Conference on Sonic Boom Research, NASA SP-255, 1971, pp. 361-371.

13. Wanner, Jean-Claude L., et al.: Theoretical and Experimental Studies of the Focus of Sonic Booms. J. Acoust. Soc. Am., Vol. 52, No. 1, 1972, pp. 13-32.

14. Haglund, G. T.; and Kane, E. J.: Effect of SST Operational Maneuvers on Sonic Boom. J. Aircraft, August 1972, pp. 563-568.

15. Ribner, H. S.: Supersonic Turns Without Superbooms. Univ. of Toronto, Inst. for Aerospace Studies, UTIAS TN 174, February 1972.

16. Ferri, A.: Airplane Configurations for Low Sonic Boom. Third Conference on Sonic Boom Research, NASA SP-255, 1970, pp. 255-275.

17. Batdorf, S. B.: On Sonic Boom Avoidance. Aeronautical Journal, September 1972, pp. 541-543. See also comments following by W. F. Hilton, p. 543, and reply by Batdorf, pp. 543-544.

18. Hayes, Wallace D.: Sonic Boom. Annual Review of Fluid Mechanics, Vol. III, M. Van Dyke, et al., eds., Annual Reviews, Inc. (Palo Alto, California), 1971, pp. 269-290.

19. Gill, P. M.: Nonlinear Acoustic Behavior at a Caustic. Ph.D. Thesis, Cornell University, 1973.

20. Wanner, J.-C.L.; Vallee, S.; Vivier, C.; and Thery, C.: Theoretical and Experimental Studies of the Focus of Sonic Booms. Proceedings of the Second Sonic Boom Symposium (1970), J. Acous. Soc. Am., 1972, pp. 52-71.

21. Cornet, E. P.: Focusing of an N-Wave by a Spherical Mirror. University of Texas at Austin Report ARL-TR-72-40, 1972.

22. Carlson, H. W.: Laboratory Sonic Boom Research and Prediction Techniques. Second Conference on Sonic Boom Research, NASA SP-180, 1968, pp. 29-36.

☆ U.S. GOVERNMENT PRINTING OFFICE: 1974—625-042/1